POLITECNICO DI MILANO

School of Industrial and Information Engineering
Department of Aerospace Science and Technology
Master of Science Degree in Space Engineering

Analysis of the ARIEL spacecraft thermal architecture in the early A Phase

Supervisor: Prof. Michèle Lavagna, Politecnico di Milano
Assistant Supervisor: Dr. Gianluca Morgante, INAF/IASF Bologna

Degree Thesis of:
Davide D'Ascanio, Matr. 804705

Academic Year 2014-2015

Aknowledgements

I would like to thank dr. Gianluca Morgante for giving me the opportunity to develop my MSc thesis at INAF-IASF Bologna on arguments of my interest, and for having always supported me during the development of the work. I would like to thank also the other researchers and staff of the INAF-IASF Bologna for sharing their experience and knowledge with me and making me feel part of the institute.

A sincere thank to prof. Michèle Lavagna for assisting me as supervisor in this work thesis that I chose. I am also grateful to her and to all the other professors of Politecnico di Milano for knowledge gained in these years.

I must express my very profound gratitude to my family for their unfailing support for the choices I made and continuous encouragement throughout my years of study.

Last but not the least, thanks also to my hometown friends, flatmates and colleagues from Milano and Bologna, great companions in this adventure.

Davide D'Ascanio

Contents

List of Figures

List of Tables

Abstract

Scientific satellites equipped with instruments that have operative temperature at cryogenic level require high precision in thermal analysis. In order to achieve those low temperatures, efficiently passive cooling systems are exploited at the cost of setting stringent requirements, mainly on orbit and attitude. When passive cooling is not enough to achieve the required operating temperatures then active solutions are considered. This thesis work analyses the thermal architecture of the ARIEL mission payload. ARIEL is one of the three candidate missions for the ESA fourth medium-class scientific mission (M4) call in the framework of the Cosmic Vision 2015-2025. Its main objective is the study of the atmospheres of several hundreds of the hottest recently discovered exoplanets. Telescope optics and detector units shall operate at cryogenic temperatures to achieve the necessary signal to noise ratio to allow successful scientific observations.

The work, started just before the end of the Phase 0 (ended in September 2015), has been focused on the payload thermal architecture at a level of details typical of an early Phase A study. A thermal mathematical model of the spacecraft has been built with the software package ESATAN-TMS, the standard ESA thermal analysis tool. Thermal performances have been investigated mainly through the analyses of the spacecraft passive cooling system, by studying the thermal design sensitivity to the most relevant parameters assumed during the construction of the model in ESATAN-TMS, like the service module dimension, radius and inclination of the V-Grooves, radiating surfaces size and others. The thesis has been conducted at INAF-IASF Bologna under the supervision of dr. Gianluca Morgante. IASF Bologna is part of the scientific consortium responsible for the ARIEL's payload, where in particular dr. Morgante is responsible for the payload thermal control system.

Keywords: active, passive thermal control system, V-Groove, ARIEL mission, M4 call of ESA, exoplanets, Phase A, ESATAN-TMS.

Sommario

Satelliti per osservazioni scientifiche equipaggiati con strumenti che operano a temperature criogeniche richiedono un'analisi termica di alta precisione. Per ottenere basse temperature, sono sfruttati efficienti sistemi di raffreddamento passivo ma al costo di porre stringenti requisiti soprattutto sull'orbita e assetto del satellite. Se il raffreddamento passivo non è sufficiente ad ottenere le temperature operative richieste, soluzioni di raffreddamento attivo sono prese in considerazione. Questo lavoro di tesi analizza l'architettura termica del payload della missione ARIEL. ARIEL è una delle tre missioni candidate per la quarta missione scientifica di classe media (M4) dell'ESA nell'ambito del programma Cosmic Vision 2015-2025. Il suo obiettivo principale è lo studio delle atmosfere di diverse centinaia dei più caldi esopianeti scoperti recentemente. Le parti ottiche del telescopio e gli strumenti di misura scientifici devono operare a temperature criogeniche per ottenere il rapporto segnale rumore necessario che permetta osservazioni scientifiche con successo.

Il lavoro, iniziato poco prima della fine della Fase 0 (conclusa a Settembre 2015), si è focalizzato sull'architettura termica del payload ad un livello di dettaglio tipico di uno studio di Fase A allo stato iniziale. Un modello termico-matematico del satellite è stato costruito con l'ausilio del pacchetto software ESATAN-TMS, lo strumento standard di analisi termica dell'ESA. Le prestazioni termiche sono state analizzate soprattutto sul sistema di raffreddamento passivo. In particolare, è stata studiata la sensibilità del design termico rispetto ai più rilevanti parametri assunti durante la costruzione del modello in ESATAN-TMS, come le dimensioni del modulo di servizio, il raggio e l'inclinazione dei V-Groove, l'ammontare della superficie radiativa e altri. La tesi è stata svolta all'INAF-IASF Bologna sotto la supervisione del dr. Gianluca Morgante. L'IASF di Bologna è parte del consorzio scientifico responsabile del payload di ARIEL. In particolare, il dr. Morgante è responsabile del sistema di controllo termico del payload.

Parole chiave: sistema di controllo termico attivo, passivo, V-Groove, missione ARIEL, esopianeti, missione M4 dell'ESA, Fase A, ESATAN-TMS.

Chapter 1

Introduction

The thesis work presented here concerns the analysis of the thermal architecture of the ARIEL mission spacecraft (S/C) through computer simulations with the software package ESATAN-TMS. ARIEL (Atmospheric Remote-Sensing Infrared Exoplanet Large-survey) is one of the three selected candidates for the fourth medium-class mission (M4) in the framework of the Cosmic Vision 2015-2025 programme of ESA. The main scientific objective is the study of exoplanets atmosphere through spectrometry. Phase 0 study has ended in September 2015, the final M4 selection will be in June 2017 after the end of the Phase A studies for all the three candidate missions. ARIEL's configuration is based on the M3 EChO mission proposal, after a major design review needed to comply to the more stringent M4 constrains. The starting point of the thesis is based on results of the studies conducted prior and during Phase 0, including the EChO heritage. From there I developed the system thermal design to a higher level of detail and accuracy, typical of a Phase A study. The work has been carried out at *INAF-IASF Bologna* which is part of the scientific multi-national consortium responsible for the payload module (PLM). Payload hardware and software provision have been split among all scientific partners. In particular, Italy main contributions to the project are the thermal system and part of the relative hardware.

In the last years, the detection of thousands of candidates has drawn the attention of the astronomical community on exoplanets science. Exoplanets are planets orbiting a star other than the Sun. So far, the observations have focused mainly on measuring the mass and the orbit radius around their star. Just in very few cases information regarding their general chemical composition was determined or somewhat predicted. ARIEL will analyse the atmosphere of several hundred exoplanets to directly measure their chemical composition and physical conditions. This will be achieved using transit and eclipse spectroscopy of the observed exoplanet-star system light. The ARIEL spacecraft, orbiting around the Earth-Sun system L2 point, will be able to observe the full sky during the 3.5 years of nominal mission duration.

One of the major issues of the spacecraft design is the cryogenic operating temperature of the scientific instruments on board, making the thermal architecture

design one of the strongest driver in the project development. To achieve the required performances, a combined passive/active thermal control system has been selected as the baseline and studied. The design main solution is based on an efficient passive cooling system, that exploits the L2 favourable conditions, in combination with an active cryocooler dedicated to the spectrometer detector. The refrigerator, a Joule-Thomson cold end fed by a mechanical compressor, is provided by RAL Space, UK.

1.1 Thesis objective and structure

The analysis of the ARIEL S/C thermal design has as objective the development of a thermal model which will be used to investigate the performances of the ARIEL S/C thermal architecture as proposed in the most recent released ARIEL study documents. The S/C thermal model has been created in ESATAN-TMS, the European Space Agency Thermal Analysis Network software - Thermal Modelling Suite. The development of the thermal model has started from the information contained in the study documents and has reached a finer level of detail which has required new assumptions on component and interface thermal properties. Assumptions on critical parameters has been made through conservative estimates typical of the early phase studies. In particular, the solved thermal model in ESATAN-TMS has allowed to:

- verify the general validity of the thermal architecture in the operative environmental condition (orbit and attitude in nominal conditions);
- analyse the sensibility of the PLM cooling performance with respect to attitude rotations in the operational orbit in compliance with scientific observational requirements;
- identify the critical PLM units in terms of thermal requirements;
- identify the S/C design parameters that have a stronger impact on the thermal performance;
- evaluate at the end of the analysis the overall thermal design robustness;
- analyse and possibly propose different S/C design solutions as a trade-off between cooling performances, dimensions and mass, fulfilling temperature requirements with margins.

The thesis is divided in the following chapters:

Chapter 2 is a general introduction to the ARIEL project. The first section is a short mission description which summarizes its main characteristics. Later sections focus on the scientific objectives and satellite design divided into payload module (PLM) and service module (SVM). Since the thesis focuses on the thermal subsystem, only the thermal characteristics are being described, while other subsystems are taken into account when they have interfaces or dependencies with the thermal one.

Chapter 3 gives an introduction to the software ESATAN-TMS environment, the main tool used for the ARIEL satellite thermal model development. This

does not represent an exhaustive explanation of whole software, focus is given only on the features used for this thesis work development.

Chapter 4 describes how the ARIEL spacecraft geometric and thermal mathematical model has been built in ESATAN-TMS. All new assumptions made, in addition to the information contained in the study documents, are also described in this chapter.

Chapter 5 shows and comments the results of the steady state temperature distribution in the thermal model described in previous chapter. Steady state temperatures in various thermal cases and with different attitudes at L2 point are analysed. The second section explains updates in the model made to obtain general better thermal performances. This updated model is assumed as the baseline, used to make comparison with all the new modifications introduced to study the model sensitivity to some parameters and described in the next chapter.

Chapter 6 investigates the influence on thermal performance of some thermal and geometrical parameters of the satellite, like dimension, inclination, relative distances of critical parts. New thermal models have been built and solved in ESATAN-TMS changing these parameters. Thermal performances are compared with the previous models to identify possible solutions for improving the system performances.

Chapter 7. Here conclusions of the thesis work are drawn. Characteristics of the final models are discussed and open points are highlighted.

1.2 Documents and information applicable to the thesis work

The work of this thesis started when the Phase 0 studies were nearly completed. The documents released at the end of the Phase 0, together with the outcome of the ESA CDF (Concurrent Design Facility) parallel study, have been used to update the work with better assumptions and more detailed results. This section explains which documents have been used as a reference to start the study, in order to highlight, later, the original contribution of this thesis work.

1.2.1 ARIEL mission proposal document

This is the document prepared by the science community submitted to ESA in response to the M4 call, containing studies conducted by researchers of the Payload Consortium. It explains scientific objectives of the mission, why this project should be chosen and shows scientific, technological, cost and schedule feasibility. The contents strongly relies on the EChO mission studies, which has not passed the last selection for M3 call. ARIEL is a revision of the EChO mission within the M4 technical, cost and schedule more stringent constrains. This document is published on the Future Mission Office page at ESA website. It corresponds to the number [1] in the bibliography list.

1.2.2 CFD Internal Final Presentation

In spring 2015 the Science Programme Committee (SPC) made a first selection among all the submitted proposals which ended up with the three ultimate candidates. For each of these three missions, a dedicated engineering team at ESA's Concurrent Design Facility (CDF) continued the work on satellite development project from a system-engineering point of view. Each spacecraft subsystem was analysed and developed iteratively in teamwork. This study, carried out by the Agency engineers with the support of the mission proposers from the scientific community, finalized the Phase 0 and ended in September 2015. Results of this work have been collected and presented in the "CDF Internal Final Presentation". This document is also published on the Future Mission Office page at ESA website. It corresponds to the number [2] in the bibliography list.

Regarding the thermal subsystem, there are important updates in comparison to the proposal document. For the payload instrumentation a complete passive cooling is not any more taken into account. On the other hand, different options of active cooling are identified in order to be later examined as trade-off studies.

1.2.3 ARIEL Environment Specification

It is a document, elaborated by the ESA science team during Phase 0 study, intended to assist the developers of instruments and spacecraft equipment for the mission to assess the effects of the space environment on their systems. It corresponds to the number [3] in the bibliography list.

1.2.4 ARIEL Science Requirement Document (SciRD)

This document details the science requirements for all aspects of the mission. It provides the main reference to understand, trace and support a detailed analysis of the relationship between the science objectives of the mission and the specification of the mission and payload. SciRD was initially derived from the science objectives illustrated in the proposal document. It has been later reviewed after the CDF study, and it will be updated continuously over the course of further studies. It corresponds to the number [4] in the bibliography list.

1.2.5 ARIEL Mission Requirements Document (MRD)

This document specifies the Mission Requirements for ARIEL. It contains a comprehensive list of all high level mission requirements (for the spacecraft including its payload, the launcher, the ground segment and operations) necessary to achieve the science goals detailed in the SciRD. The MRD will be further reviewed and updated with the results of the future studies. After the phase 0 study, ESA released the first issue of the MRD. Later issues are expected after the next study phases. It corresponds to the number [5] in the bibliography list.

1.2.6 ARIEL Payload definition document (PDD)

This document provides the description of the ARIEL baseline payload complement. The PDD was created as an output of the CDF study (Phase 0) and it will be continuously reviewed and updated during as the study goes on. First issue of the PDD contains manly the same information included in the proposal and the CDF internal presentation. It corresponds to the number [6] in the bibliography list.

Chapter 2

The ARIEL mission

2.1 Mission overview

ARIEL is one of the three candidates for the fourth medium-class mission for the Cosmic Vision 2015-2025 programme of ESA. The main objective of the mission is to observe several hundred exoplanets in order to determine chemical composition and physical conditions of their atmosphere. Europe has invested remarkable resources on exoplanets science so far, both for instruments from ground (e.g. ESO E-ELT/METIS and HIRES) and space (COROT, CHEOPS, PLATO). These missions aim to find new planets measuring mass and orbital distance from their parent star. The next scientific step is to make IR spectroscopy of exoplanets light in order to understand what those planets are made of. This will give a decisive help to constrain theoretical models regarding planetary evolution, since it will be possible to observe a lot of planets with characteristics which are not present in our Solar System. For instance, giant planets (from 1 to 10 Jupiter masses) have been discovered orbiting at distances from 0.01 AU to 0.1 AU, very close to the parent star, thus their predicted average temperature can reach in some cases values around 1500 K. Such planetary systems are expected to be still in their formation era, not in a long equilibrium configuration. This is just one example of countless planetary systems that could exist, which will enlarge scientist vision in planetary evolution theories. Here comes ARIEL: a dedicated spectroscopy survey mission for characterization of at least 500 exoplanets.

Figure 2.1 shows the concept design of the ARIEL spacecraft (S/C). It is conceptually divided into two parts: Payload Module (PLM) and Service Module (SVM). The first one will be studied and provided by the scientific consortium, the second by ESA's industrial contractors. The light coming from the exoplanet-star system is captured by the telescope and sent through a series of mirrors to the two scientific instruments on board: a spectrometer (AIRS - ARIEL IR Spectrometer) and a Fine Guidance Sensor (FGS), coupled to a NIR Photometer, located on the Optical Bench (OB) rear. They aim to detect both planet and star light simultaneously at different wavelengths. The observation of uninterrupted spectra during transit and eclipse makes possible to deconvolve

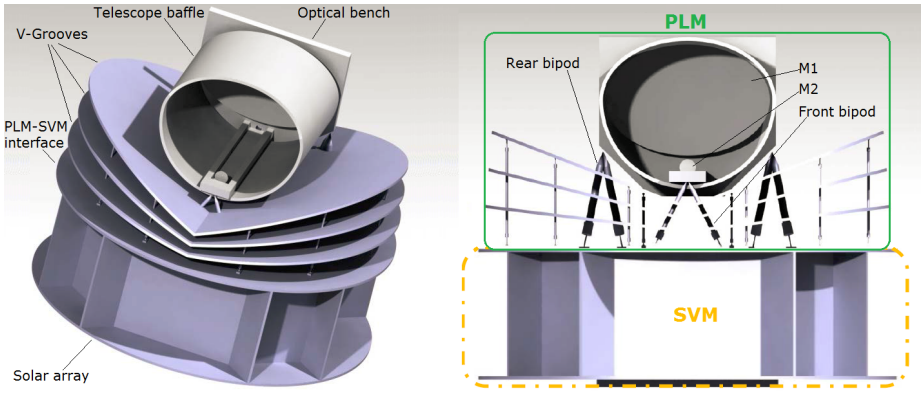

Figure 2.1: *Spacecraft design concept*

the signal in order to separate the planet contribution from the star one. AIRS and FGS/NIRP shall operate at a temperature equal or lower than 40 K and 55 K respectively to meet their scientific requirements during observations.

During the mission nominal duration of 3.5 years, the ARIEL satellite will follow a Halo orbit around the L2 point of the Sun-Earth system. The orbit has been chosen to maximize spacecraft thermal stability and sky coverage. In fact, during flight operations the satellite will have its solar array always facing the Sun while the PLM will be in shadow. At present, launch is planned from Kourou with the Ariane 6.2. A summary of the ARIEL mission main characteristics are reported in Table 2.1.

Primary mirror	Afocal elliptical 1.1 m x 0.7 m
Scientific instruments	AIRS and FGS/NIRP
Observation strategy	Transit and eclipse spectroscopy
Sky coverage	100%
Operational orbit	Halo orbit at L2 (Earth-Sun system)
Launch date	2026
Launcher	Ariane 6-2 from Kourou
Nominal duration	3.5 years
Estimated dry mass	854.8 kg (with 20% margin)
Estimated wet mass	997.7 kg
Estimated launch mass	1112.7 kg
General dimension	2.7 m x 2.7 m x 2.2 m
Expected total cost	<450 M€

Table 2.1: *Mission short summary*

2.1.1 ARIEL programmatic

In October 2015 the ARIEL project is entered in the A Phase study together with the other two candidate missions. Main scopes of Phase A are:

- review and refinement of top-level requirements
- investigation of trade-offs, alternative architectures
- identification of the design drivers and critical elements
- definition of a baseline with a feasible mission design
- risk assessment and definition of a master schedule

In March 2016, the Phase A kick-off extends the study collaboration also to industrial contractors, which work together with the scientific consortium. The information provided by each candidate studies should allow to understand whether each mission can be implemented within cost and schedule margins. Phase A is completed by the release of the Mission Selection Review (MSR), expected in April 2017. This document shall demonstrate the existence of a baseline mission which fulfils the scientific and programmatic requirements. In June 2017, thanks to the information contained in the MSR, the Science Programme Committee (SPC) selects one of the three candidates to proceed towards the B1 Phase study.

Mid-term in Phase A, the Mission Consolidation Review (MCR) is released. The MCR is similar to the scope of the MSR, it serves to identity and focus the area with critical aspects which need to be prioritized. Parallel to the MCR, the first issue of the Experiment Interface Documents part A (EID-A) is released. The EID-A contains the interface specifications applicable to the design of each payload instruments. The instrument Principal Investigator (PI) have to comply with the technical and programmatic requirements contained into the EID-A. It describe the characteristics that the spacecraft provides to the scientific instruments. Few months later, the Experiment Interface Documents part B (EID-B) is also released. It consists in the PI response to the requirements in part A, describing in detail the interface specification as inputs delivered by the scientific to the spacecraft. The EIDs documents are a formal agreement between the industrial Prime Contractor, involved in the spacecraft development, and the PIs, responsible for the scientific instrumentation. In this way, the PIs develop the instruments within the constrains imposed by the spacecraft design, and on the other side, the industrial Prime Contract can build up a spacecraft which allows successful integration of the scientific instruments. The EID-B is actually an update of the PDD. The two EIDs documents are iteratively updated and applicable to the whole duration of the mission development.

2.2 Scientific background

2.2.1 ARIEL and other planetary missions

Exoplanets are planets beyond our solar system, orbiting around other stars than our Sun. The first definitive detection took place in 1995, thanks to two astronomers of the University of Geneva. This discovery started the modern era of exoplanetary observations. Almost 2000 exoplanets have been found and confirmed so far, more than 4000 are still candidates waiting for confirmation. The first dedicated satellite mission to exoplanet search was COROT, led by

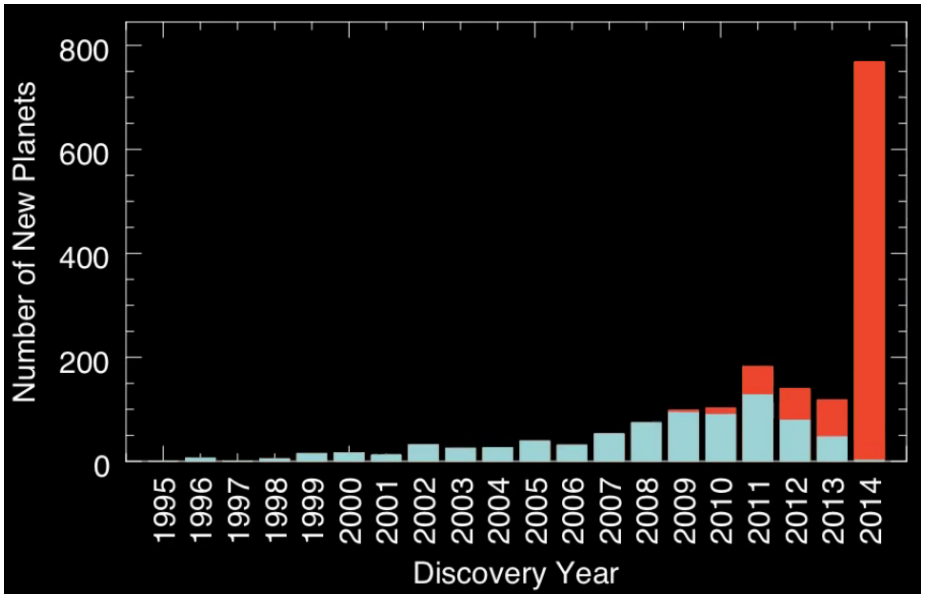

Figure 2.2: *Number of exoplanets discoveries by year for the last two decades. The red bar shows Kepler discoveries, the blue bar displays non-Kepler discoveries [7, nasa.gov].*

CNES in conjunction with ESA. During its 6 years of operation COROT discovered 32 exoplanets. The quite moderate number of revealed planets was due to the need of confirmation to be provided by ground-based telescope. Indeed in the vast majority of cases, candidate exoplanets are instead binary star systems or a combination of false positive signals. New impulse in the discovery was given by the Kepler Space Telescope of NASA. Here planets were checked using a statistical technique called "verification by multiplicity", where there is no further need to wait for additional observations. Before that mission, almost all the exoplanets confirmed were gas giant with mass comparable to Jupiter or larger, as they are easier to detect. Kepler instead is capable to find also smaller ones, from Earth to Neptune sized. In Figure 2.2 the number of exoplanets discovered through the years are displayed. The great contribution of the Kepler space telescope is clearly distinguishable in the last bar. Figure 2.3 shows the currently confirmed exoplanets, Kepler candidates are not plotted.

Next upcoming missions related to the study of exoplanets are CHEOPS and PLATO by ESA and TESS by NASA. CHEOPS, planned to be launched in 2017, will measure the bulk density of exoplanets with sizes/masses in the super-Earth – Neptune range orbiting bright stars, and to select the optimal targets for future in-depth characterisation studies of exoplanets in these mass and size ranges. PLATO, with a launch in 2024, is focused to detect terrestrial exoplanets in the habitable zone of solar-type stars. It will provide as well key informations, like planet radii, mean densities, stellar irradiation. TESS will be a more powerful survey mission than Kepler as it will be able to observe a 400x larger sky area. TESS will also look at stars nearer and brighter than Kepler, to allow the observation and study of the discovered exoplanets also from ground-based telescope. Many Kepler planets cannot be followed up by

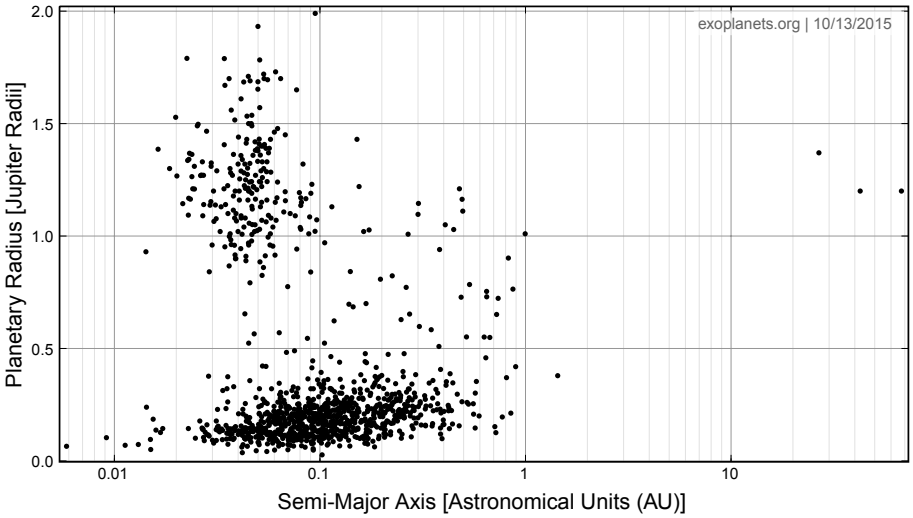

Figure 2.3: *The 1642 confirmed exoplanets up to October 13th 2015 plotted as a function of the star distance and the planetary radius. [10, Created from the "Exoplanet Data Explorer" at exoplanets.org]*

telescope on ground because their are too faint. Also the GAIA mission of ESA will improve exoplanets studies measuring masses and orbital parameters of Jupiter-size around Sun-like stars down to 14th magnitude. For known planets, GAIA may yield significant additional information. In addition to space missions, there are ground-based telescope dedicating part of their operative time to exoplanets studies. Anyway their precision is lower than a dedicated space survey due to contamination by the terrestrial environment. Moreover full-sky observations are not accessible from ground.

In spite of these discoveries, the nature of exoplanets remains largely mysterious. Planet evolution theories are based only on our solar system which is a single case. Planetary scientists have still doubts on links between planets formation, evolution and its parent star. Up to now there are no certainties on patterns linking the size, orbital parameters or the chemistry of planets to the nature of their parent star. Analysing a vast number of star systems, evidences in contrast to the actual planetary theories could arise.

2.2.2 ARIEL's scientific targets and objectives

The ARIEL mission comes as a further step in exoplanets studies, as it will investigate the atmospheric composition and physical characteristics thoroughly. It will help to answer to science questions like *what are exoplanets made of? How do planets and planetary system form and evolve?* ARIEL will be the first mission providing a large survey of spectroscopic characterization of at least 500 exoplanets. This will make possible to fully extend planetary science beyond our Solar System as none of the above mentioned missions have a spectroscopy instrument on board to study chemical composition. In summary, ARIEL main objective is not the detection of new planets but the study and characterization

of the atmosphere of the already discovered ones.

As previous said, ARIEL observation results will put the basis on formation and evolutionary theories of planetary systems. Through the survey of a large number of samples, it will be possible to find empirical correlations, elaborate classification schemes and create a taxonomy of planets, as it was done for stars in the early 20^{th} century. As a matter of fact, one could say that one of ARIEL objectives is to fill the "H-R diagram" for planets.

In order to increase the robustness of theories it is essential to know not only the atmospheric but also the bulk composition. Obviously it is impossible to have direct access to the internal layers but in some cases atmospheric composition can be directly correlated to the bulk one. This is the case of very hot planets, with temperature greater than 600 K.

> "Hot exoplanets represent a natural laboratory for chemistry and formation studies. This is because their higher atmosphere temperatures limit the effects of condensation and sinking of the volatile species, thus making the atmospheric composition more representative of the bulk one" [1].

Our Solar System is relatively cold, thus condensate clouds and sinking of volatiles of different species make impossible to observe the bulk and even the lower atmospheric layers composition. Hot planets instead should have a well-mixed atmosphere with most of their species at gas or vapour state.

In addition, hot planets represent the early stages of planetary formation from the residual nebula of the parent star. Studies of hot planets will provide scientists a key knowledge to understand mechanisms of planetary formation. For instance, the origin of water and other elements necessary for the appearance of life on Earth is linked with a primordial migration of giant gas planets. Understanding the dynamical evolution of giant planets could lead to a better comprehension of what conditions and processes have made life possible on Earth. In order to elaborate robust theories a large number of sampled objects is needed, not achievable with general purpose facilities like JWST or ground telescopes. A dedicated mission like ARIEL is thus needed.

Another reason to target to hot planets is that they orbit very close to their star. Period is thus very short so a lot of eclipses and transits happen. This makes them the best targets for spectroscopy measurements.

For all these reasons, ARIEL will target a wide number of planets ($\sim$500 are expected) hotter than 600 K. Nowadays most of these target planets have not been discovered yet but it is statistically expected that the upcoming missions (TESS, CHEOPS, PLATO) will significantly enlarge the exoplanets confirmed list in the next years.

It is important to stress that with the data collected by the instruments not only chemistry considerations can be made. Planetary energy budgets and temperaure distribution can be deduced too. Finally, the scientific tasks that the ARIEL mission will achieve can be summarized as follows:

- Detection of planetary atmospheres, their composition and structure.
- Identify chemical processes at work.

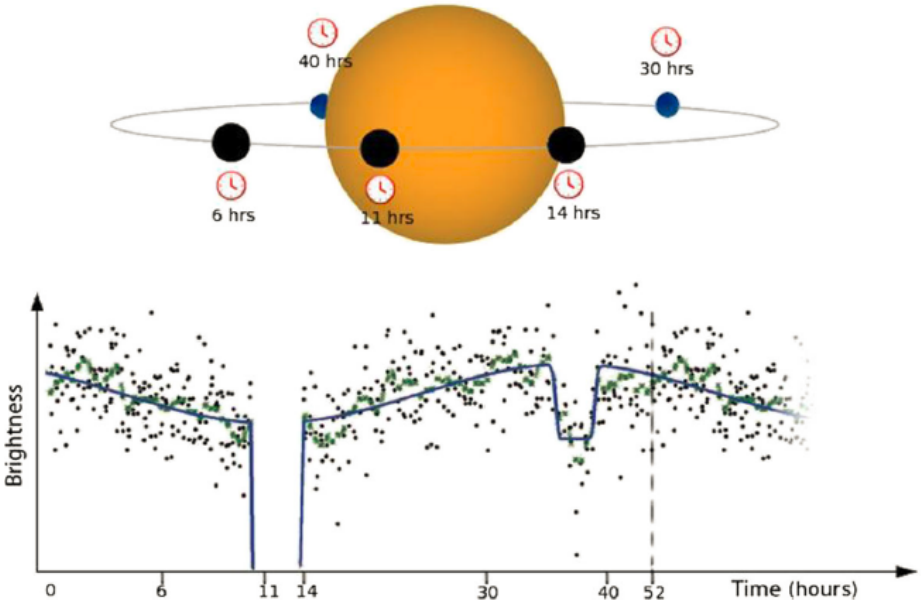

Figure 2.4: *Orbital lightcurve of the transiting exoplanet HAT-P-7b as observed by Kepler. Transit, eclipse and variations in brightness of the system due to the varying contribution from the planet's day and night-side are visible [14].*

- Determine vertical and horizontal temperature layout, their diurnal and seasonal variation.
- Quantify energy budget (albedo, temperature).
- Investigate formation and evolution models.
- Investigate the role of stellar and planetary environment on exoplanets properties.

2.2.3 Observation technique

ARIEL will investigate exoplanet atmospheres using temporal variations to separate out light from the star to analyse planet spectrum. Transiting exoplanets are required, which means planets passing in front of their parent star. Light coming from the star-planet system is observed continuously and instantaneously. Planet signal is then differentiated from the star one thanks to the knowledge of planetary ephemerides. The technique makes use of (a) planet transits, (b) secondary eclipse and (c) planet phase variations [14], same as for the EChO mission (see Figure 2.4).

(a) *Transit spectroscopy.* When the planet transits in front of its star, starlight filters through the planet's atmosphere. Comparing the in-transit with the non-in-transit spectra, it is possible to differentiate the atmospheric spectral component from the host start spectrum. The analysed atmosphere is at day/night terminator region of the planet.

(b) *Eclipse spectroscopy.* Secondary eclipse occurs when the planet is occulted by its star. In this time period only starlight is observed. Calculating the difference of flux before and after the eclipse, the planet contribution can be isolated, providing the day-side planet spectrum.

(c) *Planet phase variations.* During the transit and just before and after the eclipse, planet night-side and day-side are seen respectively. Therefore it is possible to measure the brightness time change as a function of the orbital position. From the variations, planet seasonal meteorological changes and atmospheric dynamics can be recovered [14].

Eclipsing systems allow planet characterisation without the need of spatially resolve the planet's light separate from star one. This is the great advantage of the transit and eclipse spectroscopy since there is no need to have high angular resolution telescope. The opposed method is the direct imaging, meaning a direct observation of the planets and not the star-planet system. This would extend observation to also exoplanets which do not transit in front of their star but it would require a much larger telescope in order to have a sufficient angular resolution to resolve the planet from its star.

The abundance of molecular species present in the atmosphere can be derived through spectral retrieval models applied to signals observed by ARIEL. This is possible only when both star and planet light spectra are measured together instantaneously. The AIRS and FGS instruments detect light from 1.95 µm to 7.8 µm and from 0.55 µm to 1.0 µm respectively, with the first one related to planet Infrared emission and the second to starlight. The AIRS wavelength range is optimized for warm-hot planets observation, ensuring the detection of all key chemical species (H_2O, CH_4, CO, CO_2, N_2, NH_3) and many other ones (VO, TiO, H_2S, SiO, H_3^+, C_2H_2, C_2H_4, C_2H_6, PH_3, HCN, TiH, CrH, etc.) [1].

2.3 Spacecraft general architecture

2.3.1 S/C reference frame

Figure 2.1 shows the satellite configuration resulting from the CDF study, which is very similar to the EChO phase A design. The definition of the coordinate axes used for this work is given in [5]: X is the telescope pointing axis, Z is the vertical launch vehicle symmetry axis and Y complete the right-handed triad. The origin of the reference frame is at the geometrical centre of the separation plane between the launch vehicle and the adapter of the spacecraft. Figure 2.5 shows the ARIEL spacecraft reference frame in black arrows and it is later named as Model Coordinate System (MCS). The other reference in red arrows is the telescope pointing reference frame. This is not used in this work.

2.3.2 ARIEL S/C design

The whole spacecraft configuration has been designed to reach and maintain the cryogenic temperature range required by the scientific instruments with

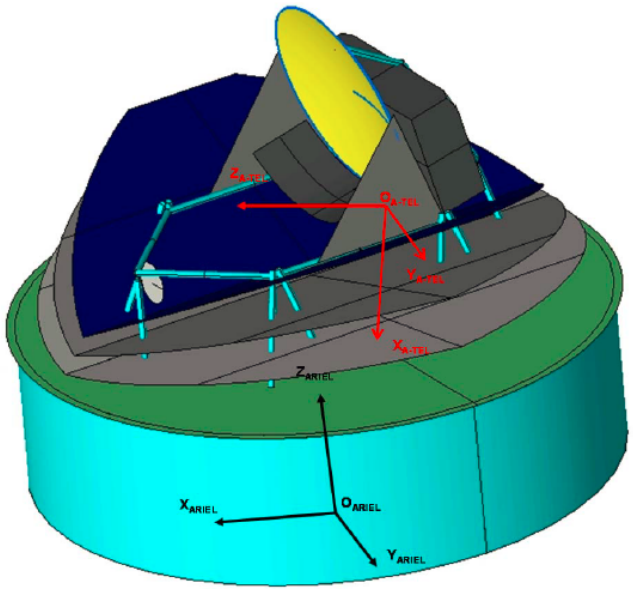

Figure 2.5: *Definition of the ARIEL S/C reference frame [5]*

low satellite efforts. The orbit around the Earth-Sun system L2 point has the unique advantage to leave the satellite in the same attitude relative to the Sun and Earth while allowing full sky coverage over the whole duration of the mission, thus offering a very stable thermal environment. This is exploited in the satellite and mission design: the spacecraft side always facing the Sun is equipped with the solar array, while on the opposite side, always in shade, the scientific payload (instruments and telescope) is located. The solar array has the double functionality of producing electric power and acting as a first shield from the solar heat flux.

The standard equipment needed to support the mission are located in the SVM, the warm section of the spacecraft, typically around room temperature. The main thermal gradient across the spacecraft follows the direction of the Z axis, from the hot solar array to the coldest part of the PLM, the telescope assembly (mirrors and baffle) and the instrument box on the optical bench at their cryogenic temperatures. It is then necessary to thermally isolate as much as possible the telescope and the instrument box from the warm units. This task is achieved by proper design of the S/C passive cooling system. This is based on a three V-Grooves (VGs) configuration. Their function is to efficiently shield the coldest part of the PLM intercepting the conductive and radiative heat leaks and rejecting them to the deep space after multiple reflection on their mirrored surfaces.

Thanks to this configuration a large thermal gradient along the Z axis can be achieved passively, with the further benefit of an overall compact design without deployable parts. A block scheme of the spacecraft architecture is shown in Figure 2.6. This architecture is mainly based on the successful Planck ESA mission, already adopted during the Phase A studies of the EChO mission. Similar concept of heat rejection after multiple reflections through consecutive

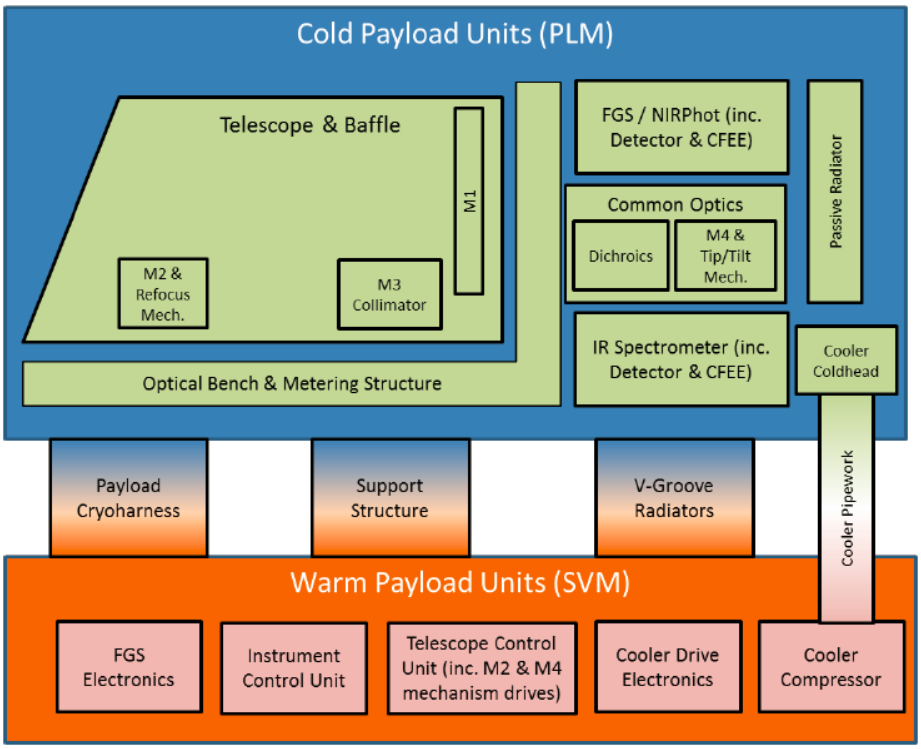

Figure 2.6: *Spacecraft architecture scheme [6]*

layers has been proven also in other previous missions (Spitzer Space Telescope) and designed for future projects like the James Webb Telescope sunshield.

2.3.3 Service module

The Service Module (SVM) accommodates the standard equipment needed to support the mission: power conditioning and distribution unit (PCDU) and batteries, on board data handling (OBDH), reaction wheels and sensor of the attitude and orbital control system (AOCS), propellant tank, thrusters and pipe lines, antenna and telecommunication units, etc. In addition, it accommodates the warm electronic units of the scientific instruments, the cooler compressor and its drive electronics.

Structural layout of the SVM is shown in Figure 2.7. Most of the equipments are inside the octagonal structure. The lower side is close by a bottom plate that supports the solar array. In the centre of the SVM the propellant tanks their supports are located. The central cone serves both as structural part as a support for units. The top plate is the SVM/PLM interface, where payloads bipods are supported and that works as the sunshield.

Structural parts of the SVM are made of sandwich panels with Aluminium honeycomb core and CFRP faceskins. This solution helps saving weight maintaining a good structural stiffness. The assumed type of honeycomb cell configuration

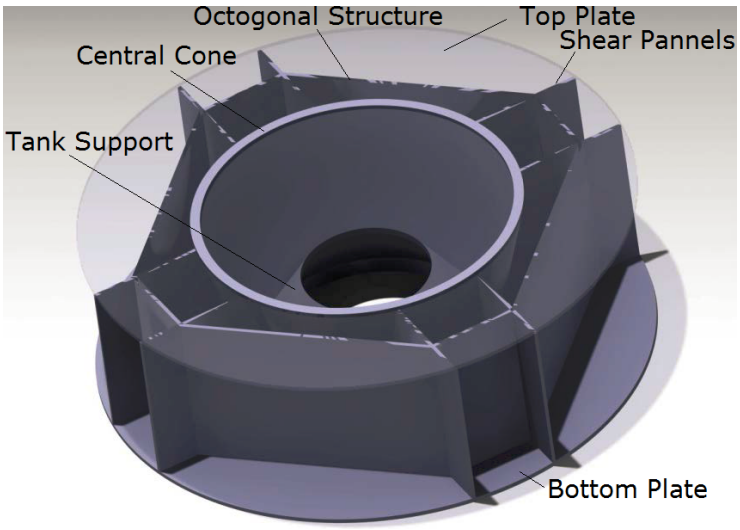

Figure 2.7: *Service module structural layout [2]*

Parameter	Value
Face-skin material	CFRP
Face-skin thickness	1.2 mm
Honeycomb material	5056 Al alloy
Honeycomb thickness, T	20 mm
Cell size, S	4.76 mm
Nominal foil thickness, δ	0.0178 mm
Honeycomb density	32 kg/m^3
Total area density of sandwich	4.93 kg/m^2

Table 2.2: *SVM structural honeycomb panels parameters*

is identified by the string "3/16 - 5056 - .0007" which corresponds to the characteristics written in Table 2.2 expressed in SI units. The three quantities T, S and δ are highlighted because they will be used later for modelling sandwich panels in the ESATAN-TMS environment (see section 4.2).

2.3.4 Payload module

The payload module (PLM) consists of all scientific equipments (telescope assembly and instruments), the VGs and the cryocooler with all the necessary supporting hardware and harness.

V-Grooves

The V-Grooves (VGs) are high efficiency, passive radiant coolers, representing the first stage of the PLM cooling system. In the ARIEL configuration, they consist in a set of three specular shields, inclined along the X axis in their halfway,

Parameter	Value
Face-skin material	Aluminium
Face-skin thickness	0.3 mm
Honeycomb material	5056 Al alloy
Honeycomb thickness, T	20 mm
Cell size, S	4.76 mm
Nominal foil thickness, δ	0.0178 mm
Honeycomb density	32 kg/m^3

Table 2.3: *VGs sandwich panels parameters*

maintaining a certain opening angle between adjacent shields (see Figure 2.1). Parasitic heat from the SVM is intercepted by the VGs and radiated to space after multiple reflections between the adjacent shields. To achieve this, VGs surfaces must have a very low emittance coating, a high reflection/mirroring material needed to reflect heat radiation. Only the upper surface of the last (upper) VG, exposed to the sky, is black coated with a high emissivity material to maximize the radiative coupling, and so heat rejection to deep space.

V-Groove design concept has been originally studied at the California Institute of Technology's Jet Propulsion Laboratory in the 80's. The Planck mission has definitely demonstrated the high efficiency of VGs passive cooling. The main advantages of this technology are:

- achieve great thermal gradient in a relatively compact volume and reduced mass with respect to a standard insulator;
- simple construction, totally passive, high reliability;
- there are no moving parts, they do not need to be deployed, vibration free.

In general, a VG configuration is able to reduce heat transfer significantly more than what is typically achieved by conventional Multi-Layer Insulation (MLI) between two parallel plates.

As reported in the CDF presentation, the ARIEL VGs are sandwich panels with both skin and honeycomb made of Aluminium. The assumed type of honeycomb cell configuration is the same as for the SVM. VGs sandwich panels characteristics are reported in Table 2.3 as done for the SVM.

Bipods and supporting struts

The PLM is supported by three bipods mounted onto the PLM/SVM interface plate. One bipod is at the front centre, connected to the telescope baffle. The other two are on the rear side of the spacecraft, attached to the OB. Bipods have hollow cylindrical shape and are made of fibreglass reinforced plastic (GFRP), a low conductive material with good structural properties.

Eight supporting struts are positioned transversally to the VGs in order to support the VGs edges. They are hollow cylinders extending from the SVM/PLM interface, where their feet are attached to, to the lower surface of the last VG.

	Quantity	Material	Diameter	Thickness
Front bipod (M2 side)	1	GFRP	30 mm	3 mm
Rear bipods (M1 side)	2	GFRP	50 mm	4 mm
Supporting struts	8	GFRP	15 mm	1.5 mm

Table 2.4: *Bipods and supporting struts characteristics*

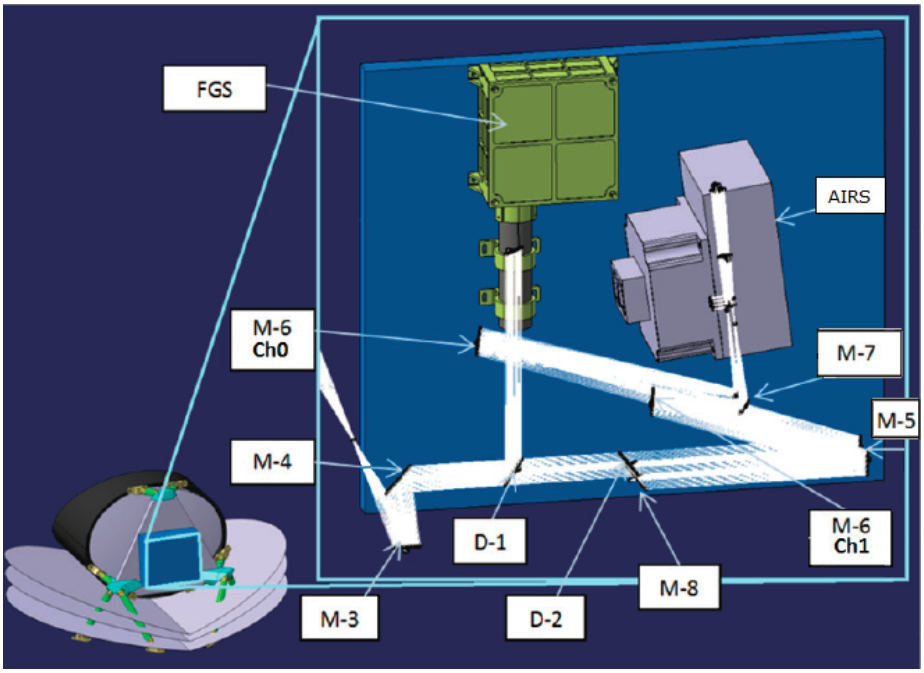

Figure 2.8: *Rear view of payload cold units [1]*

Characteristics of bipods and supporting struts taken from the CDF presentation are reported in Table 2.4.

Telescope, baffle and common optics

The ARIEL telescope is Cassegrain off-axis configuration enclosed in a baffle. The observed light first enters the baffle hitting the primary mirror (M1) and then is reflected to the secondary (M2) equipped by a re-focusing mechanisms. A third mirror (M3), located outside the baffle on the opposite side of the bench, collimates the beam before it enters the instrument box. Once in the box, the light follows a series of mirrors and dichroics referred as "common optics" (CO), which splits light to the different instruments channels. A simplified configuration of it can be seen in Figure 2.8.

The telescope is accommodated horizontally with the optical axis parallel to the spacecraft X axis. The primary mirror is supported by the OB. A baffle surrounds the telescope M1 and M2 in order to prevent unwanted stray-light from entering in the CO. A beam holds the secondary mirror with its re-focusing

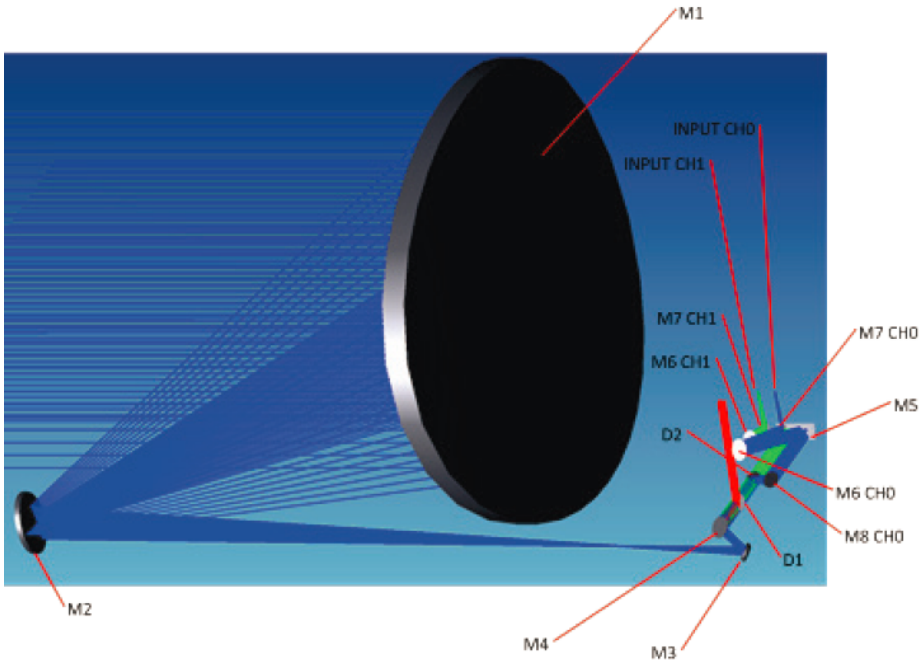

Figure 2.9: *ARIEL telescope isometric view [1]*

mechanism. An isometric view of the ARIEL telescope is shown in Figure 2.9.

Scientific instruments

The two scientific instrument modules, FGS/NIRP and AIRS, are located inside a big instrument box (IB) that shields from stray-light entering the detectors and operates as a passive radiator to provide the FGS/NIRP detectors operating temperature reference. This box is attached on the rear supporting bench. Part of the CO are also inside the IB. Detectors and relative units of each instrument are then contained in module boxes inside to the IB above the CO (see Figure 2.8).

AIRS is the prime scientific instrument of ARIEL, it is a spectrometer operating in the near-Infrared (NIR). Actually it is composed by two detectors incorporated in a single module covering ranges from 1.95 µm to 3.9 µm and from 3.9 µm to 7.8 µm respectively. Wavelength split is achieved by the D2 dichroic filter.

The FGS/NIRP has two main tasks:

- operate as a sensor for fine attitude pointing of the spacecraft,
- provide high precision IR photometry of targets for exoplanets science.

FGS ensures correct centring and guiding of telescope boresight. The FGS attitude information is elaborated together with the signal detected by the on board Star Tracker. A redundant detector is accommodated next to the nominal one, inside the same module box. As explained in the PDD, to realise both

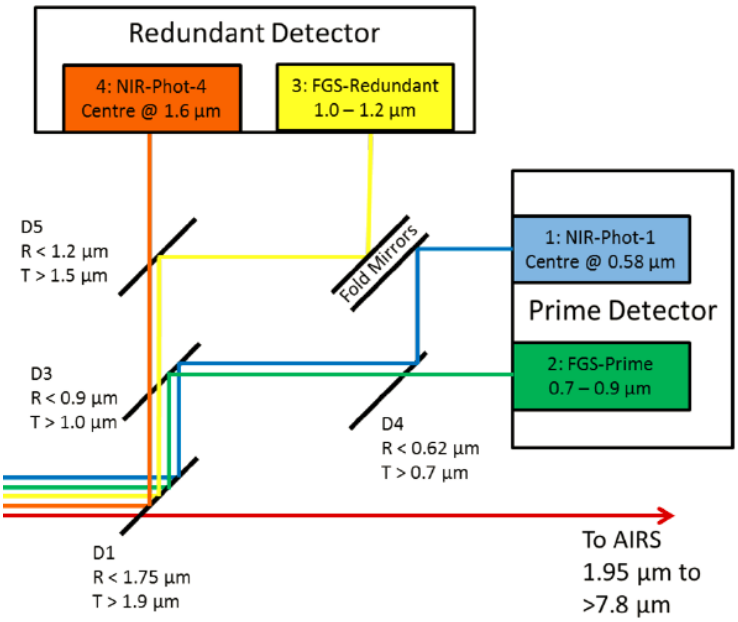

Figure 2.10: *FGS/NIRP channel splitting schematic [6]*

the guiding and the photometry targets four spectral band are defined as the baseline:

- NIR-Phot-1: Narrow-band filter centred at $\sim 0.58\,\mu m$
- FGS Prime (NIR-Phot-2): $0.7\,\mu m$–$0.9\,\mu m$
- FGS Redundant (NIR-Phot-3): $1.0\,\mu m$–$1.2\,\mu m$
- NIR-Phot-4: Narrow-band filter centred at $\sim 1.6\,\mu m$

Light is split by dichroic mirrors and sent to the relative detector channel. A schematic of the channel splitting for the AIRS and the two FGS/NIRP detectors is shown in Figure 2.10.

Next to the detectors boxes of both AIRS and FGS/NIRP there are their respective cold front-end electronics (CFEE). These electronic units provide the necessary signal and elaboration to control the detectors and should not be confused with the warm electronic units placed inside the SVM. Warm payload units have instead all level of commanding, compression, processing and I/O interface with data-handing subsystem. This splitting is needed to located away from cold payload the majority of electronics heat dissipation. Connection between cold and warm electronics is ensured by cryo-harnesses, composed by wires with optimal electrical performances and enhanced thermal insulating properties in order to minimize heat leaks from SVM to PLM.

Payload unit	T_{op} [K]	ΔT [K]	Expected load [mW]
Telescope	< 70	± 1.0	-
FGS optics	≤ 50	± 0.5	-
FGS detectors + TCS	≤ 50	± 0.05	$10 + 5$
FGS CFEE	≤ 55	± 2.0	65
AIRS optics	≤ 50	± 0.5	-
AIRS detectors + TCS	≤ 40	± 0.05	$10 + 5$
ARIS CFEE	≤ 55	± 2.0	20

Table 2.5: *Main thermal requirements of the ARIEL PLM. The heat loads include 50% margin. [1, 2]*

Joule-Thomson cooler

In order to achieve sufficient cooling of the AIRS detector a closed-cycle Joule-Thomson (JT) cooler is considered in the baseline design. The JT effect consists in the cooling of a working fluid through a constant enthalpy expansion. The fluid is firstly pumped to high pressure by a compressor and then expanded to a lower pressure through a valve. The expansion makes the fluid reduce its temperature. The cold fluid acts as an heat sink for the instrument to be cooled down. Thereafter the fluid returns to the compressor and the cycle starts again.

One of the advantages of this solution is that the compressor and its drive electronics can be accommodated at relatively large distance from the cooler cold end. In the ARIEL S/C the compressor and the electronics are located inside the SVM, where the heat dissipation and the compressor vibration are far relative to the PLM.

2.4 ARIEL thermal design

2.4.1 General thermal design

The aim of the thermal subsystem is to maintain all satellite equipments within their temperature limits in all S/C modes. The critical elements are the scientific instruments of the PLM which need to stay at cryogenic temperature range during operation. Precise temperature limits are not contained in the MRD yet, but tables with maximal temperature and electronic heat dissipation are present in both the CDF presentation and the mission proposal document. These values are estimated by the preliminary thermal analysis and downscaling of the EChO mission study results. They have been used during phase 0 studies and are also considered in this thesis work. Thermal requirements of PLM units are summarized in Table 2.5. The first column indicates the operative temperature that units must have during operation. Second column is the maximum allowed variation in temperature over a typical observation time (10 hours). Expected heat dissipations already include 50% margin.

SVM Thermal design

Since the study and realisation of the SVM and the PLM is split among different partners, thermal design of the two modules are independent. SVM internal units do not have any special thermal requirements. The SVM contains standard equipment which need to stay at room temperature. SVM thermal design is based on quite simple assumptions. The units (instrument electronics, cryocooler driving unit etc.) with the highest dissipating powers are mounted on the SVM side walls, designed as radiator to efficiently rejects the loads to deep space. Survival heaters ensures that the temperature inside the SVM is maintained above $-20\,^{\circ}\mathrm{C}$ in all S/C modes.

The SVM top plate is the SVM/PLM interface. When the two modules are assembled they must be thermo-mechanical compatible. PLM unit temperatures and their stability are influenced by the temperature variation of the SVM top plate, mechanically connected to the PLM. In order to provide the PLM the best boundary conditions, the interface should be as cold and as stable as possible. In the MRD, the thermal requirement R-THE-010 says that the SVM upper panel shall have a temperature stability of 3 K (TBC) under all possible attitudes defined in the observation requirements. The CDF study suggests as solution to consider 'oversized' radiators area on SVM panel sides and compensation heaters to stabilised the temperature of the SVM top platform at $10\,^{\circ}\mathrm{C}$ by active heating. The analysis of the influence on thermal performances of the SVM/PLM interface temperature variation is part of this thesis work.

PLM thermal design

In order to achieve scientific instrument thermal requirements it is necessary to efficiently isolate the PLM from the SVM and together to sufficiently reject heat leaks and electronic dissipations. Three main consecutive levels of cooling can be identified:

1. V-Grooves: heat leaks from SVM is intercepted by the VGs and after multiple reflections irradiated to deep space. It should achieve a cool down level around 70 K.

2. All external surface on the top of the PLM are painted with Black Paint maximizing heat rejection to space. They work as passive radiators with an expected temperature around 55 K.

3. A Joule-Thomson cryocooler with its cold plate connected to the AIRS detector, the coldest instrument on board. It provides the 40 K stage, need to meet the AIRS thermal requirement.

The first two cooling methods are passive, since they do not imply the use neither of moving parts nor power consumptions. The third instead is an active method based on the compression and expansion of fluid loop. They are analysed in the next sections. A schematic of the PLM thermal architecture is shown in Figure 2.11. The PLM passive cooling is design to achieve temperatures between 50 K and 70 K required by the instruments (telescope, FGS detector, cold FEEs).

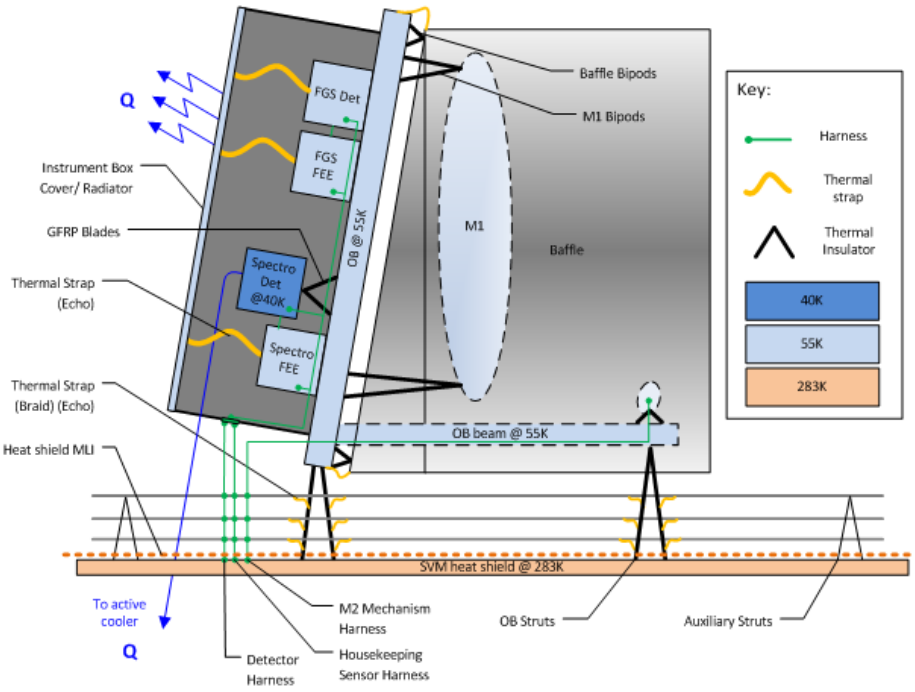

Figure 2.11: *Schematics of the PLM thermal architecture [2]*

The JT active cooling is allocated to meet the goal requirement of the AIRS detector which need to be run at 40 K, and ideally at around 35 K.

2.4.2 PLM passive cooling

The VGs represent the first cooling stage of the PLM. VGs are mechanically attached to the three bipods and also supported by eight auxiliary struts. Even if both bipods and struts are made of GFRP, which has low thermal conductivity, there will still be heat leaks going from the SVM to the PLM through solid conductivity of the bipods and struts. The task of the VGs is to intercept this heat and spread it away to deep space after multiple reflections between each VG pair. Each VG shield is tilted by a certain angle with respect to the adjacent one, creating a divergent radiative path for the reflected thermal rays. Figure 2.12 helps understand this concept.

Thermo-optical property of the VGs are of essential importance since they allow thermal isolation and heat rejection to space. The coating should have low emissivity/high reflectivity in the Infrared band. The typical solution is Vapour Deposited Aluminium (VDA) coating, used on the VGs of the Planck satellite for example, with a measured emissivity of ~ 0.045, [13]. All surfaces of the VGs are coated with VDA except for the upper surface of the topmost VG which is covered by an open aluminium honeycomb coated with black cryogenic paint. The effective emissivity of this combination is very high (> 0.9), [13].

Bipods and struts are bad thermal conductors but the thermal coupling between

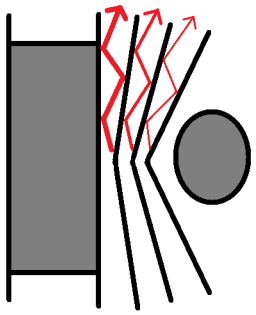

Figure 2.12: *VG heat rejection illustration*

them and the VGs should be high so that the majority of heat coming from the SVM is intercepted by the VGs and do not reach the PLM. For this reason thermal straps should connect each bipod to each VG as shown in Figure 2.11. For the same reason also the harness linking the warm electronics in the SVM to the cold ones in the SVM is thermally coupled to the VGs in order to unload their heat to the VGs. The JT cooler pipe is also thermally connected to the upper VG in order to be pre-cooled before reaching the cold end. The CDF team has considered 320 mW intercepted by the upper VG from the working fluid. All in all, the key of success of the VGs relies on their double functionality: act as thermal shield and deep space radiator at the same time.

The second cooling level is represented by the passive emitted heat by the top part of the telescope baffle and the rear side of the instrument box both facing the deep space. The emissivity of the surfaces shall be as high as possible in order to maximise heat rejection. The baseline considers the rear side of the instrument box covered with open honeycomb coated by Black paint, as for the upper surface of the topmost VG. In the A Phase it will be see if this solution is applicable also for the top side of the telescope baffle. The FGS detector and both the AIRS and FGS cold electronics are coupled with high conductive thermal straps to the radiator side of the instrument box as shown in Figure 2.11.

2.4.3 PLM active cooling

In order to run the AIRS detector at $<$40 K and ideally around 35 K, it has been decided to allocate a Joule-Thomson cooler in the baseline design. This decision was made during the phase 0 study and it is a change from the original mission proposal, in which a complete passive cooling architecture was expected. As said in the PDD document, it is not possible to achieve this low temperature and demonstrate the necessary thermal margin with a purely passive design.

A schematic illustration of the system is shown in Figure 2.13. The choice of the working fluid depends on the operating temperatures. The baseline consider Neon as the working fluid, its boiling and melting point at 1 atmosphere are respectively 27.1 K and 24.6 K. The fluid expansion generates liquid Neon in

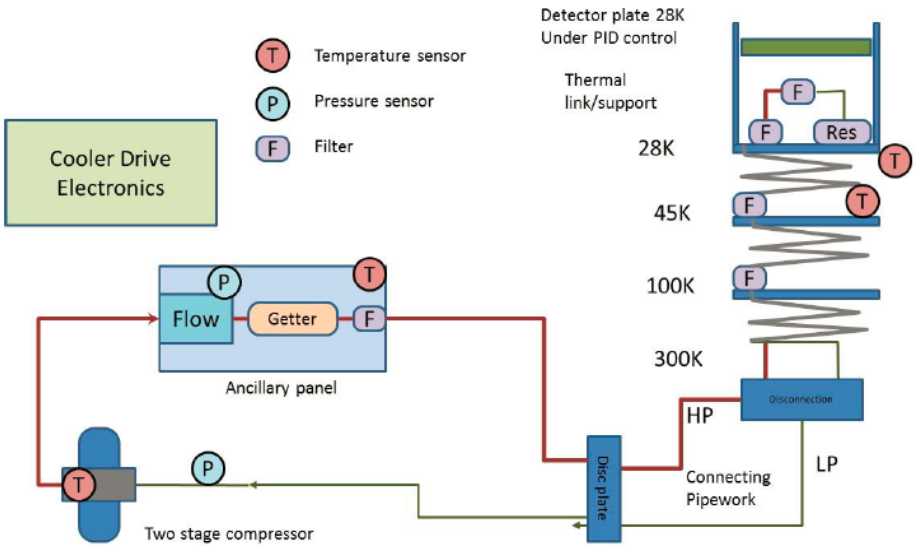

Figure 2.13: *JT cooler schematic [6]*

order to provide temperature stability of the interface of the detector. A reference temperature of 28 K is considered for the JT cold end. The spectrometer detector is the unique instrument with lowest temperature requirement (40 K). In order to avoid contamination heat from the other equipments inside the instrument box and from the OB The AIRS detector is attached to the OB with isolating supports and thermally coupled to the cold end of the JT cooler, which absorb the detector heat load. The expanded Neon passes through an heat exchanger attached to a plate where the thermal load of the AIRS is applied.

In order to maximise cooler performance, the high pressure fluid is pre-cooled during its way from the compressor towards the valve. A typical design consists in a concentric pipe heat exchanger. The tube-in-tube piping forces the warm high pressure and the cold low pressure streams to exchange heat. Before the fluid enters in the compressor and in the expansion valve the pipes are disconnected. Additional pre-cooling is achieved intercepting fluid heat by the three VGs. The pipe is thermally linked to the VG panels.

The ARIEL JT cooler is based on the heritage of the EChO mission also equipped with a similar active cooler. The EChO JT cooler has been designed by the RAL Cryogenics and Magnetics group in the UK. In the EChO mission, cooler design has been sized to provide 200 mW of cooling power at 28 K requiring approximately 35 mg/s of Neon flow [12]. ARIEL PLM requires less cooling power, so compressor and pipe lines dimension should be adapted to the new parameters. The CDF team has estimated a necessary cooling power around 50 mW including uncertainties and margins. This performance should be feasible with a small scale cooler compressor, requiring 40 W of input power. In this thesis work, different cooling power are taken into account in the ARIEL S/C thermal mathematical model (TMM) in ESATAN-TMS to investigate their influence on thermal performance.

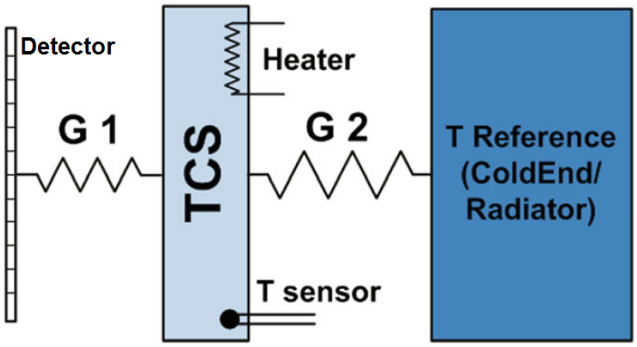

Figure 2.14: *Detector TCS scheme [12]*

2.4.4 Detectors temperature stability

Temperature stability is an additional challenging issue of the whole thermal design. Payload units have narrow allowed temperature variations (see Table 2.5). ARIEL stability intervals are base on the EChO mission requirements, therefore similar solutions are expected in the ARIEL mission as well. The most challenging stability requirement is the one on both the FGS/NIRP and AIRS detectors ($\pm 0.05\,\mathrm{K}$). In the EChO thermal architecture, detectors temperature stability is ensured by active control stages, base on a close loop circuit [12]. This solution consists in setting a Thermal Control Stage (TCS) on the detectors supporting flange. The TCS composes the active closed loop thermal control system: a heater plus thermistor couple. Each detector is thermally decoupled from the relative module box or optics to ensure optimal performance in terms of absolute temperature stability. On the other side, detectors are coupled to their last cooling stage (rear IB area as radiator for the FGS/NIRP and JT cold end for the AIRS) through high conductance links. The TCS, attached on the detector flange, operates as an intermediate stage between the detector and the cooling point, as shown in Figure 2.14.

The TCS intermediate thermal inertia represents a first level of fluctuation passive damping. Finer damping is achieved by a PID control on the TCS heater. Since the TCS mass (and therefore the thermal inertia) is very small, the thermal conductances G1 and G2 become the key parameters for oscillation damping. Their values are chosen on a trade-off between the detectors operating temperature and the minimum power needed on the TCS heater for the active control.

2.4.5 S/C attitude

The selection of an operational orbit around the Earth-Sun system L2 point offers an excellent thermal environment, as described in the previous sections. The S/C configuration has been optimized for the nominal case, when the solar array are perpendicular to the Sun rays direction keeping the PLM in shade (the S/C Z axis is aligned with the anti-Sun vector). On the other hand, the drawback of this configuration is that small variations on S/C attitude from

the nominal case could deteriorate drastically the thermal performance. In particular, S/C rotations along the X or Y axis expose the upper part of the SVM and perhaps also the PLM to direct Sun radiation.

In order to maintain PLM instruments inside their temperature limits it could be necessary to put strict requirements on the S/C attitude, with the drawback of having less versatility on the exoplanet observation strategy. In the MRD, observation constraints in the mission performance requirements say that the ARIEL S/C shall have the ability to make a rotation of:

- 360 degrees around the Z axis [R-OBS-010]
- ±25 (TBC) degrees around the Y axis [R-OBS-020]
- ±1 degrees around the X axis [R-OBS-030]

and observe the target from any of those attitudes [5]. These requirements are a direct consequence of the sky visibility requirement R-SCI-230, contained in the SciRD, which specifies the sky visibility percentage over a certain amount of time, required for scientific observations.

In the thermal section of the CDF presentation, ESA engineering team is considering rotation of ±5 degrees in along X axis and ±25 degrees along the Y axis. The analysis of the thermal performance of the ARIEL S/C at different attitudes from the nominal position at the L2 orbit are part of this thesis work.

Chapter 3

ESATAN-TMS

ESATAN-TMS is the standard European thermal analysis tool used to support the design and verification of space thermal control systems, developed by ITP Engine UK. It can predict steady-state, transient temperature and heat flows in a thermal network using the lumped parameter method. This means that the geometric model is discretized in a finite number of nodes, where the thermal properties are concentrated and considered homogeneous in the whole volume and mass assigned to each node. Nodes are then connected to each other with conductive, convective and radiative conductors, which have to be consistent with the real model. This is the thermal network. Boundary condition must be added and then the numerical calculation of the solver can be run in order to know the node temperatures.

ESATAN-TMS is optimized to solve systems in a space environment because it has embedded tools which automatically calculate radiative conductors between spacecraft nodes and the space environment (Solar, Planetary, Albedo, deep space heat fluxes) once the spacecraft orbit and attitude has been defined. The software version used in this work is the realise 7 sp2.

3.1 Overview of how ESATAN-TMS works

3.1.1 Creation of the geometrical model

It consists in the definition of all the nodes representing the satellite and the assignment to nodes of all the thermal properties needed to run the simulation. This is the first step in the creation of the thermal network. Nodes are defined by the software meshing the geometry which can be created through the ESATAN-TMS GUI (Workbench), or directly modelled with MORTRAN language (More Fortran, an extension of Fortran 77). The Workbench is an extension of ESATAN-TMS which provide facilities for automatic model generation for some geometries, automatic calculation of solid and radiative conductors and 3D visualisation. In this thesis, the geometry has been created directly through the ESATAN-TMS Workbench. The whole model geometry is

composed by primitive geometries like rectangular, disc, sphere, cylinder, etc. They represent the bricks of the whole geometrical model.

When creating a new geometry, it is necessary to assign to it bulk and thermo-optical properties; then the software will automatically elaborate these informations and assign proper values to nodes, since extensive properties like mass, area, etc, assigned to each node, depends on the chosen mesh. Next step is to connect nodes with proper conductors. Different types of conductors are available in ESATAN-TMS according to the different way that heat can be exchanged (conduction, radiation, convection). In this thesis only conductive and radiative conductors are used.

3.1.2 Linear conductors (GL)

The GL conductors are linear conductor, where the rate of heat transfer q_{ij} between nodes i and j at temperatures T_i and T_j is:

$$q_{ij} = h(T_i - T_j) \tag{3.1}$$

h, the heat transfer factor, is the value of the GL conductance. Linear conductors can be used to represent solid conductances, convection and other processes which can be treated as linear. In this thesis they are used to model solid conductance.

Four types of GL conductors can be identified in ESATAN-TMS, differentiated according to the way the software creates them:

- *GL between nodes of the same primitive geometry (intra-primitive conductors).* Since each geometry is discretized in a finite number of nodes depending on the chosen mesh, adjacent nodes need to be connect with solid conductance. They are created automatically using the information of each primitive geometry like conductivity of the assigned bulk material, area, thickness, etc.
- *Conductive Interfaces (inter-primitive conductors).* If two different primitive geometries are attached to each other, ESATAN-TMS is able to automatically detect it and calculate solid conductance between each couple of borderline nodes of the two geometries.
- *Contact zones.* This feature allows user to create a GL conductor between surfaces of two geometries which have a common contact area. A value of the thermal contact conductance [W/m^{2}K] between the two surfaces must be specified by the user. The GL is then calculated multiplying the contact conductance with the area shared by each couple of nodes.
- *User-defined conductors.* User can define a linear conductor between two nodes directly assigning the value GL. This is used where none of the previous method works because it requires manually inserting GL for each couple of node.

The first two types of GL conductors can be automatically calculated by ESATAN-TMS when the model has been created through the Workbench. The last two shall be manually defined by the user.

For lumped parameters primitives ESATAN-TMS uses an approach called the Far-Field method to calculate intra and inter-primitive GL conductors. The advantage of this method relies on the fact that it is applicable to arbitrary geometries, so also when analytical expressions for the conductance between two nodes are not available.

3.1.3 Radiative case

Once geometry and material property have been defined the next step is the radiative analysis. The ESATAN-TMS radiative module provides the facilities for the calculation of the radiative couplings between the faces of the model and, for space analysis, external heat fluxes onto the faces of the model and radiative coupling with the environment. A single radiative analysis is defined in ESATAN-TMS as a radiative case which gives the possibility to specify all the conditions which a radiative analysis depend on. A radiative case includes the definition of:

- S/C orbit and position
- S/C attitude
- Sink temperature of the environment enclosure
- The outputs to be calculated: view factors or radiative exchange factors (REFs), direct and absorbed heat fluxes from environment

In a single ESATAN-TMS model it is possible to defined multiple radiative cases to perform different radiative analyses varying the S/C orbit or attitude. Usually a radiative case consists in a set of successive S/C positions (discrete values of the true anomaly) along its orbit. For each position heat fluxes from environment are calculated. In a radiative case is possible to assign also a movements to some parts of the S/C, for example a earth-pointing satellite with its solar array always pointed towards the Sun. In this case also the REFs are calculated for each orbit position since there is a change in the satellite geometry.

The outputs of the each defined radiative case are performed in ESATAN-TMS Workbench by the Monte Carlo ray tracing method (MCRT). Conceptually it consists in firing a finite random sample of rays from the i node and trace them to see where they go to end. The ratio between the total number of rays which hit the node j and the total number of rays fired from node i gives the estimated value of the view factor F_{ij}. Taking into account the thermo-optical properties assigned to nodes i and j, it is then possible to calculate the REF.

3.1.4 Radiative conductors (GRs)

The GR conductors represent radiative conductors, where the rate of heat transfer q_{ij} between node i and node j at temperatures T_i and T_j is:

$$q_{ij} = \sigma \, \mathrm{GR}_{ij}(T_i^4 - T_j^4) \tag{3.2}$$

Calculation of GRs is not easy in a complex model since it depends on the node emissivities, area, view factors, and energy reflections which occur between node faces. The view factor, F_{ij}, between a face i and a face j is defined as the fraction of the energy emitted by the face i that is directly incident on the face j. View factors are completely determined by the model geometry, independent of the thermo-optical properties of the model's surfaces. The REF is defined as the faction of the energy emitted by the face i that is eventually absorbed by face j either directly or via multi-reflections (be these diffuse or specular) or via transmission [15]. The calculation of REFs therefore takes into account not only the geometry but also the thermo-optical properties. Moreover, REFs account also for node multi-reflections, so it is possible to have radiative coupling between nodes which are not directly in view but able to exchange heat radiatively after multiple reflection. This feature acquires importance where surfaces which high reflectivity are present, like the V-Grooves. The workbench calculates REFs for both infrared and solar bands. Computation of GRs is performed in ESATAN-TMS elaborating the REFs outputted from the considered radiative case. In particular, the VFAC function uses the values of view factors, calculated through the MCRT method, to compute the corresponding REFs taking into account multiple reflections using the method of Hottle [16].

3.1.5 Heat fluxes from environment

Monte Carlo ray tracing method is also used to calculate Solar, Planetary and Albedo heat fluxed. When the creation of the geometry of the model has been completed, the orbit and the attitude of the satellite must be defined. This information is used by ESATAN-TMS to determine the fluxes at different orbit locations and attitudes. Absorbed fluxes are added as time-dependent boundary conditions to the concerned nodes. Coupling between satellite and deep space is achieved with GR conductors between exposed nodes and a boundary node with constant temperature definable by the user (it has been considered a deep space temperature of 3 K). This node acts as an infinite thermal sink.

3.1.6 Analysis case

Before the generation of the thermal network is necessary to assign boundary conditions to concerned geometry nodes. Typical example are the definition of internal heat dissipation of electronic units or boundary temperatures of particular interfaces. The final stage in ESATAN-TMS Workbench is the generation of the thermal analysis file which is used by the thermal analyser to solve the thermal model. The definition of the analysis file is specified within an analysis case. Each analysis case include the assignment of

- one or multiple radiative cases,
- boundary conditions,
- parameters of the solution routine
- output calls

The analysis file contains all the information necessary to the solver to perform the analysis and output the requested results. Node data and GL conductors are elaborated from the whole model development through the geometry module. GRs between nodes and environment and external heat fluxes are recovered from the assigned radiative case. Boundary condition are assigned changing the initial node data of the concerned nodes. Parameter of the execution block, for instance the type of solver, time step, tolerance, etc. can be specified or default values are considered.

The analysis file is written in MORTRAN language and it accessible and editable by the user. This allows manual customisation at later time. The file could be written directly by the user with MORTRAN code without using the Workbench, but this has the disadvantages of not exploiting the automatic node meshing, calculation GL and GR conductors and heat fluxes from environment.

The thermal mathematical model is now ready to be processed and solved. For the lumped parameter approach, conservation of energy for each node can be written as:

$$Q_i + \sum_{j \neq i}^{n} GL_{ij}(T_j - T_i) + \sum_{j \neq i}^{n} GR_{ij}(T_j^4 - T_i^4) = C_i \frac{dT_i}{dt} \tag{3.3}$$

where C_i is the node heat capacity and Q_i the node heat dissipation. In steady-state case the right-hand term is zero, resulting in a set of algebraic equations. In transient case, first order differential equations result which can integrated by standard numerical methods.

3.1.7 Post-process the results

Thermal results can be loaded in the ESATAN-TMS Workbench model giving the possibility to visualise temperature node distribution, heat fluxes, etc. directly on the 3D geometry in rainbow colour scale. Anyway it is always possible to recover the vector of temperature values for all nodes and then elaborate and plot them with other software.

3.2 Time and temperature dependent variables

ESATAN-TMS allows defining quantities with a dependency on either time or temperature. This feature is particularly important since at cryogenic temperature conductivity and specific heat capacity have a strong dependency on temperature itself. Also other quantities can be dependent-defined as boundary condition, user defined conductors, spacecraft movement angles, etc. A dependent variable, called “Property” in ESATAN-TMS, can be defined as a two columns matrix where time or temperature are on the first column and thier relative quantity values are on the second column. During the solution run, ESATAN-TMS interpolates the quantity values. The interpolation method can be also user-defined, otherwise the default one is used.

3.3 Material properties

3.3.1 Bulk properties

This feature allows to define the density, specific heat and conductivity of a material that will be later assign to a shell or solid geometry. These three quantities can be defined as "Property".

3.3.2 Thermo-optical properties

Thermo-optical properties consist in the definition of coefficients for emission ε, absorption α, diffuse reflection ρ^d, specular reflection ρ^s and transmission τ for a material surface or coating. Once a optical set has been created it can be assigned to a geometry surface or face, both solid or shell. This will be used to calculate absorbed heat flux from Sun, planet and albedo; heat exchange with external environment and calculation of GR conductors between surfaces during run of the radiative case. In thermal analysis regarding space environment, it is common to divide into two non-overlapping spectral bands the radiative exchange: the Infrared band, in which model surface and planetary emission take place, and solar band, for Sun emission and planetary albedo. The Kirchhoff's law is always valid for the two spectral bands, meaning that $\alpha_{\text{ir}} = \varepsilon_{\text{ir}}$ and $\alpha_{\text{vis}} = \varepsilon_{\text{vis}}$. ESATAN-TMS follows both these assumptions. In the Infrared band ε_{ir} is considered while in visible band α_{vis}. According to the energy conservation law:

$$\varepsilon_{\text{ir}} + \rho^d_{\text{ir}} + \rho^s_{\text{ir}} + \tau_{\text{ir}} = 1 \tag{3.4a}$$

$$\alpha_{\text{vis}} + \rho^d_{\text{vis}} + \rho^s_{\text{vis}} + \tau_{\text{vis}} = 1 \tag{3.4b}$$

so once three coefficient are assigned, the fourth is automatic calculated.

3.4 Shell and solid geometries

Primitive geometries can be created as shell or solid. Basically the difference stays in the way the geometry is divided in nodes when meshed. In ESATAN-TMS Workbench, shell are sketched as surface geometries with an infinitesimal thickness. Nodes are put on the two surfaces of the shell. Even if shells are sketched with an infinitesimal thickness, it is mandatory to assign them a finite thickness which is used to calculate intra-primitive GL solid conductors both between adjacent nodes on the same surface and through the shell thickness between corresponding node pairs on the two surfaces. Shell geometries offer the possibility to assign different properties to each of the two surfaces, and to assign a user-specified GL or GR conductor across thickness between couple of nodes on the two surfaces (see subsection 3.4.2).

Solid geometries differ from shells since they have an additional set of nodes in the core of their volume. So with solids it is possible to know the core temperature, not possible with shells since nodes are just on the surfaces. Anyway

solids offer lower versatility for internal conductors: GL are calculated just by the specified bulk properties and by the geometry dimension. Additional user-specified values are not possible as for shells.

In this work most of the satellite parts are modelled through shell geometries. Solids were introduced in the last versions of ESATAN-TMS and some features, available for shells (geometry cutting, conductive interfaces between primitives, etc.), are still not developed yet.

3.4.1 Surface activity

It is possible to exclude in the thermal model radiative and/or conductive calculation nodes belonging to a surface. ESATAN-TMS surface activity can be specified as:

- ACTIVE (default), face nodes are included in radiative and conductive calculations;
- RADIATIVE, face nodes are included in radiative calculations and excluded from conductive calculations;
- CONDUCTIVE, faces nodes are included in conductive calculations and excluded from radiative calculations.
- INACTIVE, face nodes are excluded from radiative and conductive calculations.

3.4.2 Through thickness conductance and emittance

In shell geometry it is possible to specify how ESATAN-TMS connects nodes on either surface through the shell thickness. There are three possibility:

- NONE, nodes on the two surfaces are not connected;
- BULK, nodes are thermally coupled with a linear conductor GL calculated from the bulk material and thickness assigned to the shell geometry (intra-primitive conductors);
- EFFECTIVE, here it possible to specify a user-defined conductance and/or emittance per unit area. The first creates a conductive link (GL), the latter a radiative link (GR). The user-specified value is multiplied by the surface area associated to the node pair.

This feature is used to model honeycomb panels and Multi-layer insulation (see section 4.2 and 6.4).

3.5 Boundary conditions

Boundary conditions represent the interfaces between the model and the surrounding environment. For space analysis, the radiative coupling between nodes and deep space and the direct solar, albedo, and planetary infrared fluxes are

Type of BC	Allocation	Units
Initial temp.	The given initial temperature is assigned to each thermal node defined by the reference.	K
Temperature	The given temperature is assigned to each thermal node defined by the reference, and the thermal node is set to be a boundary.	K
Heat load/Unit area	A heat load is assigned to each face defined by the reference as the given value multiplied by the face's area. If the reference contains a solid, then the boundary condition is applied to the external faces of the solid.	W/m^2
Heat load/Face	The given heat load is assigned to each of the faces defined by the reference. If the reference contains a solid, then the boundary condition is applied to the external faces of the solid.	W
Total area heat load	If applied to a region including more than one thermal node, the specified heat load is divided between the nodes in proportion to the area of the faces that make up each node. If the reference contains a solid, then the boundary condition is applied to the external faces of the solid.	W
Heat load/Unit volume	A heat load is assigned to each solid defined by the reference as the given value multiplied by the solid's volume.	W/m^3
Heat load/Volume	The given heat load is assigned to each of the solids defined by the reference.	W
Total Volume Heat Load	If applied to a region including more than one thermal node, the specified heat load is divided between the nodes in proportion to the volume of the solids that make up each node.	W

Table 3.1: *Boundary condition types in ESATAN-TMS Workbench [15]*

calculated in the radiative module. Anyway it would be necessary to add internal power heat, for example to simulate electronic equipments, or assigning a boundary temperature to specific nodes. This is achieved in the ESATAN-TMS Workbench through the boundary conditions feature. Each boundary condition requires to choose the geometry or a face geometry which the boundary condition is assigned to, the boundary condition type and its value. Eight types of boundary conditions are available in the Workbench, shown in Table 3.1.

Chapter 4

The ARIEL thermal model with ESATAN-TMS

This chapter describes the construction of the spacecraft model in the ESATAN-TMS software. This model has been developed on the basis of all information available in the documents released after the end of Phase 0 study. In particular the mission proposal and the CDF outcome presentation have been the main references.

4.1 Spacecraft general dimension

The first issue consisted in fixing a starting value for the spacecraft dimensions. As the CDF team have reported neither the general dimensions of the satellite nor quotes on CAD drawings used for the study, some assumptions have been made. In particular for the solar array, sun-shield and VGs radius. It is important to remark that spacecraft dimension could have a direct impact on the thermal behaviour of the PLM largely based on passive cooling. A bigger spacecraft would accommodate larger VGs with an increased surface for heat rejection, allowing a general decrease of PLM average temperature. The spacecraft general dimensions to start the thermal analysis have been deduced indirectly by comparing units of known size in the drawings. In this way it was possible to derive general dimensions of the main units, like top and bottom plate diameter, VGs radius, octagonal structure height, etc., to be used for the starting model. The main estimated dimensions are summarized in Table 4.1. These value are used for the first ESATAN-TMS version of the S/C model, then the simulated thermal performances and the sensitivity analyses to some parameters have required dimension adjustments that will be described in the following chapters.

Parameter	Value
Bottom plate radius	1.35 m
Octagonal structure height	0.78 m
VG radius	1.32 m
Telescope baffle radius	0.56 m
S/C total height	2.24 m

Table 4.1: *Spacecraft general dimensions deduced from drawings*

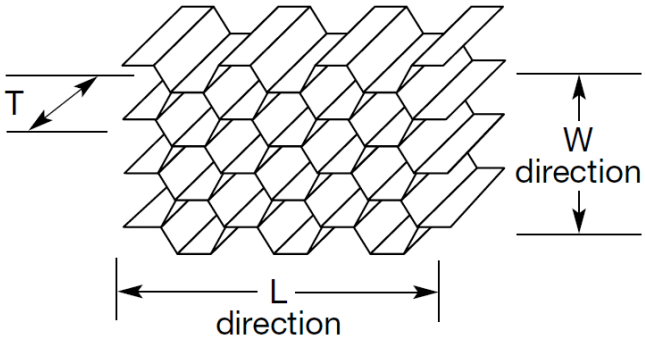

Figure 4.1: *Conventional honeycomb directions [19]*

4.2 Sandwich panels modelling

This section describe how the thermal behavior of sandwich panels has been modelled in ESATAN-TMS. Both in the PLM and SVM structural parts and other elements like the telescope baffle and the VGs are sandwich panels. A sandwich panel is composed by a honeycomb structure (core) and two panels on the two larger faces (skins). This configuration provides a very rigid structure while minimizing the mass. Being a not homogeneous structure, few considerations must be made in order to model its thermal behavior in a realistic way. Since the honeycomb cell structure has much lower density per unit volume, it cannot be modelled as a homogeneous material. Moreover honeycomb has directionally dependent conductivity since its hexagonal structure sets the heat flow along well defined paths inside the structure. Figure 4.1 shows the conventional name for honeycomb directions.

4.2.1 Honeycomb effective conductivity

As explained in [8, Appendix B], an effective thermal conductivity can be calculated along the three directions of the honeycomb. This means that it is possible to consider an apparent conductivity of the honeycomb as if it were a homogeneous material and so then apply the conventional heat transfer equations and implement it on ESATAN-TMS. Figure 4.2 shows schematically the conductive path along honeycomb ribbons in the three directions. Given the cell size S and the foil thickness δ, solid linear conductance along the three directions can be

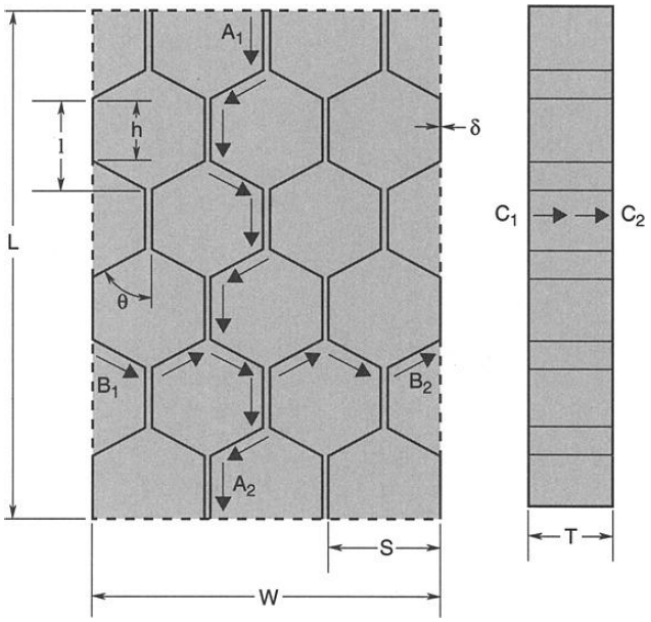

Figure 4.2: *Honeycomb scheme for effective conductivity calculation [8, Appendix B]*

approximate as:

$$C_L = \frac{3k\delta}{2S}\frac{WT}{L} = k_L\frac{WT}{L} \tag{4.1a}$$

$$C_W = \frac{k\delta}{S}\frac{WT}{L} = k_W\frac{WT}{L} \tag{4.1b}$$

$$C_T = \frac{8k\delta}{3S}\frac{WL}{T} = k_T\frac{WL}{T} \tag{4.1c}$$

where k is the core material conductivity, which actually is in all cases Aluminium alloy 5056, and k_L, k_W, k_T are the effective conductivities along the three directions. These formulas neglect the heat inter-exchange between consecutive ribbons. It is remarkable to notice that passing from k to k_i (for $i = L, W, T$) there is a factor δ/S which in our case is equal to $3.74 \cdot 10^{-3}$. So the honeycomb conductivity is three order of magnitude lower than an Aluminium solid of the same volume.

4.2.2 Honeycomb in ESATAN-TMS

The next problem is how to implement in ESATAN-TMS honeycomb panels with directional and temperature dependent thermal properties. Once defined the bulk properties (density, specific heat and conductivity) for a material, it is not possible to have a dependency on direction, but only on time or temperature. A solution to this problem has been found considering the "through conductance" feature for a shell geometry, which allows to insert a user-specified value for the conductance between nodes on the two opposite shell surfaces. Thus considering a rectangular shell, the conductance along the two planar directions (L and

W according to Figure 4.1) is defined by the bulk properties assigned to the shell geometry (intra-primitives conductors); instead the conductance along the transversal direction T is user assigned thanks to the "through conductance" feature. In this way it is possible to have two different directional conductance values. Since k_L and k_W differ by a factor 1.5, the conductivity difference between this two directions has been neglected, considering an intermediate value k_{LW}. This assumption makes sense also because the most critical sandwich plates are the VGs and the PLM-SVM interface which have circular shape. So the in-plane honeycomb conductivity can be taken as average.

The "through conductance" feature requires to set a user-defined conductance per unit surface [W/m^{2}K], not a conductivity [W/mK]. In this way linear conductors (GLs) are created by multiplying the user-defined value with the area of contact between the two nodes, which depends on the mesh applied on the shell geometry. As reported in Table 2.2 and Table 2.3, honeycomb thickness T is 20 mm for sandwich panel both in SVM and PLM, so the conductance per unit area through honeycomb thickness (T direction) is:

$$C_T = \frac{k_T}{T} \text{ [W/m}^2\text{K]} \tag{4.2}$$

Putting all assumptions together, the honeycomb thermal behavior can be modelled in ESATAN-TMS considering a shell geometry and assigning to it a bulk material with its thermal conductivity equal to k_{LW} and specifying as C_T the through thickness conductance in the shell properties. k_{LW} and C_T can be defined as "Property" in order to account for temperature dependency.

4.2.3 Sandwich panel in ESATAN-TMS

Now that it has been understood how to approximate honeycomb thermal conductivity and implement its directional dependency in ESATAN-TMS, the final step is the creation of the whole sandwich panel with two external skin panels and a central honeycomb core. The solution to this problem has been found on the use of three identical shell geometries separated by a small gap. The two external shells represent the skins, enclosing the central honeycomb core. The face-skin bulk material (Al alloy 5056 or CFRP) are assigned to the external shells while the honeycomb bulk material is assigned to the central shell. In the central shell the through thickness conductance must be specified as C_T, as explained previously.

Thermal coupling between core and skins shells must be also added to the model. This can be easily done through the contact zones feature: GL conductors are automatically created between parallel-facing honeycomb and shell nodes. The contact area is calculated by the ray tracing method. Each GL is obtained multiplying the node common area by the user-defined contact conductance. Physically, the contact zone can represent the adhesive used to bind honeycomb hexagonal to the skin panel. Adhesive should have a high contact conductance in order to allow spreading of heat over the sandwich panel. A contact conductance of 1000 W/m^{2}K has been considered in all sandwich panels. This is a reasonable value according to the expected configuration of the interfaces.

This way of modelling sandwich panels in ESATAN-TMS do not account for radiative heat exchange between internal honeycomb cell sides. In order to avoid ESATAN-TMS assigning GR conductors between the honeycomb shell nodes and the face-skin shells, surface activity of both the central shell surfaces and the internal face-skin shell surfaces is set to CONDUCTIVE, so only GL conductors are assigned between those nodes through the contact zone feature.

4.3 Bulk properties in ARIEL S/C

Before starting to build the model geometry it is important to select the optimal materials for each unit and to define the bulk and thermal-optical properties that are later assigned to geometries. At cryogenic level the thermal property dependency on temperature cannot be neglected. The thermal conductivity and the specific heat are modelled in ESATAN-TMS as a temperature dependent "Property" with values recovered from literature. Various sources have been utilized. If not specified, values are taken from the MPDB (Material Property Database) v6.69 of JAHM Software, Inc. and from [8].

4.3.1 Aluminium alloy 5056

As stated in the CDF outcome results, both PLM and SVM sandwich panels contain the Aluminium alloy 5056. Thermal conductivity k is strongly temperature dependent at cryogenic temperature. Table 4.2 reports the measured thermal conductivity of the alloy 5056 from 4.2 K to 120 K taken from the work of Baudouy [9]. In SVM and lower part of the PLM temperature are expected to higher than 120 K. Value of k at room temperature is around 160 W/mK [8]. With these values a "Property" for k has been created, allowing ESATAN-TMS to take into account temperature dependency. Values for density and specific heat are taken from [8].

As explained in section 4.2, it is necessary to create a material bulk property specific for the honeycomb. Since all honeycomb panel have the core made of Aluminium alloy 5056, the "honeycomb" material is here defined with properties shown in Table 4.3. $k_{LW}(T)$ so corresponds to the average of k_L and k_W, calculated according to Equation 4.1, where k is the thermal conductivity of the Al 5056 alloy. Considering the temperature dependency of $k_{5056}(T)$ as expressed in Table 4.2a it is then possible to define $k_{LW}(T)$ as a temperature dependency "Property" as well.

4.3.2 Glass fibers reinforced polymer (GFRP)

GFRP is used in the bipods and the VG supporting struts thanks of its low thermal conductivity together with high specific strength. Glass fibers are preferred to carbon fibers because of their lower thermal conductivity at the working temperature interval of the PLM. Figure 4.3 shows thermal conductivities of unidirectional (UD) fibers composites as a function of temperature. Glass and

(a) Thermal conductivity [9]

Temp [K]	k [W/mK]
4.3	3.7
10.1	9.1
15.0	13.9
20.0	19.2
25.1	23.1
30.2	29.0
35.0	33.5
40.0	38.4
45.2	41.6
50.2	42.9
55.1	46.4
60.2	50.4
65.1	58.2
70.3	59.6
80.4	62.8
85.1	63.1
100.5	66.5
105.2	67.5
120.7	74.2

(b) Specific heat

Temp [K]	c_P [J/kgK]
30.0	31.0
60.0	214.0
300.0	902.0

Table 4.2: *Aluminium alloy 5056 temperature dependency properties*

Parameter	Value
Density	$32\,\mathrm{kg/m^3}$
Specific heat	$c_{P_{Alu}}(T)$
Conductivity	$k_{LW}(T)$

Table 4.3: *Honeycomb bulk material properties*

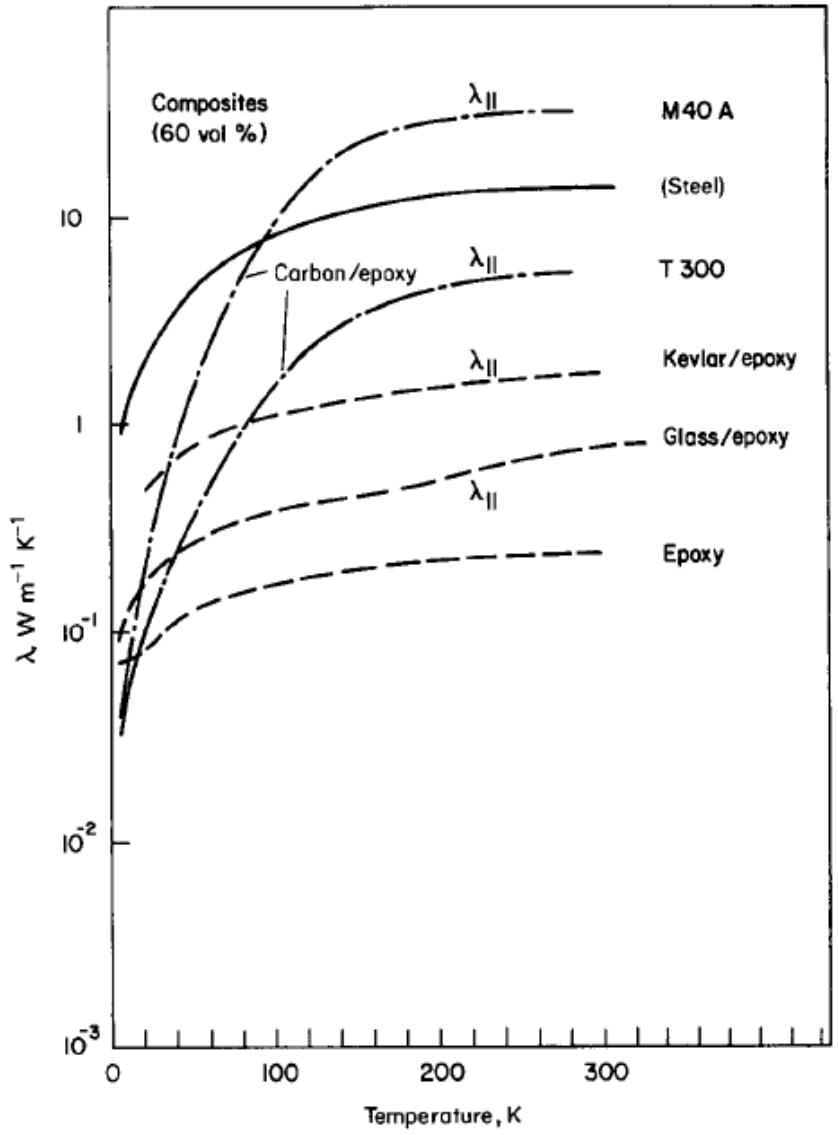

Figure 4.3: *UD fiber composites thermal conductivity versus temperature [11]*

(a) Thermal conductivity

Temp [K]	k [W/mK]
50.0	0.347
120.0	0.477
300.0	0.811
400.0	0.997

(b) Specific heat

Temp [K]	c_P [J/kgK]
40.0	126.3
300.0	880.0

Table 4.4: *GFRP temperature dependency properties*

Kevlar fibers composites have a low temperature dependence of thermal conductivity. On the contrary, carbon fibers composites show a very large temperature dependence. For temperatures greater than circa 20 K, glass fibers composites have lower thermal conductivity. Therefore in the ARIEL PLM, which has expected temperature no lower than 28 K, GFRP are more convenient for the purpose of thermal insulation. GFRP properties values used in ESATAN-TMS are shown in Table 4.4

GFRP is not an homogeneous material as it a composite made of a polymer matrix reinforced with glass fibers, with different thermal properties. In order to implement its behavior in the software it necessary to consider effective homogenised properties. Passing from element bulk properties to the homogenised ones is not easy since the result depend on geometric factors, like the number and disposition of fibers inside the matrix. Anyway, at this stage of analysis is not necessary to achieve this level of accuracy.

4.3.3 Sintered Silicon Carbide (S-SiC)

Sintered Silicon Carbide has been developed during '90 by ASTRIUM as a cost effective alternative to Beryllium for ultra-stable lightweight space based telescopes. This technology has been successfully used in space missions, including Herschel, Planck and GAIA, and it has now become a common material for telescope mirrors. S-SiC is an ideal material for that kind of application thanks to its high thermal distortion ratio, λ/α, associated with high specific stiffness E/ρ. Moreover S-Sic is extremely homogeneous, with isotropic properties. These make S-Sic the reference material for space optical payloads.

In ARIEL spacecraft SiC bulk material is used on the telescope mirror M1 and M2, and on the Telescope Optical Bench (TOB), which is the mechanical support of the M1. Table 4.5 shows the values of the thermal properties used in ESATAN-TMS to model the behavior of this material.

4.4 Thermo-optical properties in ARIEL S/C

All the thermo-optical properties used in the ARIEL S/C ESATAN-TMS model are shown in Table 4.6. Solar array are made of solar cell mounted on the supporting structure with a certain packaging factor, still undefined. Solar cell

(a) Thermal conductivity

Temp [K]	k [W/mK]
20.1	22.2
30.3	49.0
40.1	74.0
59.2	121.4
79.2	155.1
100.0	185.0
184.6	202.5
295.9	175.6

(b) Specific heat

Temp [K]	c_P [J/kgK]
20.0	0.5
40.0	5.2
70.0	36.3
100.0	100.5
300.0	667.0

Table 4.5: *SiC temperature dependency properties*

	Infrared			Solar		
	ε	ρ^d	ρ^s	α	ρ^d	ρ^s
Solar array	0.80	0.20	0.00	0.60	0.40	0.00
Aluminium	0.13	0.85	0.02	0.20	0.75	0.05
VDA	0.13	0.85	0.02	0.05	0.90	0.05
Silver	0.04	0.01	0.95	0.02	0.03	0.95
Open honeycomb	0.95	0.05	0.00	0.94	0.05	0.00
Black paint	0.90	0.10	0.00	0.90	0.10	0.00
Single-layer insulation	0.12	0.88	0.00	0.06	0.94	0.00
Gold coated Polyimide	0.03	0.97	0.00	0.30	0.70	0.00
Silvered Teflon	0.60	0.40	0.00	0.14	0.86	0.00

Table 4.6: *Thermo-optical properties used in ESATAN-TMS*

have high values of absorptivity which makes them run hot ($\alpha/\varepsilon = 0.9/0.8$). The cells are body-mounted so no radiation cooling is possible from the back. It is expected that the sun-exposed supporting structure is covered by low absorptivity/high emissivity material (solar reflector) to lower as much as possible cell temperature for efficiency maximization. A mean value of 0.6 for the solar array absorptivity has been considered.

Two different ways of modelling the MLI thermal behavior has been considered. The first one simply consists in assigning to the covered surface a thermo-optical property of a flat reflector material, which has low values of both α and ε, acting as a single layer insulator. The second method considers an additional shell geometry which has its through thickness conductance defined with an effective emittance which accounts for the MLI internal layers. Two different outer-layer material for the MLI have been considered. One is gold coated Polyimide with a particularly low emittance. Values of α and ε are taken from [18]. The other is silvered Teflon surface finish which minimize thermal impact of solar exposure thanks to its low α/ε ratio. Values are taken from [8]. This second method of MLI modelling is explained in section 6.4.

4.5 SVM modelling

As already mentioned, the SVM design will be developed by ESA prime industrial contractors, so no specific thermal requirements have been specified with the exception for the sunshield top surface. For this reason a SVM model has been built in order to have a complete and realistic geometry of the spacecraft, so, when the thermal behaviour is analysed as a function of different satellite attitudes, reliable results are obtained. The simpler solution would have been not to build the SVM and assign to the SVM/PLM interface plate a fixed boundary temperature.

4.5.1 SVM solar array

Solar array is body-mounted on the external side of the SVM bottom plate. Since no specific information is available about the structural interface which connects the solar cells to the bottom of the SVM panel, the mounting structure is assumed made of the same sandwich panels of the SVM structural parts. Solar array is thus model together with the SVM bottom plate as sandwich panel of circular shape. Three primitive disc shells are sketched, they represent the bottom skin, core and top skin of the sandwich plate. Radius of the disc is 1.35 m, equal to the SVM/PLM interface radius. CFRP bulk material is assigned to the face-skin shells and honeycomb to the central shell. Shell thickness is defined according to Table 2.2.

"Solar array" thermo-optical property is assigned to the bottom surface of the lower disc shell, which is the one exposed to the solar rays. The top of the upper shell disc should be covered by an insulating material. The "Single-layer insulation" thermo-optical property has been assigned to it. All the other

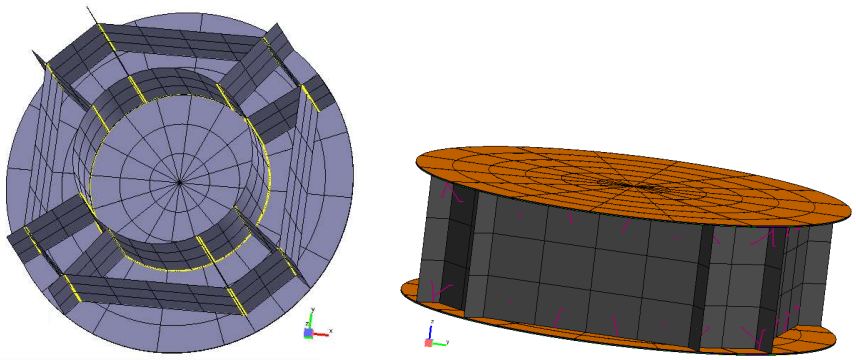

(a) Condutive interfaces **(b)** User-defined conductors

Figure 4.4: *SVM inter-primitive conductors*

surfaces do not need optical properties because they are set as CONDUCTIVE, as explained in the sandwich modelling section.

4.5.2 SVM structure

SVM structure is created referring to the drawing shown in Figure 2.7. Even if structural parts are made of sandwich panels, it has been decided to model them with just a single shell in contrast of the three shells used for example in the solar array. Indeed here it would be necessary to use a high number of rectangular and cylindrical primitive geometries in order to represent the layout of the structure similar to the drawing in Figure 2.7, and the use of three shells for each part of the structure would increase to much the complexity of the model without bringing additional useful details in the solved temperature distribution. Moreover the CFRP and the honeycomb thermal conductivity have quite similar values in the same temperature rage ($k_{CFRP} = 1.5\,\mathrm{W/mK}$, $k_{LW} = 0.80\,\mathrm{W/mK}$ both at $300\,\mathrm{K}$). According to these two reasons, SVM structure has been modelled with single shells. Shell thickness is the sum of the two skin thicknesses and the honeycomb one, totally equal to 22.4 cm. Bulk material assigned to all shells is honeycomb. Thermo-optical property assigned to all surfaces is "Aluminium".

Octagonal sides, shear panels and central cone have been sketched in ESATAN-TMS in a way that the software can created automatically conductive interfaces at each shell edge, so assigning GL conductors between nodes of different shells which are in contact to each other. Figure 4.4a shows in yellow the conductive interfaces in the SVM. It can be noticed from the same figure that there are no yellow lines connecting the bottom edges of the octagonal sides and of the shear panels to the solar array top skin shell. ESATAN-TMS is not able to create conductive interfaces because those shells do not share their free edges. This problem has been solved connecting manually with user-defined conductors each face node of the structure to the nearest face node of the solar array and solar shield surfaces. User-defined conductor connections are shown in pink in Figure 4.4b. The GL value assigned at each user-defined conductor has been approximated by the rectangular mono-dimensional conduction formula

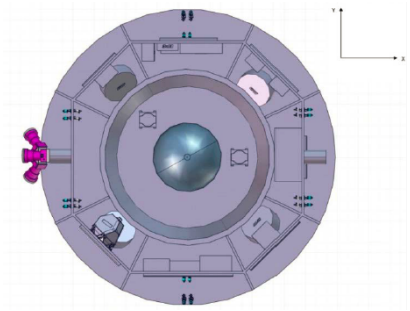

(a) Internal components from CDF study, [2]

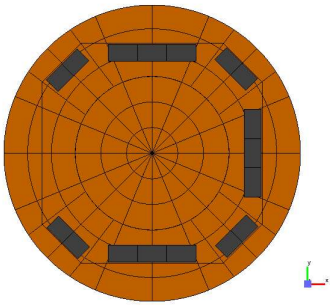

(b) Internal components in ESATAN-TMS

Figure 4.5: *SVM internal components distribution*

Unit	Enclosure	Dissipation [W]
RTU	+X	20
RW, OBC	+X-Y	33
ICU, FGS WE	-Y	120
RW, Gyro	-X-Y	45
-	-X	-
RW, Batteries	-X+Y	26
Comms units	+Y	64
RW, STR, EU	+X+Y	32

Table 4.7: *SVM enclose distribution and heat dissipation [2]*

GL(n_1,n_2)=$k\frac{A}{l}$, where k is the Aluminium conductivity, A is the contact area between sandwich and structural panels, so the structural panel thickness, and l is the average distance between the two face node centers. The mesh of SVM primitive geometries has been chosen to have in all shells similar node face dimension.

4.5.3 SVM internal components

No detailed information regarding number, size and distribution of internal components of the SVM is available. It has been decided to add just the components which have an internal heat dissipation, so which have an impact on the thermal behavior. CDF study has proposed a distribution shown in Figure 4.5a. Table 4.7 lists the units enclosure distribution and their relative heat dissipation.

In ESATAN-TMS, the units in each enclosure are represented by a solid rectangular geometries, as shown in Figure 4.5b in dark grey. They are thermally connected to the relative octagonal side by a contact zone with a contact conductance equal to 100 W/m^2K.

4.5.4 SVM/PLM interface plate

The SVM/PLM plate (or sunshield) has been sketched in ESATAN-TMS identical to the solar array. The only difference lies in the thermo-optical property assigned to the external surface. Here both external surfaces are covered by MLI, therefore the assigned optical property is "Single-layer insulation". In chapter 6 (section 6.4), the thermal behavior of the MLI covering both side of the SVM/PLM plate is simulated with a refined model.

4.6 PLM modelling

The main objective of the thermal analysis required to the ARIEL Consortium, and in particular the to INAF-IASF Bologna, is the PLM model. For this reason, the PLM is built with a higher level of detail with respect to the SVM.

4.6.1 VG honeycomb panel

V-Grooves design is a key issue of the ARIEL thermal performance. Accurate modelisation is necessary to obtain realistic and reliable results. No information has been specified for the VGs shape and inclination. Looking at the drawings included in the proposal document and the CDF presentation it can be supposed that a flat circular shape has been considered, which is the simplest choice. A constant step of 7° has been assumed for the VGs inclination, resulting in a set of 7°-14°-21°. V-Grooves are sandwich panels with hexagonal honeycomb core. CDF team has suggested the sandwich type with the characteristics reported in Table 2.3. Each VG has been sketched in ESATAN-TMS with three plus three half disc shell geometries connected at their free edge. ESATAN-TMS is able to calculate a conductive interface along the edge automatically creating GL conductors between right and left sided half discs. Aluminium bulk material is assigned to each face-skin shell and honeycomb to the central shell. "VDA" optical is assigned to all VG surfaces except for the upper one of the topmost VG which is "Open honeycomb", as explained in subsection 2.4.2. A front and isometric views of the three VG as modelled in ESATAN-TMS are shown in Figure 4.6. The gaps between the VGs at their half is 10 cm.

4.6.2 VG bipods and supporting struts

The three bipods and the eight supporting struts have been modelled with a cylindrical shell geometries with thickness and assigned bulk material according to Table 2.4. At the head and at the two feet of each bipod, box shells has been added representing the mechanical interface where the bipods legs are attached to. All bipods feet are attached to the top surface of the SVM/PLM plate, the front bipod head is supporting the telescope baffle, the rear bipod heads are attached to other small box shells representing the mechanical connections with the Telescope Optical Bench (TOB) and the Instrument Optical Bench (IOB). Conductive thermal coupling between shell boxes and the surface where they

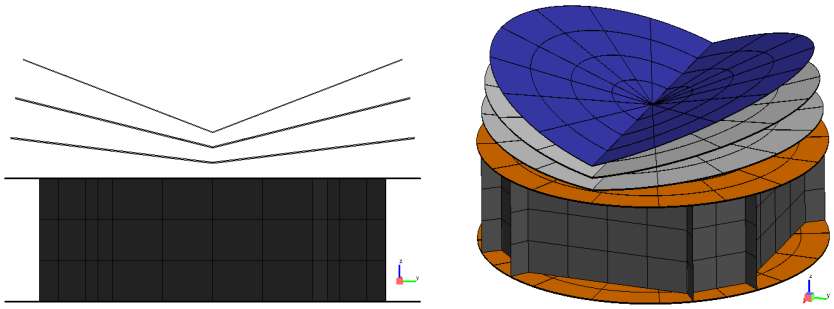

Figure 4.6: *VGs over the SVM, front and isometric views*

are attached to is achieve through contact zones. Also in these cases a contact conductance of 100 W/m^2K has been assigned.

Supporting struts extend from the SVM/PLM plate top surface to the lower surface of the topmost VG. Conductive connections between those interfaces is simply achieved through user-defined conductors: the lowest struts node is connect to the nearest face node of the SVM/PLM and the highest strut node to the nearest face node of the lower surface of the third VG. The thermal conductance assigned is again approximated with the formula $GL(n_1,n_2)=k\frac{A}{l}$. Bipods and supporting struts cylinder shells are meshed with 10 face nodes since it is expected an high thermal gradient along their direction: from the SVM/PLM plate room temperature down to the third VG around 60 K–50 K. A general view of the three bipods and the eight supporting struts attached over the entire SVM is shown in Figure 4.7.

Bipods and supporting struts are attached to the VGs with high conductive interfaces as explained in the subsection 2.4.2. These connections are modelled through user-defined conductors with a conductance assigned value of 1 W/K. The surface contact conductance of the bipods, with enhanced conductive property, is assumed to be around 1000 W/m^2K, a reasonable value for bolted interfaces. The contact area between the pods and the VG surface is estimated on the order of 10 cm^2: the contact conductance is then calculated as close to 1 W/K.

The bipod legs on the ESA Planck mission have been filled with a special foam with the aim of enhancing their stiffness. The foam material has low thermal conductivity to limit heat leak from the SVM to PLM. In the ARIEL ESATAN-TMS bipods, the foam has been modelled with cylindrical solid geometries with height and diameter a little bit smaller of the bipod legs. No information has been found in literature regarding the bulk properties of such a type of foam. It has been hypothesised that the foam thermal conductivity has a lower order of magnitude with respect to the GFRP. A bulk material which has the values of the GFRP divided by 10 has been assigned to foam solid geometries. Conductive coupling between the foam lateral surfaces and the internal bipod leg surfaces have been achieved through contact zones with an assigned contact conductance of 100 W/m^2K. Foam and internal leg surfaces are set to CONDUCTIVE, so no radiative coupling between them is considered in the thermal model. Figure 4.8

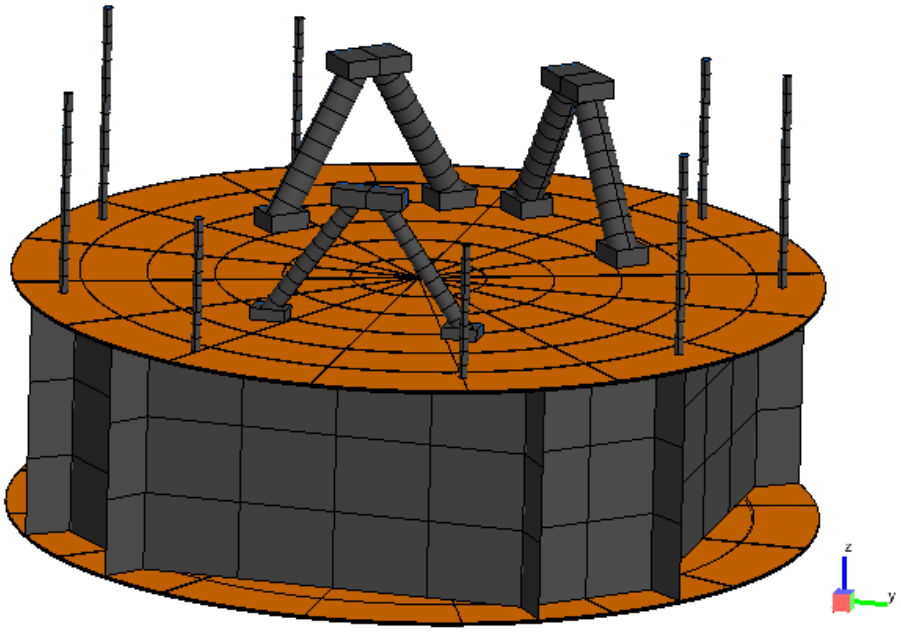

Figure 4.7: *Bipods and supporting struts over the SVM*

shown only the front bipod with the right leg shell transparent. The internal solid cylindrical geometry (green) representing the foam is visible.

4.6.3 Telescope and its baffle

The telescope is composed by many mirrors which direct and split the incoming light to the different instrument channels. For what concern the PLM thermal behavior, the impact of the small mirrors belonging the the Common Optics (CO) is very small. Only the bigger M1 and M2 have been sketched in ESATAN-TMS while all the other mirrors have been neglected since they would complicate the model without bringing any contribute to it. When the instrument box will be detailed designed, then it is more reasonable to consider them.

Firstly, the telescope baffle has been modelled. It has been sketched using a cylindrical shell geometry of 0.55 m radius and 1.8 m height cut by two planes at the two ends. The cutting plane at the front is inclined along the Y axis of 45°, the rear plane of 105° along the same axis. The baffle rear is closed the Telescope Optical Bench (TOB), an elliptical shell realised by a 105° inclined plane cut by the a cylinder of the same radius of the baffle. At the centre-bottom of the TOB a small half-round hole as been made where light path between M2 and the CO is.

According to the CDF outcome results, the baffle structure is CFRP-skin/Al-honeycomb sandwich (as of SVM, Table 2.2). Two concentric shell cylinders (representing the sandwich skins) have been added external and internally to the first shell cylinder, one with 0.60 m radius and the other with 0.50 m, with

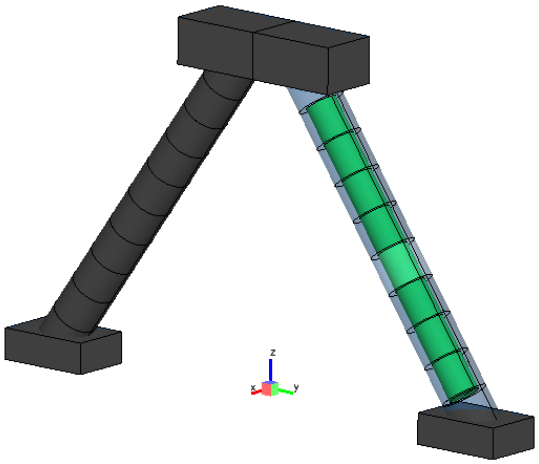

Figure 4.8: *Front bipod with visible internal foam*

the same type of cuts. A problem has been encountered when ESATAN-TMS calculates the GL conductors between honeycomb central shell and external skin shells through the contact zone feature. In particular, when the conductor calculation routine reaches those nodes, the software suddenly crashes producing a fatal error report. It is possible that there is a bug when ESATAN-TMS deals with contact zones defined between geometries which have been cut. For this reason, the baffle has been modelled with a single shell. "Honeycomb" bulk material has been assigned to the shell, the thickness is the sum of the honeycomb and the two skin thicknesses: 0.0224 m. The TOB assigned bulk material is SiC, an hypothetical thickness of 0.01 m has been considered. Thermo-optical property of both baffle and TOB is "black paint".

The M1 has been realised cutting a paraboloid shell by a cylinder of 0.38 m radius, inclined of 135° and 110° along the X and Y axis respectively. This cut operation creates a good approximation of the real mirror geometry. The M1 is accommodated on the TOB inside the baffle. Conductive connection between the two elements high achieved by a contact zone. The M2 is simply sketched by a shell disc of 0.08 m radius, inclined by 85° along the Y axis. It is accommodate in the bottom-front of the baffle. Thermo-mechanical connection is modelled through two user-defined conductors between one M2 face node and two baffle face nodes. A value of 0.01 W/K has been assigned to both the user-defined conductors. Bulk material assigned to both mirrors is SiC, "silver" as thermo-optical property. Front and rear isometric views of the telescope assembly are shown in Figure 4.9. User-defined conductor connections are shown in magenta lines.

Even if the TOB and the baffle geometries share their free edge, ESATAN-TMS is not able to create a conductive interface between them because these two geometries have been realised by cuts. User-defined conductors have been manually added between baffle and TOB nodes at their free edge. Conductance values assigned have been approximated by the usual rectangular mono-dimensional conductive formula. Both baffle cylinder and TOB ellipses are meshed with

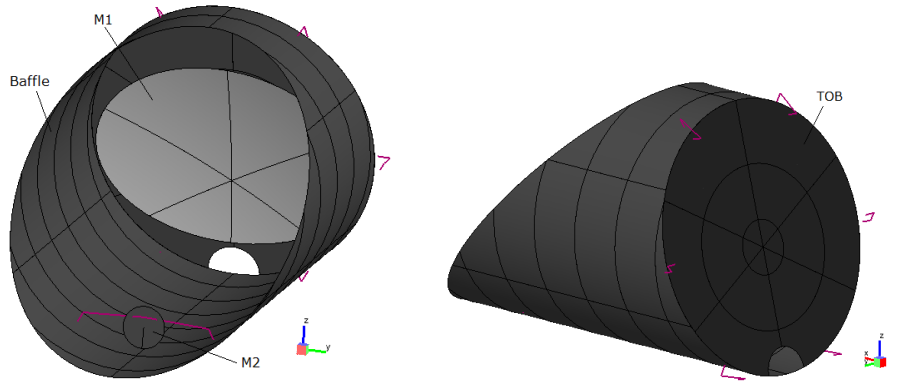

Figure 4.9: *Telescope assembly views*

the same number of nodes along the radial parametric direction (the baffle is divided into a 6x8 mesh and the TOB in a 6x3). This facilitates the estimation of contact area and node distance to be used in the formula. The contact area between each node couple has been estimated with

$$A = \frac{2\pi r}{n} t = \frac{2\pi \cdot 0.55}{6} \cdot 0.0224\,\mathrm{m}^2 = 0.0129\,\mathrm{m}^2 \tag{4.3}$$

where r is the baffle/TOB radius, n is the mesh number along the radial direction and t is the baffle thickness. Looking at the rear view of the telescope assembly in Figure 4.9, it can be notice that the distance between node face centres is not the same for all the six node couples. A value of 0.20 m has been used for the two upper node couples, 0.10 m for the lateral, and 0.15 m for the bottom ones. The thermal conductivity k used in the formula is k_{LW}.

4.6.4 Instrument optical bench (IOB) and box (IB)

The Instrument Optical Bench (IOB) is a part of the entire OB/metering structure consisting in a supporting plate for the PLM cold scientific equipments. It has been sketched in ESATAN-TMS simply with a squared shell of side 0.72 m. The bulk material is Al alloy to minimize thermal gradients, a thickness of 0.01 m has been assumed.

The IOB is mechanically connected to the TOB/Baffle assembly at its top, and to the bipod heads at the right and left bottom. The top support has been design as an upside-down bipod with its head attached to the IOB and the two feet to the TOB. Bipod legs are cylinder shells with 0.01 m radius and 2 mm thickness. Bottom mechanical interfaces are sketched as small rectangular box shaped geometries. Conductive thermal coupling between rectangular boxes, the TOB, the IOB and the bipod heads are modelled through contact zone. The bulk material of all those geometries is Al alloy while thermo-optical is black paint in order to maximise heat rejection to deep space.

The Instrument Box (IB) contains the two scientific instruments and the JT cooler cold end. It should contain also the mirrors of the CO but, as previously

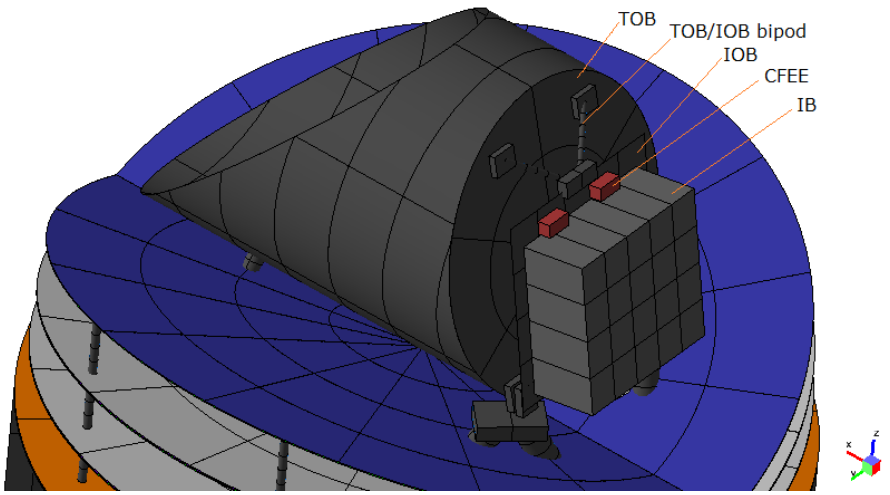

Figure 4.10: *Explained external PLM rear view*

said, they have not been considered in the development of the ESATAN-TMS thermal model. The IB has been sketched as a rectangular box of dimensions 0.6 x 0.6 x 0.25 m, with a thickness of 5 mm. Assigned bulk material is Al alloy to minimize thermal gradients. Lateral surfaces have black paint as assigned thermo-optical property, while the rear squared surface has open honeycomb. The IB is conductively connected to the IOB thought a 100 W/m^2K contact zone.

The CFEEs of the two scientific instruments have not be specified if they shall be accommodated inside or outside the IB. It has been decided to put them outside, just above the IB to distance away their heat dissipation from the detectors. They have been sketched in ESATAN-TMS with two identical solid rectangular geometries of dimension 0.05 x 0.1 x 0.05 m. Conductive thermal coupling between the CFEEs and the IOB is enhanced in order to spread their dissipation heat over the IOB and metering structure which are radiatively coupled to the deep space thanks to their black paint coating. For this reason, a 500 W/m^2K contact zone between the two CFEEs and IOB has been assumed. A view of the elements explained in this section can be seen in Figure 4.10.

4.6.5 FGS/NIRP, AIRS and JT cooler

The IB contains the two scientific instruments and the JT cooler cold end. No internal IB drawing is available yet. The instruments are composed by a module box containing the detector and the Temperature Control Stage (TCS). FGS module box has been sketched with dimensions 0.22 x 0.22 x 0.16 m, while AIRS box bigger with 0.4 x 0.25 x 0.16 m, because it contains some CO parts which have not been modelled in ESATAN-TMS as they are not thermally relevant at this level of analysis. The module boxes are mechanically and thermally anchored on the IB. Connections are modelled through 100 W/m^2K contact zones. Each detector has been sketched as a rectangular solid geometry of 0.1 x

0.8 x 0.8 m. Two detectors have been considered for the FGS/NIRP instrument according the Figure 2.10. Each detector has its own TCS. They have been designed through a simple rectangular shell geometry, which has the same area of the facing detector surface. JT cold end is also simply a rectangular shell, facing the AIRS TCS.

As explained in the subsection 2.4.2, the detectors should be thermally decoupled from their module boxes while thermal contact with the cooling stage (IB rear surface radiator or JT cold end) is optimized. In the EChO mission thermal design, the interfaces between modules and IB have been considered sized stainless steel (304L or 316L) stands which reach resistance values on the order of 10^3 K/W [12]. A precautionary value of 0.01 W/K has been assigned to the user-defined conductors connecting each detector to its relative module box.

A key role in detectors' thermal behavior is played by the GL values of the conductive interfaces between detector and TCS, and between TCS and the relative cooling stage (G1 and G2 conductance in Figure 2.14). The reference cold stage for the FGS/NIRP is the IB rear surface, while for the AIRS is the JT cold end. The G1 and G2 values must be carefully optimized in order to find the best trade-off between maximum conductance and minimum control power. An high conductance value would let the detector temperature run close the its cooling stage temperature but it would require a greater TCS control power since most of this heat is absorbed by the cold stage and not by the detector. On the contrary, a low conductance value would require less control power and more stable detector temperature but at the cost of increasing the detector working temperature. In the EChO thermal control system design, the chosen optimal conductances are on the order of 0.1 W/K between TCS and the cooling stage, and 0.01 W/K between detector and TCS [12]. These value have been used for the first ARIEL ESATAN-TMS model version. Sensitivity on these parameter is later investigated and optimised for the ARIEL case. These conductive connections between detector, TCS and cooling stage are achieved through user-defined conductors.

Electronic connection between CFEE and detector is achieved through cryo-harnesses, which are wires with enhanced thermal resistivity. In ESATAN-TMS the connections have been modelled through user-defined conductors with a conductance of 0.001 W/K.

Figure 4.11 shows the component accommodation inside the IB of the ESATAN-TMS ARIEL model. The IB has been hidden and both the FGS and AIRS module boxes are transparent for better comprehension. The JT cold end is inside the IB but outside the AIRS module box. No detailed information is provided on the material composition of the elements describe in this subsection. For simplicity, the bulk material assigned to all geometries is Al alloy and "black paint" for thermo-optical property.

4.7 Radiative cases

The construction of the first version of the ARIEL S/C thermo-mathematical model has concluded. The next step is the definition and run of the mission

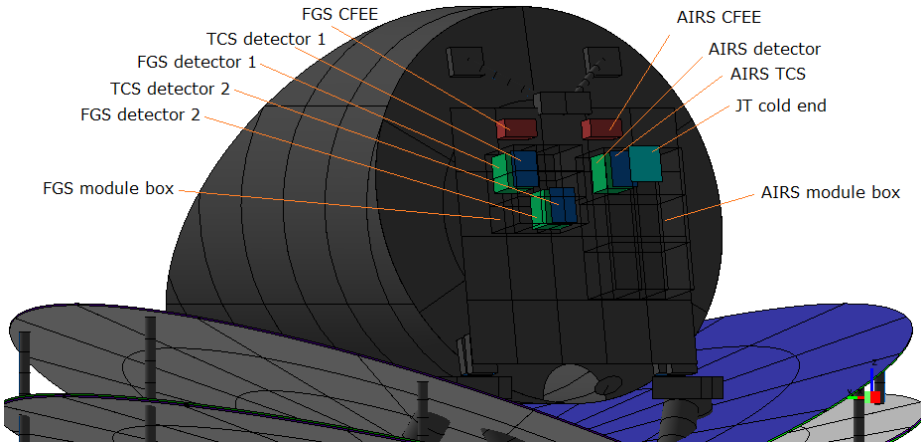

Figure 4.11: *Component description inside the IB*

radiative cases. They include the definition of the satellite orbit and attitude. The investigation of the spacecraft thermal performance at different attitude from the nominal one is part of the thesis work. It has been decided to perform steady-state analyses at increasing attitude inclination along both the S/C X and Y axes with a constant angle step of 5°. A single radiative case has been defined for each satellite attitude.

4.7.1 Nominal case

The first radiative case that has been set the S/C at the L2 Earth-Sun system point with its Z axis aligned with the anti-Sun vector. The baseline operational orbit of the ARIEL S/C is a large amplitude Halo orbit at the Earth-Sun system L2 point [3]. This virtual point is located about 1.5 million km from the Earth in the anti-Sun direction. It is so far away that the Earth albedo and infrared radiation can be ignored. Only the solar radiation is taken into account. ESATAN-TMS offers the possibility to define a radiative case into an Earth or a Sun orbit. The virtual L2 point moves around the Sun as the same rate of the Earth rotation, describing an almost circular orbit of $1\,\mathrm{AU} + 1.5 \cdot 10^6\,\mathrm{km} \simeq 1.5 \cdot 10^8\,\mathrm{km}$ radius. Since Earth do not play a role in the S/C orbit thermal environment, the defined orbit in the ESATAN-TMS radiative case is a Sun-centred orbit of $1.5 \cdot 10^{11}$ m radius on the Ecliptic plane.

A way to define the S/C attitude consists in specifying the orientation of the Model Coordinate System (MCS) with respect to the Inertial Coordinate System (ICS). For Sun-centred orbit the ICS origin coincides with the centre of the Sun, X and Y axes lay on the Ecliptic plane, Z axis is perpendicular to the plane forming a right-handed triad. By default, the X axis direction is defined from the Sun to the Vernal Equinox. In order to fully constrain the satellite attitude it is necessary to specify two MCS vector with respect to the ICS. In ESATAN-TMS this is achieved specifying the primary and secondary pointing vectors and directions. Pointing vectors refer to the MCS while pointing direction to the ICS. The satellite is thus oriented at each orbital position by firstly

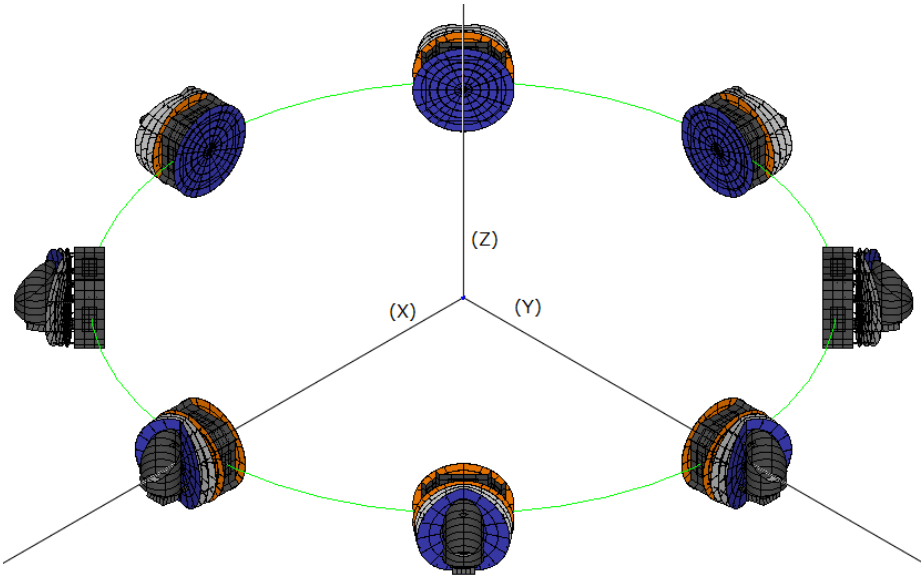

Figure 4.12: *S/C orientation in the ICS of the nominal radiative case*

aligning the primary pointing vector to the primary pointing direction and then rotating about the primary pointing vector to achieve the best alignment of the secondary pointing vector with the secondary pointing direction. In the nominal case, the S/C Z axis is pointing the anti-Sun vector. The S/C Z axis, [0.0, 0.0, 1.0], is thus defined as the primary pointing vector and the anti-Sun as the primary pointing direction. The definition of the secondary direction is not straightforward since, according to the observation mission requirements discussed in subsection 2.4.5, the ARIEL S/C shall be able to make a rotation of 360° around the Z axis, so assuming all the attitude definable in the secondary movement. For convenience, the ARIEL X axis and the normal-to-orbit direction have been defined respectively as secondary pointing vector and direction. S/C orbit and attitude for the nominal case are represented in Figure 4.12 for eight orbital positions, orbit radius and model dimension are not in scale. Since the thermal environment is identical at each orbit position, only one position can be analysed reducing the computation efforts.

4.7.2 S/C rotated along X and Y axes

A set of radiative cases have been defined at different satellite attitudes to study their influence on the S/C thermal performance. Six cases have been defined for rotation from $-15°$ to $15°$ along the X axis with a step of $5°$ and ten cases for rotation from $-25°$ to $25°$ along the Y axis with the same angle step in response to the observational requirements discussed in subsection 2.4.5.

In ESATAN-TMS, attitude rotation from the nominal case are easily obtainable through the "User defined movement" feature. After the S/C Z axis has been aligned to the primary direction (anti-Sun), and then rotated along the Z axis so that the S/C X axis is aligned to the normal-to-orbit vector, additional attitude

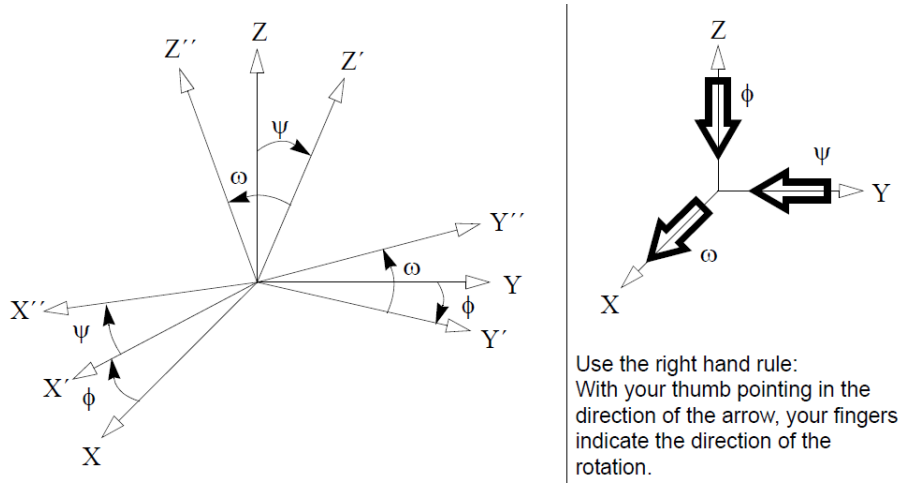

Figure 4.13: *Euler angles in ESATAN-TMS Workbench [15]*

movements can be defined by means of a set of Euler angle rotations, ϕ, ψ, ω, applied in the MCS. These rotations are illustrated in Figure 4.13 together with the convention adopted for positive rotations. Attention must be paid for rotation along the Y axis: in ESATAN-TMS positive ψ rotations are obtained pointing the thumb towards the anti-Y axis direction.

Single radiative cases have been defined for $\omega = -15, -10, -5, 5, 10, 15$ degrees (rotation along the MCS X axis), and for $\psi = -25, -20, -15, -10, -5, 5, 10, 15, 20, 25$ degrees (rotation along the MCS -Y axis). Figure 4.14 illustrates two defined radiative cases, the first with $\omega = 15°$, the second with $\psi = 25°$. Reference frame axes painted in both figure bottoms are from the ICS.

A total of seventeen radiative cases have been so defined: one nominal case (no rotation), six for X axis rotation, ten for Y axis rotation. Cases are run one by one by ESATAN-TMS, which calculates the radiative exchange factors (REVs), solar direct flux (SDF), and solar absorbed flux (SAF). REVs are calculated by the MCRT firing 10000 from each face node of ACTIVE geometries. The SAF is the solar power absorbed by each faced node, which depends on the SDF and node thermo-optical property. When the analysis file is created, the REVs are used for the GR radiative conductors calculation, non-zero SAF are assigned to each relative node as an internal heat load. The value of the SDF can used to check the correctness of the defined orbit in the radiative cases. The solar flux is inverse proportional to the square of the distance to the Sun. The ARIEL Environment specification document considers a solar flux average value of $1339\,\mathrm{W/m^2}$ at the L2 point. In the ARIEL ESATAN-TMS model the SDF value in the nominal case for each node exposed to direct Sun illumination is $1352\,\mathrm{W/m^2}$. The values are acceptably close to each other.

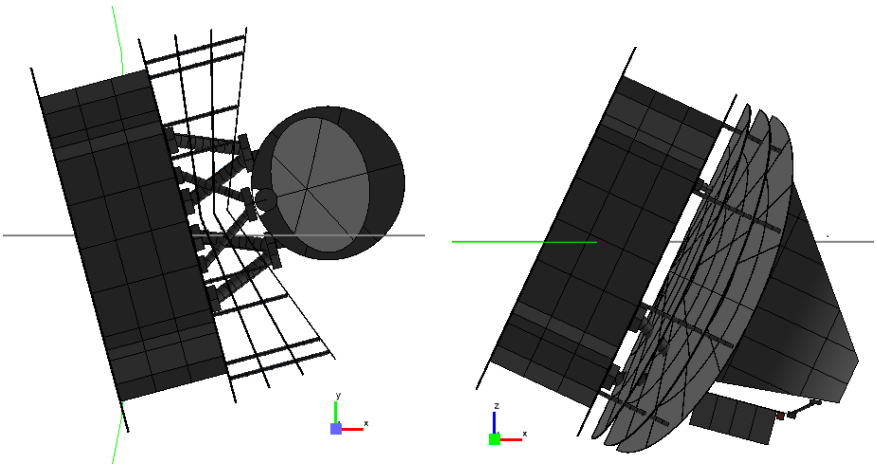

(a) $\omega = 15°$ **(b)** $\psi = 25°$

Figure 4.14: *S/C attitude at L2 point for* $\omega = 15°$ *and* $\psi = 25°$

4.8 Boundary conditions

The boundary conditions (BC) are necessary to simulate the thermal behavior of electronic units, which dissipate heat, and of the JT cooler, which absorbs heat at its cold end. Environmental boundary conditions, like the deep space temperature and the solar heat flux have been already taken into account in the radiative cases. The mission proposal document, the PDD and the CDF results give applicable values for equipment heat dissipation and JT cooler behavior. These values have been assigned to a first set of analysis cases. Some of them have been later modified in order to understand their sensibility on the PLM thermal performance. New analysis cases have been created with the new BC values in the same ESATAN-TMS model.

4.8.1 BC values from reference documents

The PLM and SVM internal components heat dissipation are summarized respectively in Table 2.5 and Table 4.7. The CDF study has considered 26 mW of absorbed power at the JT cold end and a total power load of 320 mW at the third VG which includes pre-cooling of the warm JT Neon stream and heat interception from harness. With all these values a set of BC have been created and assigned to the corresponding geometry in the ESATAN-TMS model.

The SVM internal components have been sketched as rectangular solid geometries. A total volume heat load BC has been assigned to each component with its relative dissipating heat according the table values.

The heat loads BC assigned to the PLM components as modelled in ESATAN-TMS with values based on the reference documents are shown in Table 4.8. Total area heat loads are applied to shell geometries, while total volume to solids. The BC heat load values is divided between the nodes in proportion to the area or

Geometry	Type of BC	Value [mW]
FGS detector 1	Total volume heat load	10
FGS TCS 1	Total area heat load	5
FGS detector 2	Total volume heat load	10
FGS TCS 2	Total area heat load	5
FGS FEE	Total volume heat load	65
AIRS detector	Total volume heat load	10
AIRS TCS	Total area heat load	5
AIRS FEE	Total volume heat load	20
JT cold end	Total area heat load	−26
VG3 (single face node)	Total area heat load	320

Table 4.8: *"JT26mW" set of BC assigned to PLM geometries*

volume that make up each node in the geometry. The BC on the VG3 is instead applied to a single face node of the upper VG3 surface mesh. The chosen node is beneath the instrument box, where the JT cooler pipe is supposed to pass through. As explained in subsection 2.4.4, temperature variation on FGS and AIRS detectors are damped by dissipating a specific amount of heat calculated through a close loop control. In order to take this extra power dissipation into account, a heat load boundary condition of 5 mW has been applied in each TCS (also in the redundant FGS detector). EChO mission study results [12] showed that, for worst case temperature fluctuation at the 45 K–50 K detector stage, 2 mW–3 mW are sufficient to meet the stability requirements. This set of BC is identified by the string "JT26mW" because of the BC type and value assigned to the JT cold end.

4.8.2 Other BC considered

The JT cooler characteristics pose questions on the best BC which model its thermal behavior. In the ESATAN-TMS Workbench is not possible to model heat transfer in fluids. This can be done outside the Workbench using the Fluid Heat Transport System (FHTS) extension which enables the combined thermal/hydraulic solution of piped fluid networks. The fluid network shall be programmed in the ESATAN-TMS language (MORTRAN) and eventually inserted in the Workbench generated analysis file. This solution can be potentially developed at a later analysis levels when the PLM and in particular the JT cooler characteristics and its interfaces are more detailed.

Two ways of modelling the JT cold end with the available BC types in the Workbench are:

- assigning a total area heat load (Neumann BC type),
- assigning a fixed boundary temperature (Dirichlet BC type).

Both solutions are a simplification of the real thermal behavior. As explained in subsection 2.4.3, the expanded Neon shall be liquid at its boiling temperature in order to provide stability with the AIRS detector interface. This assumption

Case name	JT cold end BC type and value	VG3 BC value
JT26mW	Total area heat load, −26 mW	320 mW
JT50mW	Total area heat load, −50 mW	500 mW
JT100mW	Total area heat load, −100 mW	500 mW
JT150mW	Total area heat load, −150 mW	500 mW
JT28K	Temperature, 28 K	500 mW

Table 4.9: *Difference between the five considered BC cases*

can be satisfied or not, having at the cold end a complete liquefied Neon, a two-phase fluid or still Neon at vapour state, depending on the thermal network solution.

Other sets of BC have been considered to see how the different JT cold end modelling approaches affect the thermal solution. The "JT26mW" BC set is considering a total area heat load of −26 mW. Three additional sets with increased total area heat load have been considered: −50 mW, −100 mW and −150 mW. Since the JT cryocooler heat lift is higher, it is also expected that the Neon mass flow is increased and consequently the pre-cooling heat interception at the VG3. A value of 500 mW heat load on the VG3 node has been considered for all these three BC cases. Another case specifies the BC on the JT cold end as a 28 K boundary temperature, and 500 mW of heat load on the VG3. The differences between the five different BC cases are highlighted in Table 4.9.

4.9 Analysis cases

The final stage in ESATAN-TMS Workbench is the generation of the thermal analysis file which is used by the thermal analyser to solve the thermal model. The definition of the analysis file is specified within an analysis case. Each analysis case has been defined including a single radiative case (one S/C attitude) and a single BC case. Considering the seventeen radiative cases and the five BC case there are 85 possible analysis cases to be defined. The ARIEL S/C first version in ESATAN-TMS has been study with 17 analysis cases each one with one of the different attitude cases and all with the same "JT26mW" BC case. Other analysis cases defined by different combinations of radiative and BC cases have been solved in the updated and modified models. In the following chapters, each analysis case is identified by the a string which specify first the BC case and then the Euler angle value and rotation axis of the radiative case. For example, "JT150mW-y-10deg" refers to the analysis case which has been assigned the JT150mW BC case and the radiative case with a rotation along the Y axis of $\psi = -10°$.

The solution routine adopted in all analysis cases is the "SOLVFM" which calculates the model steady state solution by full matrix inversion. The output calls generate a TMD file which stores thermal information to visualize results directly on the 3D model in the Workbench and a comma separated value files containing the temperature, capacitance, internal power of each node, the GLs

and the GRs between each couple of nodes. The data contained in those csv files has been post-processed using MATLAB.

Chapter 5

Updates to the baseline model and results

This chapter describes the iterative process that staring from the results of the first version of the ARIEL S/C model, built in the previous chapter, has led to the ARIEL S/C baseline in ESATAN-TMS.

5.1 Results of the first version

In the ARIEL S/C first version Workbench, 17 analysis cases have been defined and solved, each one corresponding to a different satellite attitude. The BC case assigned to all them it the "JT26mW". Figure 5.1 shows the temperature distribution results of the "JT26mW-0deg" case. In this case, the SVM temperatures go from the solar cells at around 358 K to the SVM/PLM plate upper surface at 250 K. SVM internal components are at room temperature: electronic box with the lowest temperature is at 280 K while the one with the highest assigned power dissipation is at 320 K.

The VGs have average temperatures of 170 K, 101 K and 52 K. The bottom figure shows a detailed view of the PLM main units with a finer temperature scale, which allows to appreciate detailed thermal gradients. The effect of the 320 mW heat load BC applied on one VG3 node is visible on the VG3 temperature distribution which is not uniform. The node where the BC is applied is the one with the highest temperature ($\sim$ 55 K), coloured in dark red. TOB, IOB and IB temperatures are around 44 K, representing the last PLM passive cooling stage. M1 and M2 are also around 44 K, well below their requirements limit (70 K). FGS and AIRS components are at around 45 K. They are just few Kelvin below their requirement limits, except for the AIRS detector which, having the lowest temperature requirement (40 K), is above the limit. The 26 mW absorbed heat BC, the JT cold end is at 41 K, not enough to bring AIRS detector below its limit.

Even if not all temperature requirements are respected, the first results are

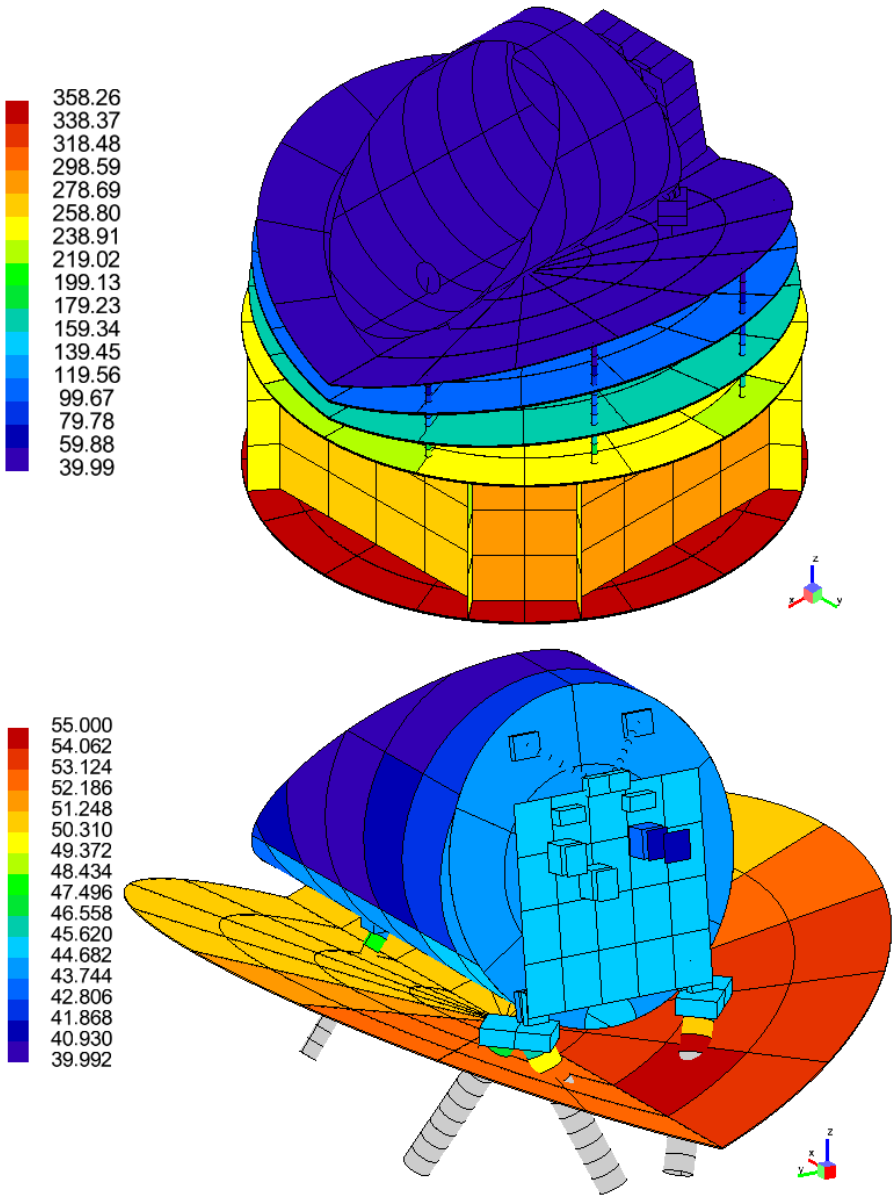

Figure 5.1: *ARIEL 1.0 temperature distribution ESATAN-TMS solution for the "JT26mW-0deg" case. Entire spacecraft (top), cold PLM main units (bottom). The IB and the FGS/AIRS module boxes are hidden to show internal components.*

very encouraging because, in general, the built ARIEL S/C in ESATAN-TMS as described in the previous chapter is consistent with the scientific consortium and ESA studies. The good correspondence of the estimated components' temperatures can be considered as a general confirmation of the validity of the ESATAN-TMS built S/C.

Problems arise when satellite attitude is changed through the considered rotations around the X and the Y axes. Figure 5.2 shows the FGS and AIRS components temperatures for all rotated attitude considered with "JT26mW" BC. The steady state solutions of the analysis cases defined with rotated attitudes shows substantial PLM temperature increase with respect to the nominal case. After 10° rotations AIRS-FGS temperatures overstep the requirement limits.

Temperature increases for positive and negative attitude rotations along the X axis are approximatively the same. This is not true for Y axis rotation: AIRS and FGS experience an higher temperature increase for positive ψ Euler angles. This happens because externally the ESATAN-TMS S/C is symmetric with respect to the X-Z plane and not to the Y-Z plane. A positive ψ causes the Sun to illuminate the X-negative satellite side. The entering solar power is then concentrated on the back side of the satellite, where the IOB and IB are located. The attitude case with $\psi = +25°$ is therefore considered the worst case.

Figure 5.3 plots the maximal, mean and minimal node temperature of the three VGs. The mean is weighted by nodes capacitance. Figure 5.4 shows the total solar absorbed power by each VG. Both figures refer to rotations along the Y axis. The second VG experiences the highest increase of temperature because it has a higher absorbed solar power. It can be noticed that for $\psi = \pm 5°$, the VGs' temperature increase is much lower than for higher rotation angles. In fact, the absorbed solar power for $\psi = \pm 5°$ is zero for all VGs' and the AIRS-FGS components remain below the requirements limits. The same behavior occurs for rotation along the X axis. The correlation between VG absorbed solar power and VGs/scientific instrument temperature increases, makes clear that ARIEL PLM thermal performance decisively deteriorates if the solar rays enter the PLM.

These first solved analysis cases show that the first version of the ARIEL S/C in ESATAN-TMS is completely not able to maintain PLM scientific instrumentation below corresponding temperature limits for rotation angle greater than $\pm 5°$. This issue suggests to review the geometrical assumptions made for the VGs sketching in order to avoid the Sun entering the PLM. For the zero rotation case, FGS/AIRS components are close to their requirement limits (telescope mirrors are well below the limit). AIRS detector is instead above. This second issue suggests instead to analyse the BC applied on the JT cold end and the GL values assigned between FGS/AIRS equipment and their interfaces.

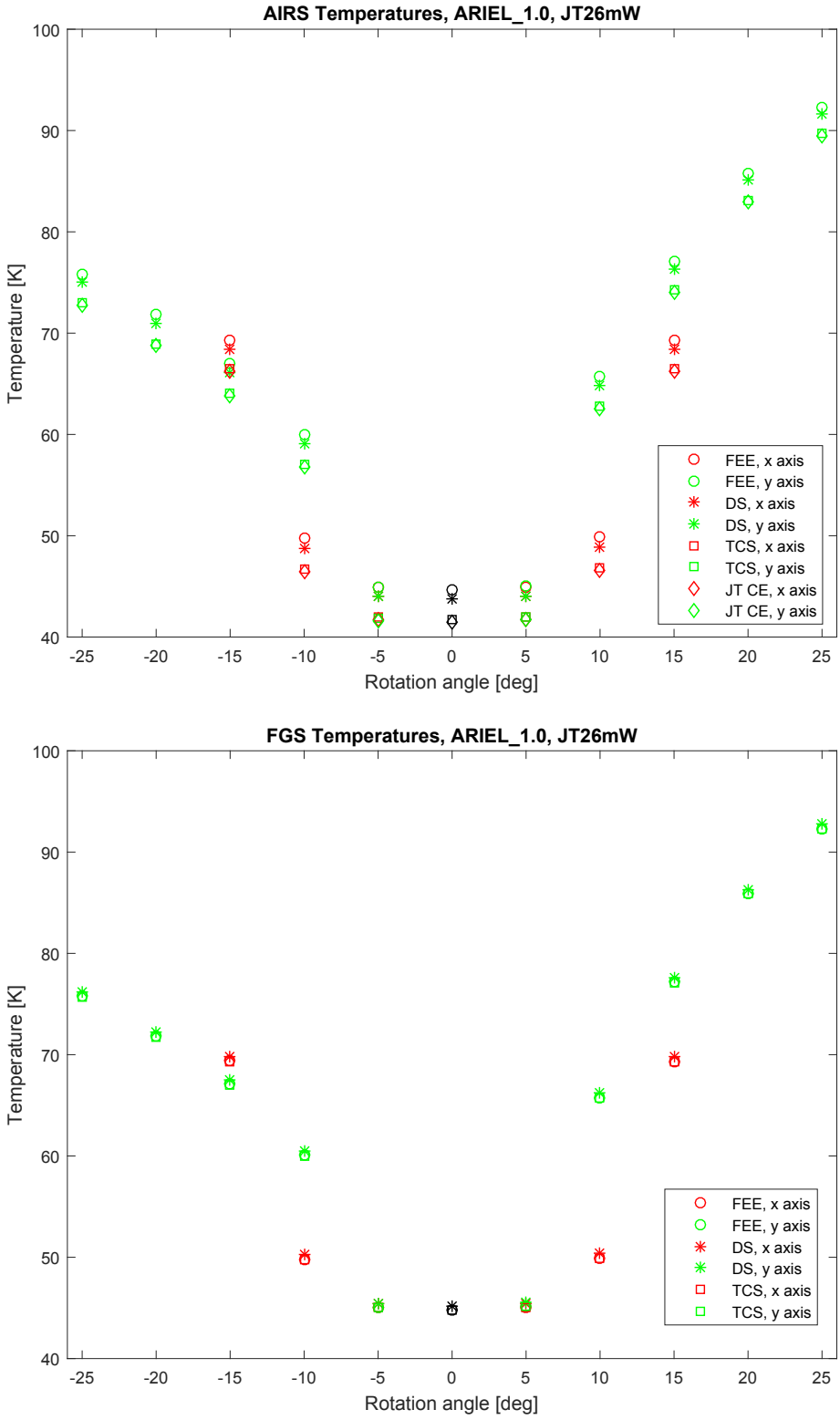

Figure 5.2: *ARIEL 1.0 AIRS and FGS temperatures for all attitude cases and JT26mW BC case*

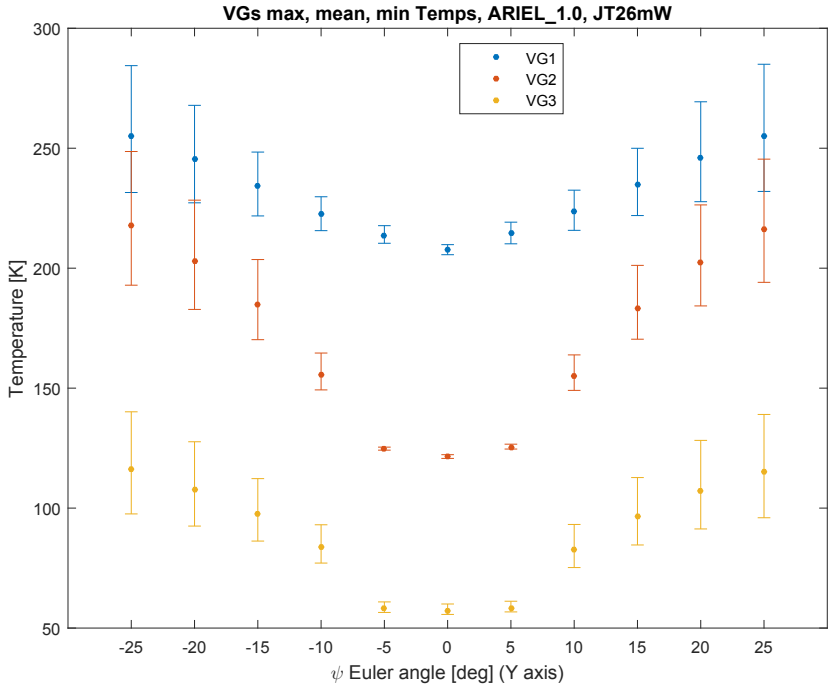

Figure 5.3: *ARIEL 1.0 VG temperature for rotations along Y axis*

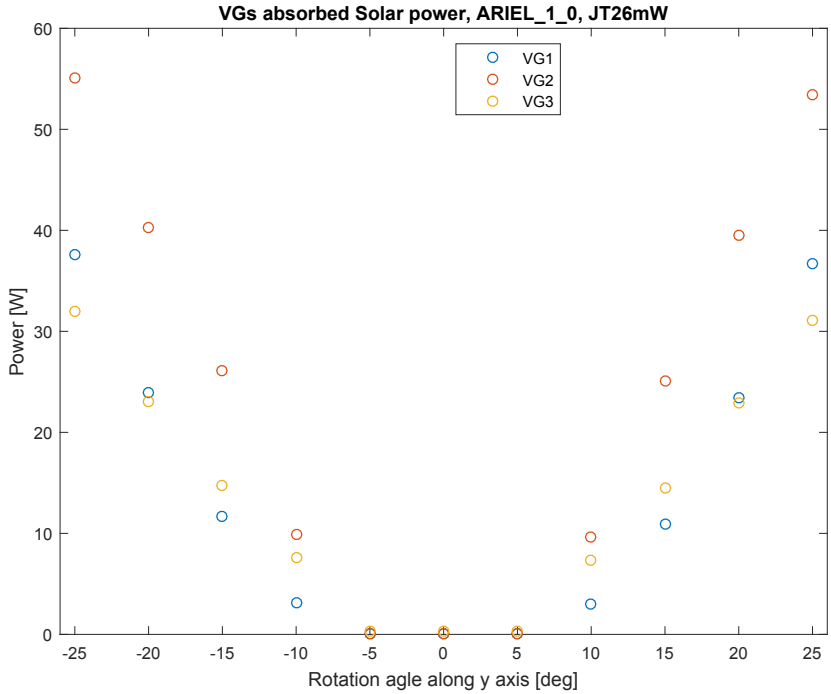

Figure 5.4: *ARIEL 1.0 VG solar absorbed power for rotations along Y axis*

	Case 1	Case 2
Model name	ARIEL 1.1	ARIEL 1.2
Modified parameter	SVM top and bottom plate radii	VG radii
Original value	1.35 m	1.32 m
Modified value	1.53 m	1.15 m
Expected total Δm	+12.64 kg	−17.37 kg

Table 5.1: *Parameter of the two trade-off cases in geometrical update.*

5.2 Updates in the ESATAN-TMS model

5.2.1 Geometrical updates

In order to avoid the Sun rays hitting the VGs two possible solutions have been considered:

1. increase the solar array and SVM/PLM plate radii, maintaining the same dimension of the VGs.
2. decrease the VGs' radii, maintaining the same dimension of the SVM plates.

Both solutions have advantages and drawbacks. In particular, lowering the VGs' radii means to decrease the available radiating area for heat rejection to deep space, corresponding in an average increase of the VGs' temperatures and, consequently, of the cold PLM instruments. On the other side, increasing the SVM solar array and SVM/PLM plate radii generates a heavier and bigger satellite. A trade-off between the two cases must be found. In both solutions the radii have been modified from the initial values as minimum as possible to avoid the Sun hitting the VGs for attitude rotations up to 25°. Thicknesses have been left unchanged. In the first solution, SVM plates radii have been increased from 1.35 m to 1.53 m. The S/C dimension increase is still within the volume limitation of the launcher fairing both of Ariane 6.2 (baseline) and Soyuz ST (backup). In the second solution, VGs' radii have been decreased from 1.32 m to 1.15 m. From the mass budget contained in [2], the SVM bottom and top plate masses are respectively 24.83 kg and 19.60 kg, VGs' total mass is 72.22 kg, which divided by three gives 24.07 kg. Considering the shape of the SVM plates and the VGs as discs and maintaining the original thickness in each element, in the first solution the SVM bottom and top plate mass gains are 7.09 kg and 5.55 kg respectively. In the second case there is a mass reduction of 5.79 kg for each VG. Table 5.1 summarizes the characteristics of the two cases. For each case, a new ESATAN-TMS model has been created form the first version and modified. The first case has been called ARIEL 1.1, the second ARIEL 1.2. The "JT26mW-0deg" and "JT26mW-y25deg" analysis cases, representing so far the cold and hot conditions, have been solved in both models.

In the ARIEL 1.2, after the VGs' radii reduction, for a rotation with $\psi = 25°$ the top right and left edge of the IB are exposed to direct solar rays. Even if the illuminated area is very small it is enough to warm the IB bringing detectors temperatures over the limits. Solution to this problem has been found changing

	ARIEL 1.1 mean T [K]		ARIEL 1.2 mean T [K]	
Component	$\psi = 0°$	$\psi = 25°$	$\psi = 0°$	$\psi = 25°$
SVM/PLM plate	229.8	277.0	236.6	277.7
VG1	151.7	187.5	154.7	186.0
VG2	93.3	114.0	94.6	113.0
VG3	50.4	55.9	53.2	58.1
TOB	43.6	47.2	44.8	47.9
IOB	43.9	47.5	45.1	48.2
M1	43.6	47.3	44.8	48.0
M2	42.6	46.9	44.3	48.0
FGS CFEE	43.9	47.5	45.1	48.2
FGS TCS	43.9	47.5	45.1	48.2
FGS detectors	44.4	48.0	45.6	48.7
AIRS CFEE	43.9	47.5	45.1	48.2
AIRS TCS	40.8	44.5	42.0	45.1
AIRS detector	42.9	46.5	44.1	47.2
JT Cold end	40.6	44.2	41.7	44.9

Table 5.2: *Main component average temperatures of the two trade-off cases in geometrical update. BC are the "JT26mW" in all cases.*

the IOB/IB inclination and reducing the IB box dimension so that it is always in shade even for $\psi = 25°$. The IOB inclination has been turned from 100° to 105° which is the same inclination of the TOB. All geometries attached to the IOB, including the IB, have undergone the same change. The IOB mechanical supports have been also adapted to this modification. The supporting bipod between top side of the TOB and IOB has been sketched smaller. The same modifications have been made also in the ARIEL 1.1, so that the differences between the two are only the dimensions of the SVM plates and VGs. The analysis cases have been solved again. Average temperatures of the main S/C components are summarized in Table 5.2. Geometrical differences and temperature distribution can be visualized in Figure 5.5.

In both ARIEL 1.1 and ARIEL 1.2, the VGs are not exposed to solar radiation in all rotation cases, which was the aim of the geometrical update. Without solar absorbed power by the VGs, the PLM component temperature excursions are lowered significantly. In the first version, ARIEL 1.0, FGS and AIRS components go from circa 44 K at zero angles (cold case) to 92 K at $\psi = +25°$ (hot case) (see Figure 5.2) As shown in Table 5.2, both ARIEL 1.1 and ARIEL 1.2 FGS/AIRS temperature excursion between cold and hot case in around 3 K. The geometrical update is successful in both modified models.

Comparing the computed temperature of ARIEL 1.1 and 1.2, it can be noticed that, in general, PLM temperatures in ARIEL 1.1 are lower than in ARIEL 1.2, as expected. Focusing on the FGS/AIRS components, which are the equipments with temperature close the requirement limits, the difference in each case is around 1 K–1.5 K. The ARIEL 1.1 achieves lower temperature but at the cost of an estimated mass increase of 30.0 kg with respect to the ARIEL 1.2. In both

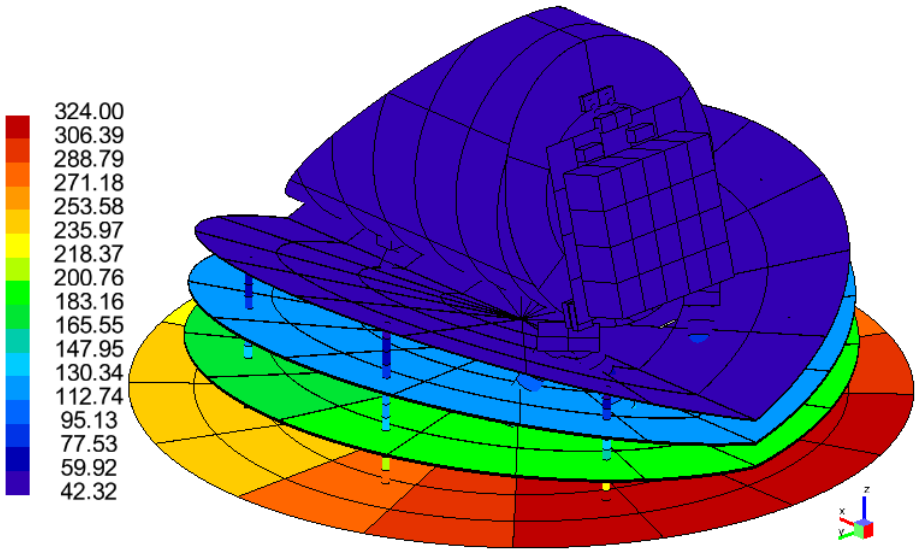

(a) ARIEL 1.1 ($r_{\mathrm{SVM}} = 1.53\,\mathrm{m}$, $r_{\mathrm{VG}} = 1.32\,\mathrm{m}$)

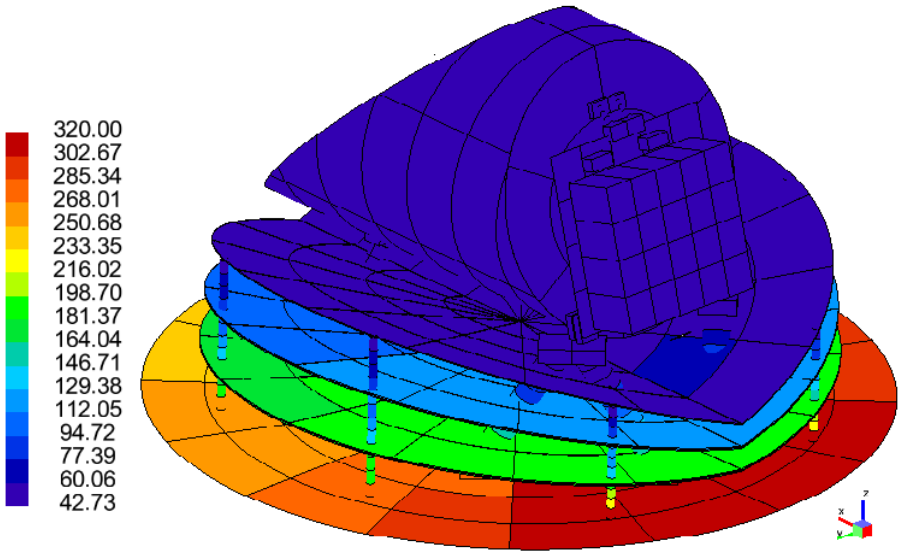

(b) ARIEL 1.2 ($r_{\mathrm{SVM}} = 1.35\,\mathrm{m}$, $r_{\mathrm{VG}} = 1.15\,\mathrm{m}$)

Figure 5.5: *ARIEL 1.1 and 1.2 SVM top plate and PLM temperatures for* $\psi = 25°$

	GL(detector,TCS) [W/K]	GL(TCS,JT cold end) [W/K]
ARIEL 1.2	0.01	0.1
ARIEL 1.3	0.05	0.2
ARIEL 1.4	0.05	0.1

Table 5.3: *Assigned GL values between AIRS detector, TCS and JT cold end for the three considered cases.*

model the AIRS detector is the only component which oversteps the requirement limit (40 K). The other FGS and AIRS components are few Kelvin below their limits. As described in subsection 2.4.2 and in 2.4.3, the FGS and AIRS detectors thermal designs are different: the first is based on only passive cooling while the second is thermally connected to the cold end of the JT active cooler. It is expected that the AIRS detector temperature can be lowered increasing the cooling power delivered by the JT fluid loop. The different design in ARIEL 1.1 and 1.2 impacts the passive cooling performance of the PLM, affecting steady state temperatures of the equipments designed to be cooled by passive means. Since all PLM components, except for the AIRS detector, are still below their limits in both model, it has been decided to keep the lighter ARIEL 1.2 model for the next analyses, more challenging in terms of temperature. In the next chapter parametric analysis on critical S/C design parameter investigates if additional temperature margin can be achieved having less increase on mass and dimension.

5.2.2 Thermal updates

AIRS detector is few Kelvin above the requirement limit (40 K). The JT cold end temperature excursion goes from 41.7 K to 44.9 K suggesting that an increase in JT cooling power is necessary. In addition, the temperature gap between TCS and detector is much larger than the one between TCS and JT cold end. The two couple of GL values between these elements can be optimized in order to help the detector achieving a lower temperature. As reported in subsection 4.6.5, in ARIEL 1.0, and consequently in ARIEL 1.2, the following values have been assigned to the user-defined conductors: GL(detector,TCS)= 0.01 W/K and GL(TCS,JT cold end)= 0.1 W/K. To lower the temperature gap between JT cold end and the detector, it has been decided to increase the GL conductances.

An new model 1.3, identical to the 1.2, with GL(detector,TCS) changed to 0.05 W/K (five times higher) and GL(TCS,JT cold end) to 0.2 W/K (two times higher) has been created. A mixed case, named 1.4, with GL(detector,TCS)= 0.05 W/K and GL(TCS,JT cold end)= 0.1 W/K has been considered. Table 5.3 summarized the GL values assigned in the three considered cases. Figure 5.6 compares the AIRS component steady state temperature at different boundary conditions for the worst case condition ($\psi = 25°$). For the first 4 BC cases (imposed power at JT cold end) the detector temperatures are approximatively the same in the three models in each BC case. With a Neumann boundary condition (the power absorbed is fixed) detector steady state temperature has a very low dependence on the GL values. TCS and JT cold end temperatures

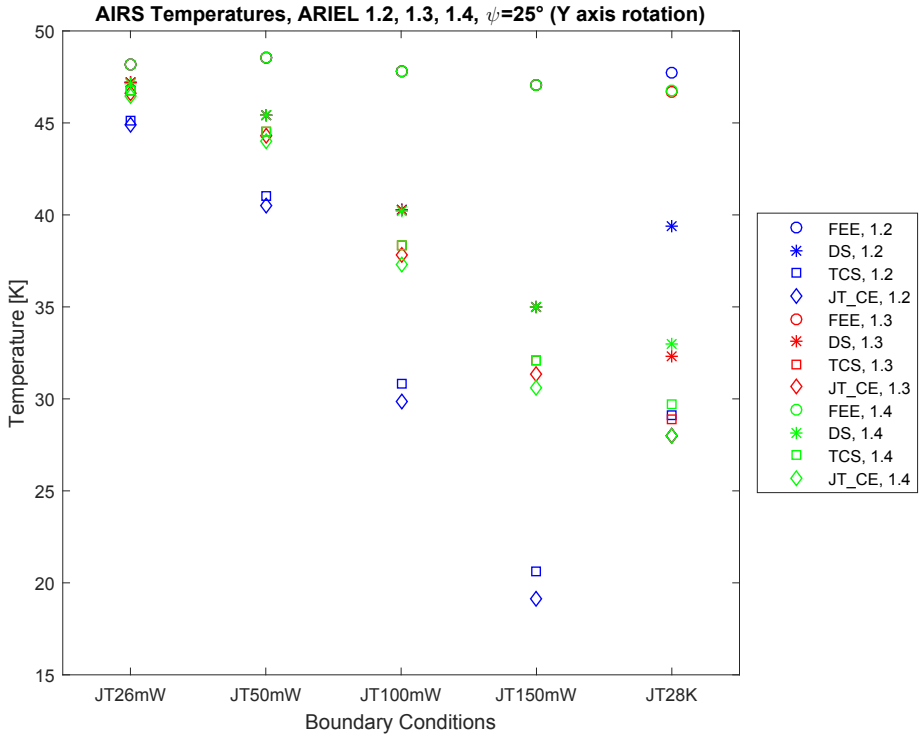

Figure 5.6: *AIRS component temperatures in the three model with different GL values. The plotted analysis cases are for all BC at* $\psi = 25°$.

depend instead on the chosen JT cooling power. In the JT28K case, Dirichlet boundary condition is applied on the JT cold end (temperature is fixed), detector steady state temperature depends on the GL values. In ARIEL 1.3 and 1.4 the gap between TCS and detector temperature is lower with respect to the 1.2, consistent with the increased GL value between them. The gap between TCS and JT cold end is higher in ARIEL 1.4 than in ARIEL 1.3 because of the lower GL value connecting these two elements. These differences can be better appreciated looking at the JT28K case where the JT cold end is fixed at 28 K. In ARIEL 1.2 the detector is at 39.4 K and the TCS at 29.1 K, which is a quite high gap. With higher GL values, in ARIEL 1.3, detector and TCS temperatures are reduced to 32.3 K and 28.8 K respectively. AIRS detector is brought enough below its requirement limit. Passing from ARIEL 1.3 to ARIEL 1.4 only the GL(TCS,JT cold end) is lowered causing a small increase in detector and TCS temperatures. The ARIEL 1.4 has been selected as the best case since it maintain more balanced temperature gaps between detector, TCS, and cold end. It is expected that this would bring benefit in the active temperature stabilization through a PID controller on the TCS, without increasing to much the detector working temperature. This is a compromise between detector temperature and necessary efforts to achieved the required temperature stability.

The BC case JT150mW and JT28K achieve similar temperatures in AIRS components and maintain the AIRS detector at a temperature around 33 K–35 K, having a 5 K margin from its requirement limit. The similarity between the two

cases means that the two BC are approximately exchangeable in the thermal network, built through the ESATAN-TMS Workbench in the ARIEL 1.4. The Neon expanding through the JT orifice becomes liquid at an average temperature of 28 K. The Neon experiences at this temperature a phase change absorbing latent heat maintaining constant its temperature. Therefore the JT28K condition can be considered a more realistic representation with respect to the JT150mW to simulate the the JT cold end and other nodes thermal behavior. The assumption of a fixed temperature BC should be compatible with the cooling power available in the JT cooler which mainly depends on the fluid loop mass flow. In this case, a 28 K temperature at the cold end is achieved with a cooling power around 150 mW.

5.3 Baseline results

The geometrical and thermal updates has led to the model ARIEL 1.4 which is now considered the baseline.

5.3.1 Temperature results

Table 5.4 shows the maximal, mean and minimal nodal component temperatures of the ARIEL 1.4 main components for the cold (no rotation) and hot ($\psi = 25°$) cases. BC are the JT150mW. The results show that in general the proposed PLM cooling architecture is valid to bring the cryogenic instruments at their design working temperatures. The SVM internal units are always at room temperature due to the very stable environment in the operational orbit which maintains S/C approximatively at the same distance from the Sun and without eclipses. At this level of analysis they do not represent any issue. The two telescope mirrors have maximum temperature which is well below their limit (70 K). The FGS/NIRP and AIRS components have simulated temperatures which are closer to the requirements limits. In the FGS/NIRP module, the detector has the highest temperature and the lowest limit. The CFEE has lower temperature since it is outside the IB, directly coupled radiatively with the environment and conductively with the IOB. The detector, instead, is inside its module box which is contained into the IB. FGS detector is thus more isolated from its cooling stage. In the hot case, the detector is around 2.5 K and 3.0 K below the requirement while the CFEE 8.0 K. Concerning the AIRS instrumentation, the CFEE has similar temperature to the FGS one and same limit. These two units have been sketched identically and assigned same thermal properties. The detector temperature is at 35.0 K, so 5 K below the limit. The FGS and AIRS detectors are the components which are closest to their temperature limits.

5.3.2 Discussion on margins

For space systems operating at cryogenic temperatures, a margin on heat loads is more adequate than margins on temperatures. For a program in the early development stage a heat load margin of 50% is suggested [8]. Heat loads applied

	No rotation		$\psi = 25°$	
Component	Min T [K]	Mean T [K]	Mean T [K]	Max T [K]
Solar array	357.3	359.4	351.9	353.6
SVM unit +X	268.9	269.0	270.4	270.5
SVM unit +X-Y	296.5	296.7	298.7	298.8
SVM unit -Y	317.7	318.0	324.7	324.8
SVM unit -X-Y	304.7	304.9	326.9	326.9
SVM unit -X+Y	284.0	284.2	309.5	309.6
SVM unit +Y	290.6	290.9	324.7	324.9
SVM unit +X+Y	290.7	290.9	293.1	293.2
SVM/PLM plate	215.7	236.6	277.7	320.4
VG1	153.3	154.7	185.9	196.8
VG2	94.3	94.7	112.1	113.3
VG3	52.6	54.1	58.7	62.4
TOB	43.8	43.9	47.1	47.2
IOB	43.9	43.9	47.1	47.1
M1	43.9	43.9	47.1	47.1
M2	44.7	44.7	48.3	48.3
FGS CFEE	43.9	43.9	47.1	47.1
FGS TCS	44.0	44.0	47.1	47.1
FGS detectors	44.4	44.4	47.6	47.6
IB	43.8	43.9	47.0	47.0
AIRS CFEE	43.9	43.9	47.1	47.1
AIRS TCS	28.8	28.8	32.1	32.1
AIRS detector	31.7	31.8	35.0	35.0
JT Cold end	27.3	27.3	30.6	30.6

Table 5.4: *Main component maximal, average and minimal node temperatures of the ARIEL 1.4. for the "JT150mW-0deg" and "JT150mW-y-25deg" cases.*

on the cryogenic FGS/NIRP and AIRS components are derived from the values considered in the proposal document [1], summarized in Table 2.5. In these values a 50% margin has been already taken into account. Additionally, some conservative thermal assumptions have been made during the development of the thermal model in the ESATAN-TMS Workbench. The most important are summarized below.

- The MLI on both external sides of the SVM/PLM plate has been simulated assigning a low emittance/low absorptivity thermo-optical property directly on the SVM/PLM external surfaces;
- The power intercepted by the three VGs, coming from harness and JT fluid pre-cooling, has been assigned to a single node of the topmost VG. Additionally, this node is at the intersection of one of the rear-central bipod leg.
- The assigned conductance between the two facing nodes of the AIRS detector and its module box geometries is 0.01 W/K, instead of the assumed 0.001 W/K in the EChO design.

- The considered heat load of the FGS and TCS detector has been applied also to the redundant detector and the relative TCS.
- The assigned optical property to the IB rear surface (the side facing the deep space) is black paint ($\varepsilon = 0.90$) instead of open honeycomb ($\varepsilon = 0.94$).

The simplified model of the MLI does not take into account the thermal gradient between internal and external layers of the MLI because no nodes are allocated for the MLI. SVM/PLM plate external surface and the MLI are considered through the same node, so they have the same temperatures. This model acts as a single layer insulation neglecting the insulating effect of multi layers which would create a thermal gradient between the two outer layers. This single-layer model is conservative since leaves the SVM/PLM plate more sensitive to thermal environment variations. The solar radiation is directly absorbed by the SVM/PLM nodes and not by the MLI external layer which would then create a temperature gradient from the plate. SVM/PLM plate nodes run hotter incrementing the heat leaks to bipods and struts which are directly connected to the plate. A more refined model of the MLI should consider an additional set of nodes allocated for the external layer. These nodes are then thermally coupled with an appropriate insulating conductance to the surface plate nodes. A MLI refined model is treated in section 6.4.

The harnesses connecting cold PLM electronic equipments to the SVM units and the JT fluid pipe are thermally connected the all three VGs in order to intercept the heat before it reaches the cold PLM components. Allocating the whole estimated heat in the top VG is a worst case assumption since the heat is concentrated closer to the PLM cold components as it would be in the real case. In particular, the node, where the total heat load BC has been applied, is connected with a 1 W/K user-defined conductance to the relative bipod leg node. The heat has a shorter path in the thermal network to the FGS/AIRS components. In the real design, heat interception occurs at different points in all the three VGs in order to distance the heat from sensible PLM equipments and distribute it as much as possible over the VGs' radiating area.

The AIRS detector should be decoupled from its module box and the IB as much as possible in order to isolate it from heat coming from the other components supported on the IB (CFEEs, FGS/NIRP equipments). A higher conductance of its interface with the IB has as consequence an increase in its average temperature, requiring a higher cooling power from the JT cold end.

In addition to the 50% margin on cryogenic component heat loads and the conservative assumptions made in the development of the ESATAN-TMS S/C model, according the ESA margin management [17], a 5 K margin on the temperature of cryogenic components has been considered. One of the goals of the ARIEL S/C thermal architecture analysis is to build a thermal model compliant with the temperature requirements with margins. The margins on temperatures and heat loads, combined with the conservative assumptions should provide a thermal design with an adequate level of reliability for an early phase A mission project.

Figure 5.7 shows the temperature excursion between cold and hot conditions of the PLM units with thermal requirements in ARIEL 1.4. The dark grey bars

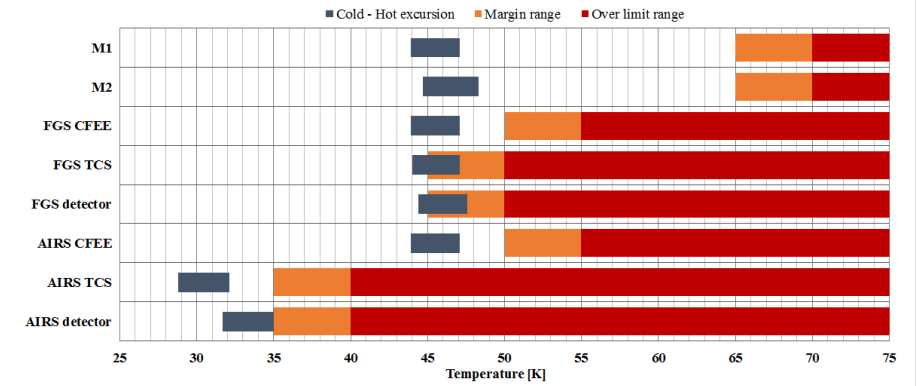

Figure 5.7: *Temperature bar chart for PLM units with thermal requirements in ARIEL 1.4*

describe intervals from the minimal node temperature in cold case to the maximal in hot case. Red bars represent the temperature ranges for each component over its requirement. The orange bars account for the assumed 5 K margin. The critical components are the FGS and AIRS detectors which are the closest to their temperature requirements. The FGS detector in the hot case is inside the margin range. The AIRS detector, with the 150 mW of JT cooling power, is exactly at the margin limit. The next chapter analyses different S/C models to understand how critical design parameters influence the PLM thermal performance with the aim of finding new possible solutions to increase the margins on the results.

Chapter 6

Parametric analysis

The influence on thermal performances of some critical geometrical and thermal parameters is analysed in this chapter. Each modification has been made on a ESATAN-TMS model copy of the baseline ARIEL 1.4.

6.1 The PLM passive cooling

The VGs are the most efficient component for the PLM cooling. They are able to create passively a thermal gradient going from the SVM/PLM plate at room temperature to the 60-50 K of the third VG in around 50 cm of vertical space. Also the telescope baffle, black paint coated, contribute to the PLM cooling rejecting heat to the deep space. This section analyses the thermal influence of these elements considering hypothetically configurations with a lower or higher number of VGs or without the baffle, in order to understand the cooling contribution of each element.

6.1.1 Description of cases

Firstly, a new model, called ARIEL 2.1, has been created from the baseline deleting the VG1 (bottom VG). Another model, named ARIEL 2.2, has been created adding a new VG. In ARIEL 2.2, the lowest and topmost VG have maintained the original inclination (7° and 21° respectively) while the two intermediate VGs have been inclined by 12° and 17°. The vertical distance between the VGs has been rearranged in order to maintain approximately the original distance between each VG couple (10 cm). In particular, the topmost VG has been shifted a few centimetre upward to allow the additional VG accommodation. The model ARIEL 2.3 is identical to the baseline but without the telescope baffle. This is actually a non realistic case since the baffle is necessary to the scientific observation activities. The last case considered, ARIEL 2.4, is composed by a baffle which has an assigned bulk material with enhanced thermal conductivity. Looking at Figure 5.1 (bottom), there is a thermal gradient along the telescope baffle. Temperature difference between the TOB and baffle nodes with with the

Model name	Modification
ARIEL 2.1	VG1 deleted, only two VGs remain
ARIEL 2.2	a fourth VG is added
ARIEL 2.3	Telescope baffle deleted
ARIEL 2.4	Tel. baffle bulk material is Al alloy 5056 instead of honeycomb

Table 6.1: *Modifications of the four considered cases in PLM passive cooling analysis*

lowest temperatures is around 5 K. Baffle heat rejection to deep space could be increased enhancing the thermal conductance along the baffle structure from the TOB/IOB. In the baseline the bulk material assigned to the telescope baffle is the honeycomb, as explained in subsection 4.6.3. In ARIEL 2.4 the Al 5056 alloy has been assigned to the baffle. The thickness has been maintained as the original (0.0224 m). Table 6.1 summarizes the considered cases.

From mass budget of the CDF results [2], a VG has approximately a mass around 25 kg. The ARIEL 2.1 would decrease the S/C total mass of one VG, while the ARIEL 2.2 would increase it of one VG neglecting the mass of mechanical interfaces and end-fittings. The other two cases are actually unrealistic. A baffle with the same volume but made of Al alloy would have a mass greater than 500 kg, which is almost two times the total PLM mass. Anyway these two cases can be useful to better understand parameter influence on thermal performance.

6.1.2 Discussion of results

Analysis cases representing the hot and cold case conditions have been solved in each model. The cold case is for zero attitude rotation (the nominal case), the hot case is for a $\psi = +25°$ rotation. The cold case never represents a concern since the SVM internal components are always above the required $-20\,°C$ limit, and for the PLM scientific equipments, the colder they are the better it is. For this reason, focus is given on the hot condition results which are close to violate the requirement limits. Analysis cases with JT150mW and JT28K have been solved to see if the two conditions remain approximately exchangeable as for the baseline solution. Table 6.2 reports the main component temperatures for the "JT150mW-y25deg" analysis case of the baseline model (ARIEL 1.4) and of the modified models considered in this section (ARIEL 2.x). Figure 6.1 shows the simulated temperature distribution for the ARIEL 2.1 and 2.2, displayed on the PLM and SVM/PLM plate.

ARIEL 2.1 Result of the ARIEL 2.1 shows a substantial increase in the FGS component temperatures. With just two VGs passive cooling is less efficiency as expected. FGS detector and its module box, containing its related optics, overstep the requirement limit (50 K). With respect to the baseline, FGS temperatures have increase of around 6 K, which is quite a lot considering that FGS components are cooled passively, so there no other possibilities in this thermal design to bring down temperature passively in a way more efficient in term of

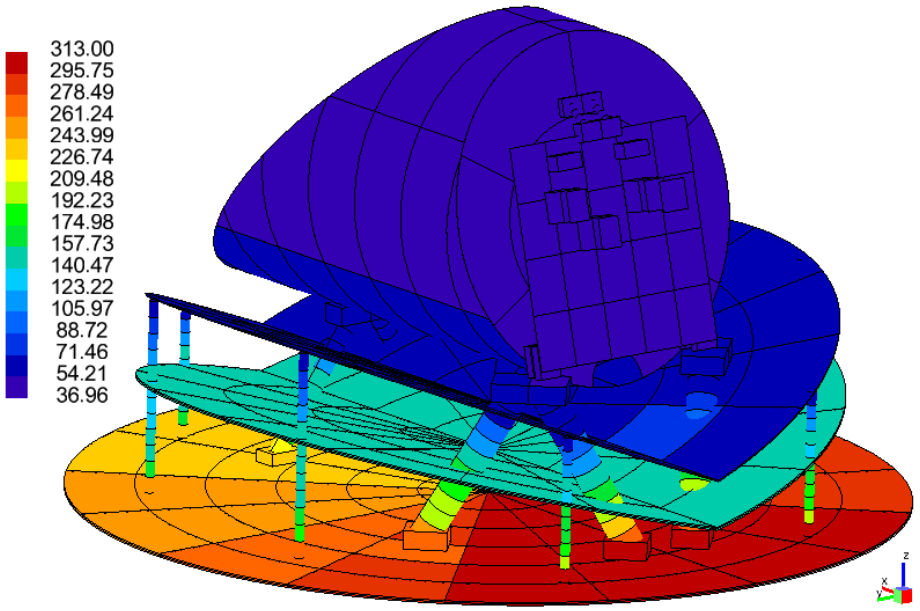

(a) ARIEL 2.1

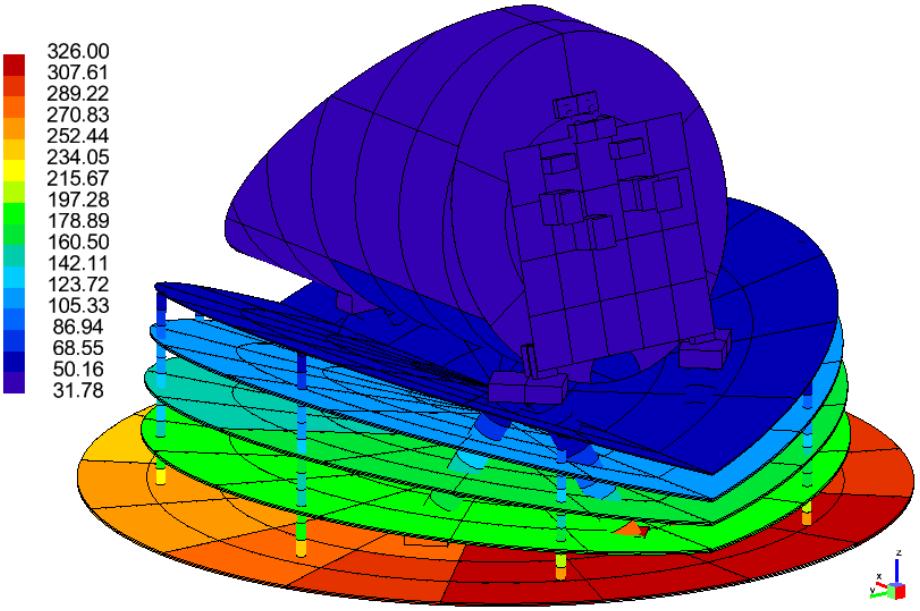

(b) ARIEL 2.2

Figure 6.1: *ARIEL 2.1 and 2.2 SVM top plate and PLM temperatures for "JT150mW" BC and $\psi = 25°$ attitude rotation. The IB and the FGS/AIRS module boxes are hidden to show internal components.*

	Mean T [K]				
ARIEL	1.4	2.1	2.2	2.3	2.4
SVM/PLM plate	277.7	273.0	281.5	277.7	277.5
VG1	185.9	147.1	191.2	186.0	185.8
VG2	112.1	68.1	162.3	111.9	112.0
VG3	58.8	–	108.4	56.4	58.4
VG4	–	–	60.7	–	–
Baffle	46.8	53.0	47.7	–	46.5
TOB	47.1	53.3	48.2	46.7	47.0
IOB	47.1	53.3	48.2	46.7	47.0
FGS CFEE	47.1	53.3	48.3	46.7	47.1
FGS TCS	47.1	53.3	48.3	46.7	47.1
FGS detectors	47.6	53.8	48.7	47.2	47.6
AIRS CFEE	47.1	53.3	48.2	46.7	47.0
AIRS TCS	32.1	38.4	33.3	31.7	32.0
AIRS detector	34.9	41.3	36.2	34.6	34.9
JT Cold end	30.6	37.0	31.8	30.2	30.5

Table 6.2: *Comparison between baseline model (ARIEL 1.4) and modified models (ARIEL 2.x) main component average temperatures. Temperatures refer to the analysis case defined by the "JT150mW" BC and $\psi = 25°$ attitude rotation.*

mass. In addition, the computed JT cold temperature is 37.0 K (absorbed power of 150 mW), which is almost 10 K far from the nominal temperature (28 K) of the JT cold end, meaning that the JT shall deliver additional cooling power to have liquid Neon. In the configuration with just two VGs the heat load on both the FGS and AIRS components is too high. As seen in the previous chapter, enlarging the VGs and consequently the SVM plates with an increase in mass of around 30 kg would bring FGS temperature down of circa 1.5 K. It is thus better to maintain the third VG, which with an estimated mass of 25 kg is able to maintain FGS component temperature below the requirement limit.

ARIEL 2.2 Results of case with four VGs are quite unexpected since there is a general increase in the temperatures of the PLM components. The mean temperature of the topmost VG is almost 2 K higher with respect to the baseline. The fourth VG actually deteriorates the thermal performance in the PLM passive cooling. In this modified configuration, the VGs are quite close to each other, the heat rejection to deep space requires more multiple reflections since now the VG divergent path is narrower. A higher quantity of the heat emitted by the VG surfaces is reabsorbed.

ARIEL 2.3 The configuration without the telescope baffle gives cold instrument temperature distribution which is in general 0.5 K lower with respect to the baseline. The VG1 and VG2 have similar temperature while the there is a 2.4 K difference between the VG3. The assigned thermo-optical property to VG3 upper surface is open-honeycomb with an emissivity of $\varepsilon = 0.95$. The emissivity of the baffle external surface is instead black paint ($\varepsilon = 0.9$). The

configuration without the baffle allows higher heat rejection to deep space since now the VG3 upper surface has a greater view factor to the cold space. The suppression of the radiating area offered by the baffle is compensated by the VG3 central area which was prior obstructed by the baffle. Since the VG3 has a little higher emissivity, the heat rejected increased and FGS/AIRS temperatures are few tenth of Kelvin lower.

ARIEL 2.4 Temperature differences between the model with the baffle made of Al alloy and the baseline are on the order of the hundredth of Kelvin. The help in heat rejection to deep space given by an enhanced conductive baffle seems to offer benefits which are negligible related to the mass gain that they would require.

Conclusions The results have shown that the PLM configuration with three VGs offers the best condition for the FGS/AIRS temperature requirement fulfilment. The baffle dimensions seem to influence much less the PLM passive cooling ability rather than the VGs. A reduction in the baffle dimension, and thus the available radiating area, is compensated by the upper surface of the topmost VG which would have a larger view factor to deep space. The case with four VGs has put questions on the influence on thermal performance of the VG parameters, like the inclination and the distance between each others. In the next section, parametric analysis focuses on VG design parameters.

6.2 VGs dimension and inclination

The baseline ESATAN-TMS model has the VGs with the same radius equal to 1.15 m. VG radii have been lowered from the initial value of 1.32 m in order to avoid the Sun to illuminate them for all attitude rotation considered cases. This section considers model where the VG radii, inclination and vertical distance have been modified to analyse the impact on the thermal performances.

6.2.1 Description of cases

In previous models, the VGs have the same radius. A new model, ARIEL 3.1, with different VG radii have been sketched in the Workbench. The VG1 radius has been increase to 1.25 m, the VG2 to 1.20 m, the VG3 has been left with the original radius (1.15 m). It is expected that a VG radius increment offers more radiating area to heat rejection to deep space, so a benefit in passive cooling. It must be avoided to let the solar rays enter in the PLM. The VG1 is closer to the SVM/PLM so it remains in shade also for a higher radius enlargement. The VG3 is already at the limit. In geometrical updates of the previous chapter, it has been found the maximum radius value which allowed the VGs to be kept in shade for the highest considered attitude angle rotation. Increasing the VG3 radius would require also to increase the SVM/PLM plate radius.

Model name	Modified parameters	New parameter values
ARIEL 3.1	VG radii	1.25-1.20-1.15 m
ARIEL 3.2	VG inclination angles	7°-16°-28°
ARIEL 3.3	VG inclination angles	5°-10°-15°
ARIEL 3.4	VG inclination angles	3°-6°-9°
ARIEL 3.5	Vertical distance between VGs	5 cm each

Table 6.3: *Cases with modified VG parameters*

Another parameter in VG design that could affect their thermal performance is their angle inclination set. In the baseline, VG inclination set is 7-14-21 degrees. Three cases has been considered which have different angle inclination sets: ARIEL 4.2 with 7°-16°-28°, ARIEL 4.3 with 5°-10°-15°, and ARIEL 4.4 3°-6°-9°. The first has the VGs more inclined while in the other two the VGs are less divergent. It is expected that increasing the inclination angles, VGs are able to reject more heat to deep space, since the divergent path is enlarged for emitted ray multiple reflection.

The distance between the centerline of each VG couple and between the bottom VG and the SVM/PLM plate has been set to 10 cm in the baseline. The model ARIEL 4.5 considers a distance of 5 cm to see how this parameter influences the VG cooling. Lowering the distance could bring benefit in terms of S/C compactness, making the S/C smaller. The VGs are sketched closer to the SVM leaving additional free space between the topmost VG and the telescope baffle. Lowering the bipods and supporting struts would lower the S/C vertical dimension. The disadvantage is that shorter supports would less thermally isolate the PLM from the SVM since the their length is smaller. Anyway for this kind of analysis, the bipods and supporting struts have been left at their original height in order to understand the influence on only the VG vertical distance. Table 6.3 summarizes the considered cases with modified VG parameters

6.2.2 Discussion of results

Also in this parametric analysis, focus is given on the results of the analysis cases "JT150mW-y25deg" and "JT28K-y25deg". Table 6.4 reports the main component temperatures for the "JT150mW-y25deg" analysis case of the baseline model (ARIEL 1.4) and of the modified models considered in this section (ARIEL 3.x).

ARIEL 3.1 The case with increased first and second VG radii lowers the FGS/AIRS components temperatures around 0.2 K with respect to the baseline. In ARIEL 3.1, SVM top plate, VG1 and VG2 have higher temperatures while the VG3 lower with respect to the baseline. The VG1 and VG2 are able to isolate better the VG3 from the SVM top plate, maintaining a few tenth of Kelvin higher thermal gradient between the SVM and PLM. The cost of lowering the scientific instrument temperature of 0.2 K is paid on the mass increment of the VG1 and VG2. Considering a 25 kg mass for each VG [2], with the first

	Mean T [K]					
ARIEL	1.4	3.1	3.2	3.3	3.4	3.5
SVM/PLM plate	277.7	281.8	277.8	279.4	281.6	281.7
VG1	185.9	188.6	184.3	190.5	196.4	194.3
VG2	112.1	112.6	109.3	117.4	125.0	126.3
VG3	58.8	58.4	58.5	60.0	62.5	67.4
Baffle	46.8	46.6	47.5	47.2	48.4	53.2
TOB	47.1	46.9	47.7	47.6	49.1	53.5
IOB	47.1	46.9	47.7	47.6	49.1	53.7
FGS CFEE	47.1	46.9	47.7	47.7	49.2	53.7
FGS TCS	47.1	46.9	47.8	47.7	49.2	53.8
FGS detectors	47.6	47.4	48.2	48.1	49.6	54.2
AIRS CFEE	47.1	46.9	47.7	47.6	49.1	53.7
AIRS TCS	32.1	31.9	32.7	32.6	34.1	38.8
AIRS detector	34.9	34.8	35.6	35.5	37.1	41.7
JT Cold end	30.6	30.4	31.2	31.1	32.7	37.3

Table 6.4: *Comparison between baseline model (ARIEL 1.4) and modified models (ARIEL 3.x) main component average temperatures. Temperatures refer to the analysis case defined by the "JT150mW" BC and $\psi = 25°$ attitude rotation.*

original radius (1.32 m), enlarging the VG1 radius from 1.15 m to 1.25 m gives an estimated mass increase around 3.5 kg, and 1.7 kg for the VG2. The total is 5.2 kg.

ARIEL 3.2 This is the case with the highest set of VG inclination angles. It can be noticed that the VG temperature are lower with respect to the baseline but the overall temperatures of the TOB/IOB and scientific boxes and instruments are around 0.6 K higher. This apparent contradiction can be explained by the fact that in this case the VG3, with an inclination of 28°, has reduced its view factor with the deep space and increased the view factor with the telescope baffle and the rear TOB/IB. The emitted heat from the VG3 upper surface is absorbed by the Baffle and the TOB/IB. Figure 6.2 shows the computed REFs to environment in the Infrared band for the PLM ARIEL 1.4 (baseline) and ARIEL 3.2. It can be noticed that in the ARIEL 3.2, the VG1/VG2 external nodes have a higher REF to the environment with respect to the ARIEL 1.4, meaning an higher radiative coupling to the deep space. The VG3, baffle and TOB nodes instead have lower REF values. The greatest value differences are in the central VG3 nodes, the TOB nodes, and the later baffle nodes. The reduced radiative coupling to the deep space of the VG3 and upper PLM elements is not enough counterbalanced by the increased coupling of the VG1 and VG2.

ARIEL 3.3 and 3.4 These two cases with reduced set of VG inclination angles shows a general deterioration in PLM passive cooling. What is happening here is the opposite of the ARIEL 3.2: the REFs to environment of the VG3, baffle and TOB are increase but at the cost of lowering the REFs of the VG1 and VG2. Also in ARIEL 3.3 and 3.4, the reduction of the VG1/VG2 radiative

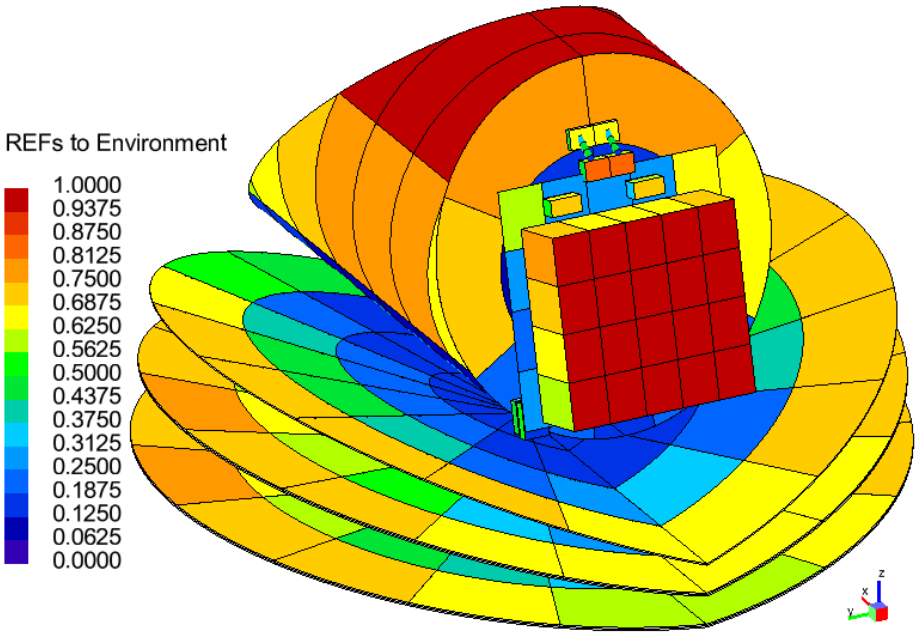

(a) ARIEL 1.4

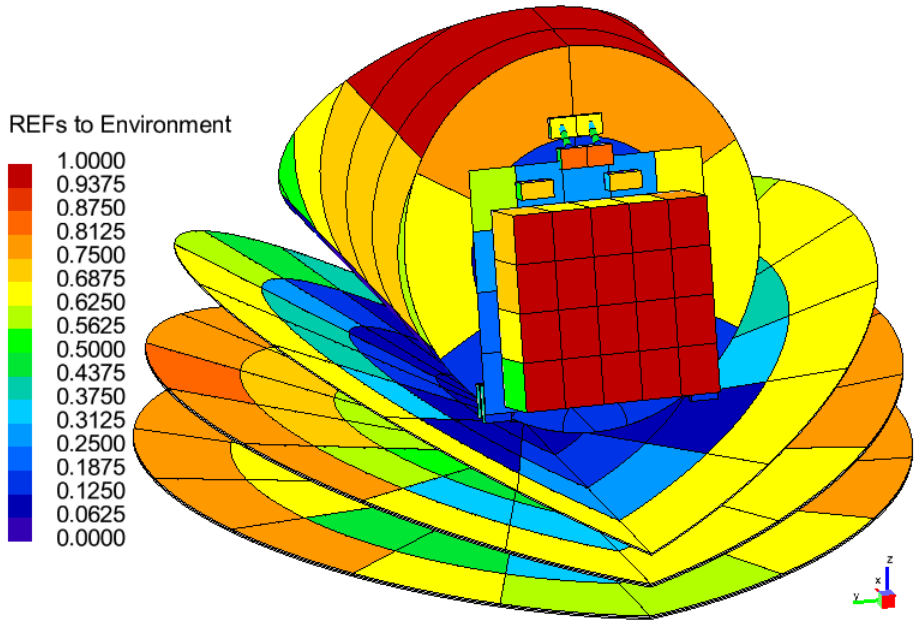

(b) ARIEL 3.2

Figure 6.2: *ARIEL 1.4 and 3.2 IR REFs to environment of the PLM for the $\psi = 25°$ radiative case. Bipods and supporting struts are hidden.*

coupling to deep space generates worse effects than the benefit of the enhanced REF values of the VG3, baffle, TOB/IB. Figure 6.3a shows the computed REFs to deep space in the IR band in the PLM ARIEL 3.4.

ARIEL 3.5 The case with the reduced vertical distance between the VGs is the worst condition. FGS/AIRS components experience a temperature increase of around 7 K with respect to the computed baseline temperatures. Figure 6.3b shows the computed REFs to environment in the Infrared band for the PLM ARIEL 3.5. The same consideration made for the 3.3 and 3.4 cases are also here valid: the enhanced cooling ability provided by greater REFs of the upper PLM nodes is less to the reduced cooling power of the VG1/VG2 with lower REF values.

Conclusions The only case which provides a benefit in the passive cooling of the PLM scientific instruments is the ARIEL 3.1. In this case, VG inclination angle and vertical distance have been kept as the baseline but the VG1 and VG2 radii have been increased. Modifying the VGs distance and inclination seems not to bring any benefit in the passive cooling performances. The baseline VG angle set (7°-14°-21°) is the best for this general PLM configuration. In order to increase the VG3 radii it is necessary to enlarge the SVM/PLM plate in order to avoid the Sun hitting the VG3 surface. The next parametric analysis considers models where the SVM plate and VG dimension have been modified.

6.3 SVM plate and VG dimensions

The solar array and the SVM/PLM plate shield the PLM from direct Sun illumination. If the satellite has its $-Z$ axis directed to Sun, solar rays are perpendicular to the solar array and the SVM/PLM plate is completely in shadow. When the S/C rotates around the X or the Y axes, the SVM/PLM plate starts to be illuminated by the Sun. As the rotation angle increases, its solar absorbed power and therefore its average temperature increase. Passing from zero attitude rotation (nominal case) to $\psi = 25°$ rotation (worst case) there is a circa 3 K increase in both AIRS and FGS components. This section analysis some different model with enlarged dimensions of the VGs and/or the SVM plates.

6.3.1 Description of cases

Different cases have been considered and then results have been compared to the baseline. Firstly, one case with the SVM solar array radius increased (ARIEL 4.1) and a second case with the SVM/PLM plate radius increase (ARIEL 4.2) have been sketched. In both cases, the radius has been enlarged from the baseline 1.35 m to 1.45 m. The third case (ARIEL 4.3) has both the SVM plates with a radius increased to 1.45 m. ARIEL 4.4 is identical to the 4.3 but with enlarged VGs. Their radii are increased to 1.25 m. In the previous chapter it has been seen also that in a model with VG and SVM plates radii respectively equal to 1.32 m and 1.53 K, FGS/AIRS temperature are lowered of circa 1 K

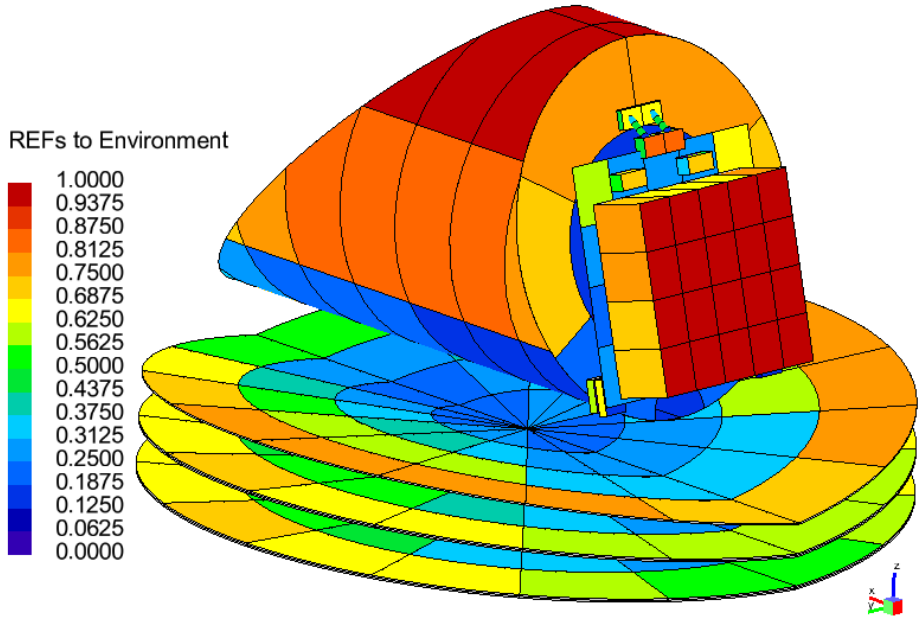

(a) ARIEL 3.4

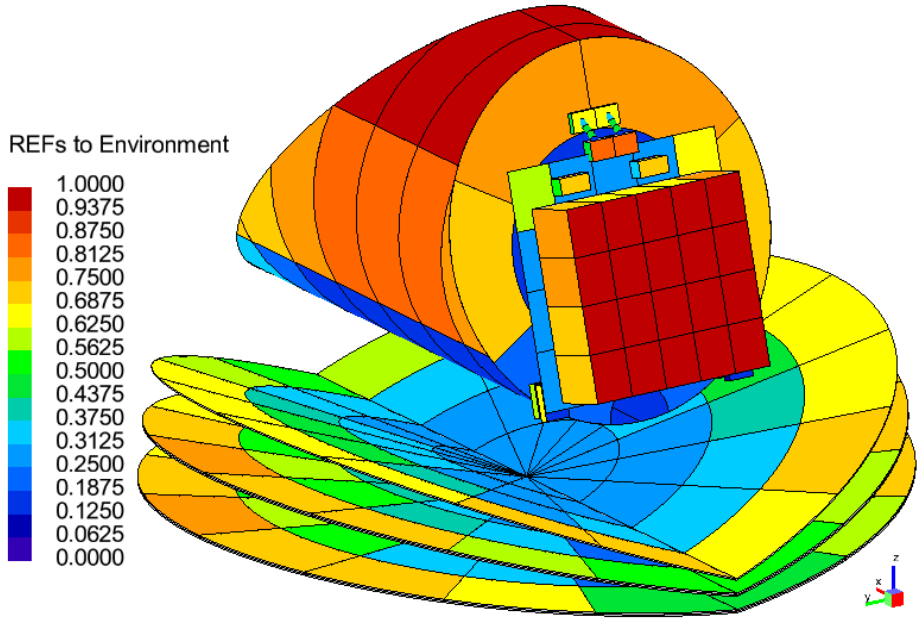

(b) ARIEL 3.5

Figure 6.3: *ARIEL 3.4 and 3.5 IR REFs to environment of the PLM for the $\psi = 25°$ radiative case. Bipods and supporting struts are hidden.*

Model name	Modified parameters	New parameter values	Est. Δm
ARIEL 4.1	SVM bottom plate radius	1.45 m	4 kg
ARIEL 4.2	SVM upper plate radius	1.45 m	4 kg
ARIEL 4.3	both SVM plate radii	1.45 m	8 kg
ARIEL 4.4	both SVM plate radii VG radii	1.45 m 1.25 m	18 kg
ARIEL 4.5	both SVM plate radii VG radii	1.53 m 1.32 m	25 kg
ARIEL 4.6	SVM bottom plate radius	1.72 m	16 kg
ARIEL 4.7	SVM bottom plate radius SVM top plate radius VG radii	1.55 m 1.35 m 1.25-1.20-1.15 m	13 kg
ARIEL 4.8	SVM bottom plate radius SVM top plate radius VG radii	1.55 m 1.40 m 1.30-1.25-1.20 m	20 kg
ARIEL 4.9	SVM bottom plate radius SVM top plate radius VG radii	1.55 m 1.45 m 1.35-1.30-1.25 m	27 kg

Table 6.5: *Cases with modified SVM plate and VG dimensions*

with respect to the baseline. This case is again considered (ARIEL 4.5) with the GL conductance between AIRS TCS and JT cold end modified as explained in subsection 5.2.2. ARIEL 4.6, has the SVM bottom plate enlarged to the minimum radius which guarantees the SVM top plate to be in shade from the Sun for the maximum rotation angle considered ($\psi = 25°$). The found value for the radius is 1.72 m. The last models, ARIEL 4.7, 4.8, 4.9 are mixed cases. The SVM bottom plate has the same radius (1.55 m) in all the three cases and the SVM top plate and the VGs' radii have incremental values of 5 cm between each case.

An estimate mass gain has been calculated for each considered model in order to compare the temperature variation with the mass increase. Mass increments have been estimated as in the previous sections, except for the SVM top plate which has been considered to have the same mass of the bottom one. Table 6.5 summarizes the cases considered in this section reporting the modified parameter and the estimated mass increase.

6.3.2 Discussion of results

Tables 6.6 and 6.7 report the main component temperatures for the "JT150mW-y25deg" analysis case of the baseline model (ARIEL 1.4) and of the modified models considered in this section (ARIEL 4.x). First row of the table reports the solar power absorbed by the SVM/PLM. The value is the sum of the power absorbed by all nodes of the plate.

ARIEL	**1.4**	**4.1**	**4.2**	**4.3**	**4.4**	**4.5**	**4.6**
				Solar absorbed power [W]			
SVM/PLM plate	128.7	95.3	214.1	167.7	167.7	183.8	0.0
				Mean T [K]			
SVM/PLM plate	277.7	267.3	289.0	277.8	278.9	277.0	235.8
VG1	185.9	179.1	194.0	187.4	187.9	187.5	154.2
VG2	112.1	108.3	118.5	114.7	113.8	114.1	94.4
VG3	58.8	57.7	61.4	60.3	57.4	56.5	54.0
Baffle	46.8	46.1	49.1	48.2	46.3	45.9	43.4
TOB	47.1	46.4	49.5	48.6	46.6	46.3	43.8
IOB	47.1	46.4	49.6	48.7	46.7	46.3	43.9
FGS CFEE	47.1	46.4	49.6	48.8	46.7	46.4	43.9
FGS TCS	47.1	46.5	49.7	48.8	46.7	46.4	43.9
FGS detectors	47.6	46.9	50.1	49.3	47.2	46.9	44.4
AIRS CFEE	47.1	46.4	49.6	48.7	46.7	46.3	43.8
AIRS TCS	32.1	31.4	34.6	33.8	31.7	31.3	28.8
AIRS detector	34.9	34.3	37.5	36.7	34.6	34.2	31.7
JT Cold end	30.6	29.9	33.1	32.3	30.2	29.8	27.3

Table 6.6: *Comparison between baseline model (ARIEL 1.4) and modified models (ARIEL 4.x) main component average temperatures and SVM/PLM plate absorbed solar power. Values refer to the analysis case defined by the "JT150mW" BC and* $\psi = 25°$ *attitude rotation.*

ARIEL 4.1-4.2-4.3 In ARIEL 4.1, the enlarged SVM bottom plate has the effect to reduce sun-illuminated area on the SVM top plate, thus reducing the total absorbed power and consequently its average temperature of 10 K. Thanks to that, FGS and AIRS components reduce their average temperature of circa 0.5 K. In ARIEL 4.2, the enlarged SVM top plate has the opposite effect: greater area is illuminated by the Sun with an increase in the absorbed power and average temperature. ARIEL 4.3 its an intermediate condition between the previous two. The scientific equipment temperatures are higher than the baseline. The three cases shows that, in general, enlarging the SVM bottom plate is favourable. The solar array acts as a first sunshield, absorbing solar power away from the SVM/PLM interface. A bigger bottom plate makes the PLM less sensible to attitude rotations since it keeps a higher portion of the SVM/PLM plate in shade. Figure 6.4 shows the ARIEL 4.1 VGs' and FGS components' temperatures for rotated attitude considered with "JT150mW" BC. For rotation angles up to $\psi = \pm 5°$ the SVM/PLM plate remains shaded by the solar array plate. The VGs and consequently the FGS/AIRS components experience a small temperature variation.

Enlarging the SVM top plate instead would bring solar power much closer to the PLM, negatively affecting the PLM average temperatures. Anyway, the SVM top plate is necessary to avoid the Sun hitting the VGs and the rest of the PLM. The compromise between the two considerations is to chose the SVM/PLM plate dimension no bigger than what is necessary to shield the PLM from the Sun for the maximum attitude rotation angle. In the next considered

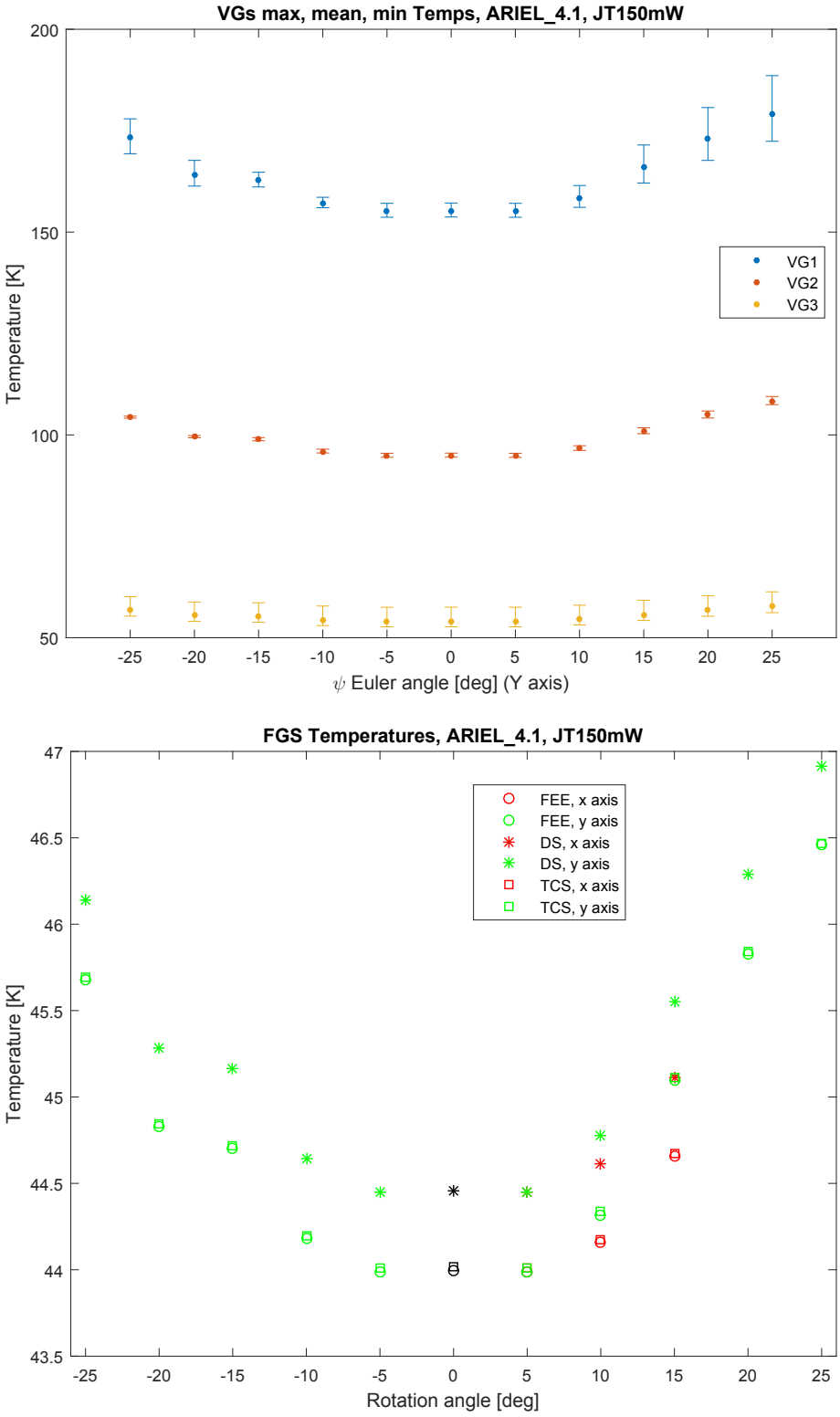

Figure 6.4: *ARIEL 4.1 VG and FGS temperatures for the considered attitude rotation angles and "JT150mW" BC case.*

cases the SVM/PLM plate radius is chosen as the minimum which guarantees complete PLM shield from the Sun.

ARIEL 4.4-4.5 In ARIEL 4.3 the SVM plates have been enlarged to a 1.45 m radius, so there is available room to increase the VG dimension maintaining them protected from the Sun. In ARIEL 4.4, VGs have been enlarged with the maximum radius which maintain them in shade (1.25 m). Comparing temperatures between 4.3 and 4.4, the benefits of the increased radiating area of the VGs is evident since there is a temperature difference of circa 2 K in FGS/AIRS components. Anyway, 4.4 temperature are still few tenth of Kelvin higher than the 4.1 case (just the SVM bottom plate enlarged). These comparisons suggest that is more convenient to enlarge only the SVM bottom plate and maintain the SVM top and VGs at the original dimension rather than enlarge all of them. The greater solar power absorbed by a bigger SVM/PLM plate is not enough counteracted by the enhanced radiative cooling of bigger VGs. ARIEL 4.5 is like the 4.4 but with greater SVM plates and VGs. Temperature of the 4.5 are almost similar to the 4.1. In the 4.5 case, it has been necessary to increase the SVM bottom and top plate in order to allow an enlargement of the VGs, with an estimated mass of 25 kg. The same temperatures have been reached in ARIEL 4.1 with only an increase of the SVM bottom plate to a smaller radius than the ARIEL 4.5.

ARIEL 4.6 Figure 6.5 shows the ARIEL 4.6 SVM/PLM plate, VG and FGS component temperatures for rotated attitude considered with "JT150mW" BC. The large SVM bottom plate shields the SVM top plate from the Sun for all rotation angles. Without absorbed solar power and protected by a low emissivity coating, the SVM top plate maintains approximately the same temperature distribution for all rotation angles. Consequently, also the VGs maintain their temperature excursion in the same range. The small temperature variation due to attitude change can be appreciated in the FGS plot, where each component experiences a temperature variation around 0.2 K. In ARIEL 4.6 the cold and hot cases has reversed: the zero rotation has the highest temperature while with $\psi = 25°$ PLM temperature are lowest. The attitude change makes the SVM/PLM nodes to higher their view factor to environment, increasing the radiative coupling to the deep space. In all previous model, this small increment in radiative cooling was much more counterbalanced by the incoming solar radiation to the SVM top plate.

The ARIEL 4.6 has also the advantage to create a very stable environment on the SVM/PLM interface with general benefit on the active stability control. The drawback to pay, apart from the mass increment, is the large increment in the S/C dimension. The horizontal dimension is the SVM bottom plate diameter equal to 3.44 m. This value is still below the diameter of the internal available volume of the Ariane 6 (4480 mm) and Soyuz ST (3720 mm) fairings [2].

ARIEL 4.7-4.8-4.9 Table 6.7 compares baseline, 4.6, 4.7, 4.8, 4.9 cases. The ARIEL 4.6 PLM temperatures represent the minimum reachable with the baseline configuration and dimensions of the SVM/PLM plate and VGs. In order to

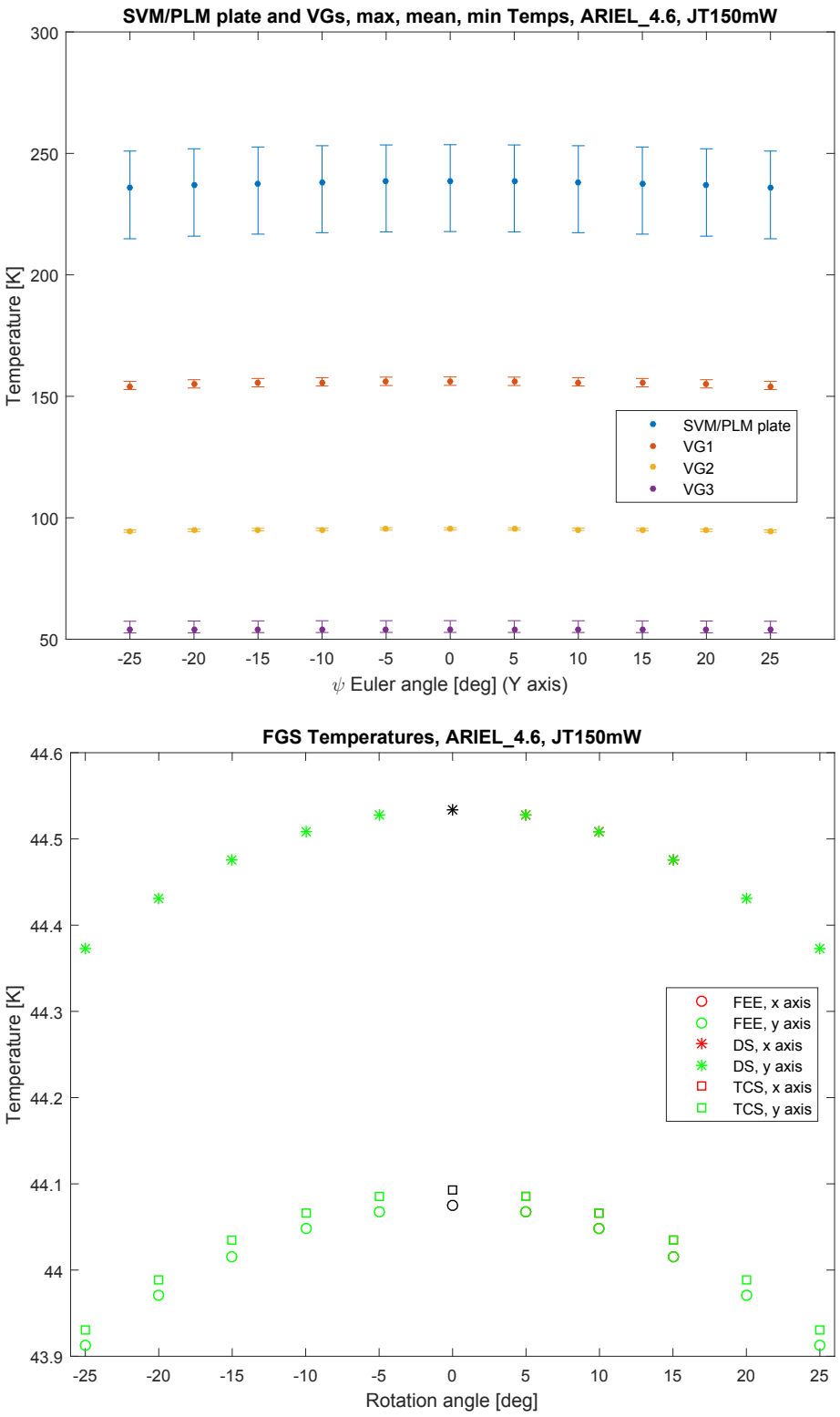

Figure 6.5: *ARIEL 4.6 SVM/PLM plate, VG and FGS temperatures for the considered attitude rotation angles and "JT150mW" BC case.*

ARIEL	**1.4**	**4.6**	**4.7**	**4.8**	**4.9**
			Solar absorbed power [W]		
SVM/PLM plate	128.7	0.0	50.5	87.7	109.0
			Mean T [K]		
SVM/PLM plate	277.7	235.8	254.5	262.4	265.8
VG1	185.9	154.2	168.9	168.6	177.8
VG2	112.1	94.4	101.9	101.9	107.5
VG3	58.8	54.0	55.7	54.9	55.6
Baffle	46.8	43.4	44.6	44.9	45.0
TOB	47.1	43.8	45.0	44.7	45.4
IOB	47.1	43.9	45.1	44.8	45.4
FGS CFEE	47.1	43.9	45.1	44.8	45.5
FGS TCS	47.1	43.9	45.1	44.9	45.5
FGS detectors	47.6	44.4	45.6	45.3	45.9
AIRS CFEE	47.1	43.8	45.0	44.8	45.4
AIRS TCS	32.1	28.8	30.0	29.7	30.4
AIRS detector	34.9	31.7	32.9	32.6	33.3
JT Cold end	30.6	27.3	28.5	28.2	28.9

Table 6.7: *Comparison between baseline model (ARIEL 1.4) and the last modified models (ARIEL 4.6-9) main component average temperatures and SVM/PLM plate absorbed solar power. Values refer to the analysis case defined by the "JT150mW" BC and $\psi = 25°$ attitude rotation.*

increase the PLM passive cooling it is necessary to enlarge the VGs' dimension and consequently the SVM top plate to shield them from the Sun. Temperatures of the models 4.7, 4.8 and 4.9 show that for a given SVM bottom plate dimension an increase in VGs' and SVM top plate dimensions is convenient until a certain point. The cases 4.7, 4.8 and 4.9 have the same SVM bottom plate radius and incremental SVM top plate and VGs' dimensions. Comparing the temperature of these three cases, the lowest are reached in the 4.8 case which has intermediate VGs' and SVM top plate dimensions. Enlarging the VGs and SVM top plate has the benefit to increase the radiating area of the VGs but, on the other hand, it increases also the SVM plate area illuminated by the Sun and consequently the solar absorbed power. For the considered angle rotation ($\psi = 25°$), passing from the 4.7 to the 4.8 is convenient but from 4.8 to 4.9 no more. The ratio between the SVM top and bottom plates' radii of the ARIEL 4.8 optimizes the passive radiating performance of the PLM. The ratios for the 4.7, 4.8 and 4.9 are respectively 0.87, 0.9 and 0.93. The 0.9 is the optimum ratio in the considered design for a rotation angle of $\psi = 25°$. Comparing ARIEL 4.6 and ARIEL 4.8, the 4.6 achieves lower temperature with a lower estimated mass increase. The 4.6 design has the drawback to create a S/C which is large and not so compact, almost at the Soyuz ST fairing available volume limit. The 4.8 case represents a compromise between S/C dimensions and final FGS/AIRS temperatures but heavier in terms of mass. In ARIEL 4.8 the computed FGS detector temperature is 0.3 K above the margined limit. Its temperature can be lowered incrementing the GL conductance between TCS and the cold stage

node as done in the previous chapter for the AIRS detector. Considering a GL value of 0.05 W/K, instead of the original 0.01 W/K the final FGS temperature detector is 44.9 K, enough to respect the margined limit.

Conclusions The analysis in this section has concluded that it is better to protect the SVM/PLM plate from incoming heat rather than try to increase the passive cooling from the PLM. The most efficient way in terms of mass to decrease PLM temperatures is to enlarge the SVM bottom plate as mush as possible up to completely shield the SVM top plate from the Sun for the highest rotation angle. There is around 3.2 K difference in FGS/AIRS instruments between the baseline model (ARIEL 1.4) and the ARIEL 4.6 with the SVM bottom plate which completely shades the top one. Additional passive cooling power can be achieved increasing the SVM top plate and the VGs' dimensions maintain a ratio between the bottom and top SVM plates around 0.9. This additional increment in dimensions brings less benefit in temperature lowering related to the mass gain. The optimum ratio between SVM bottom and top plate depends on the insulation property of the MLI on the SVM top plate. The more the insulating efficiency, the lower the sensibility to Sun illumination, and therefore the higher the optimum ratio between SVM plates' radii. A more efficient MLI makes an enlargement of the SVM/PLM less problematic since the solar ray are better shielded allowing a reduction of the SVM bottom plate. (the optimum ratio is greater, closer to 1). The next and last section deals with a different way of modelling MLI in ESATAN-TMS.

6.4 MLI on SVM/PLM plate

As said in the PLM thermal design description, both sides of the SVM/PLM interface plate are covered by MLI in order to minimize absorbed solar power and heat radiation from the SVM to the PLM. In general, a realistic simulation of the MLI thermal behavior is a difficult task as the performance depends on multiple factors (shape, seams, holes, interfaces, adhesive, etc...). An ideal MLI have all its layers separated with no contact between each others. In reality this is not possible to achieve, in particular when the surface to cover has geometrical irregularities, curves and all sorts of mechanical interfaces and supports between MLI and covered surface. The number and the extension of these contact zones between MLI layers in very difficult to estimate and therefore to simulate with thermal software. At this level of analysis, it does not make sense sketching in ESATAN-TMS detailed MLI geometry since there is no such detailed information.

In literature it is common to define the effective emittance, ε^*, for a MLI, which represents a fictitious emittance that radiatively couples the two external layers of the MLI. ε^* accounts for both conductive and radiative thermal couplings between all internal layers. The higher the isolation efficacy of the internal layers, the lower the value of ε^*. Typical value of ε^* for space application is around 0.015-0.030 [8]. In all previous models, the MLI has been modelled in ESATAN-TMS simply assigning to the SVM plate external surfaces the "Single-layer" thermo-optical property. A different way of MLI modelling has been tried

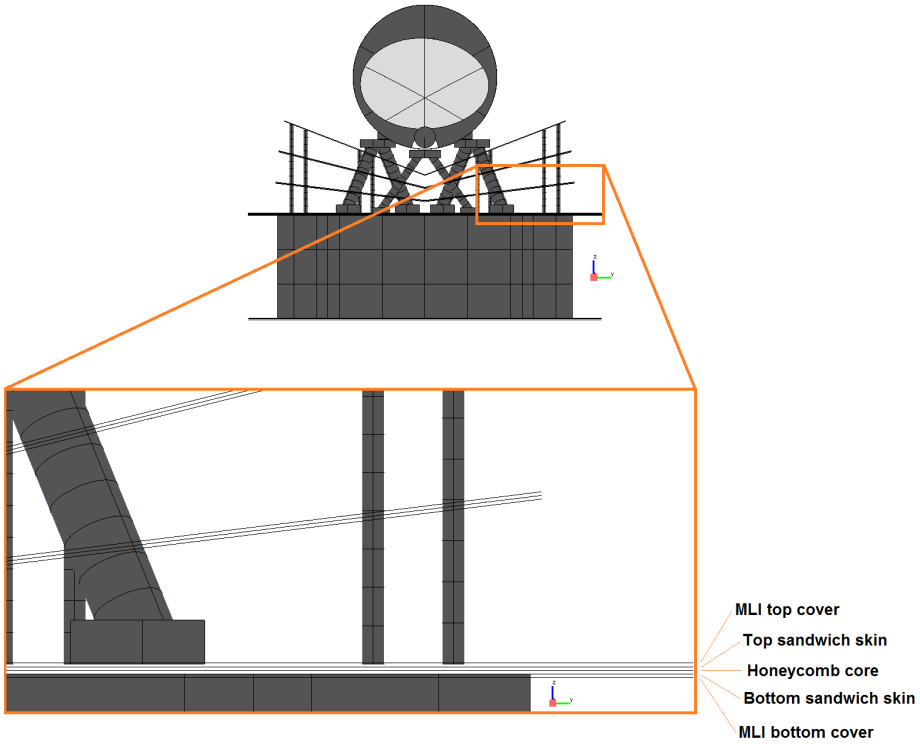

Figure 6.6: *Front view of ARIEL 5.1 and 5.2 with zoom on MLI covers*

in a new version of the ARIEL S/C in ESATAN-TMS.

6.4.1 Description of cases

For the SVM/PLM plate, the new modelling method for MLI in ESATAN-TMS considers an additional shell geometry identical to one of the three discs which accounts for the sandwich panel. It can be created copying and translating the face-skin shell externally of few millimetres. The new created shells represent the top and bottom MLI covers on the SVM/PLM plate. Figure 6.6 is the front view of the new models with the two additional shells accounting for the MLI top and bottom covers. The zoomed part of the figure explains the layout. The MLI top shell is few millimetres above the lower ends of the bipods feet and supporting struts. In this way the contact zones between SVM/PLM and bipods and struts are valid as before. In fact, the bipods and struts must be connected to the SVM/PLM plate, not to the MLI upper surface since they would have different temperature with the consequence to underestimate the amount of conductive heat leak from the SVM to the PLM.

The internal layers thermal behavior is modelled through the "through thickness conductance", setting it to EFFECTIVE and assigning a user-defined effective emittance of 0.030. The MLI shell side which is facing the SVM/PLM plate shall be thermally connected with it. As previous said, the thermal coupling between

Model name	MLI outer cover optical property			
	Lower side	α/ε	Upper side	α/ε
ARIEL 5.1	"Single-layer"	0.06/0.12	"Single-layer"	0.06/0.12
ARIEL 5.2	Silvered Teflon	0.14/0.60	Gold coated Polyimide	0.30/0.03

Table 6.8: *Cases with modified MLI on SVM/PLM plate*

MLI and its covered structure is difficult to estimate. A contact zone with very low contact conductance ($10\,W/m^2K$) has been used between SVM/PLM plate and MLI shell surfaces. It is left to defined the optical properties of the MLI external surfaces, the upper one facing the PLM first VG, the lower one looking at the SVM and exposed to solar radiation when the satellite attitude is rotated. In MLI design, the properties of the outer layer are important since they define the radiative coupling with the environment. In the first considered model, named ARIEL 5.1, the "Single-layer" optical property has been assigned to both the upper and lower external layers, the same optical property used in all previous model, in order to compare how the additional shells representing the MLI affect the thermal performance. In a second model, the MLI outer layer optical properties has been chosen to better adapt to the environment and their function. In particular, it has been previously seen that for satellite attitude rotations the absorbed solar power by the SVM/PLM lower surface affects negatively the PLM final temperatures. Therefore it has been chosen for the lower outer cover layer a material with a low absorptivity in the solar band and high emissivity in the infrared. A typical solution is a silvered Teflon surface finish over its supporting material. Values of $\alpha = 0.14$ and $\varepsilon = 0.60$ has been considered [8]. The function of the MLI covering the upper SVM/PLM plate is instead to minimize the radiative heat from the SVM to the PLM. For this reason, it has been chose a outer cover material with low emissivity in the infrared. Absorptivity in the solar band is not playing a role since this side of the SVM/PLM and its covering MLI is not exposed to solar ray. Gold coated Polyimide covers have extremely low emissivity and moderate solar absorptivity. Values of $\alpha = 0.30$ and $\varepsilon = 0.03$, taken from [18],has been considered. The ARIEL ESATAN-TMS model with silvered Teflon and Gold coated Polyimide is the ARIEL 5.2. Table 6.8 summarizes the assigned optical properties in the two cases considered.

6.4.2 Discussion of results

Table 6.9 reports the main component temperatures for the "JT150mW-y25deg" analysis case of the baseline model (ARIEL 1.4) and of the modified models considered in this section (ARIEL 5.x). First row of the table reports the solar power absorbed by the MLI outer layer covering the SVM/PLM lower surface. The value is the sum of the power absorbed by all nodes on the surface of the shell geometry.

Temperatures of ARIEL 5.1 show a general reduction of 2.3 K–2.6 K in cold PLM components. The simulated insulation effect of the internal MLI layer is able to create a temperature gradient from the average 320 K of the outer

ARIEL	**1.4**	**5.1**	**5.2**
	Solar absorbed power [W]		
SVM/PLM plate	128.7	-	-
MLI lower ext. layer	-	128.7	150.0
	Mean T [K]		
MLI lower ext. layer	-	319.7	257.1
SVM/PLM plate	277.7	267.3	240.2
MLI upper ext. layer	-	213.7	209.2
VG1	185.9	161.4	144.7
VG2	112.1	98.3	89.4
VG3	58.8	54.9	52.6
Baffle	46.8	44.1	42.3
TOB	47.1	44.5	42.9
IOB	47.1	44.5	42.9
IB	47.0	44.5	42.9
FGS CFEE	47.1	44.6	43.0
FGS TCS	47.1	44.6	43.0
FGS detectors	47.6	45.0	43.4
AIRS CFEE	47.1	44.5	42.9
AIRS TCS	32.1	29.5	27.8
AIRS detector	34.9	32.4	30.7
JT Cold end	30.6	28.0	26.3

Table 6.9: *Comparison between baseline model (ARIEL 1.4) and modified models (ARIEL 5.x) main component average temperatures and SVM/PLM plate and MLI absorbed solar power. Values refer to the analysis case defined by the "JT150mW" BC and $\psi = 25°$ attitude rotation.*

layer to the 267 K of the internal layer - SVM/PLM plate. MLI internal surfaces connected with the SVM/PLM have almost the same temperature of the SVM/PLM plate which is averagely around 10 K lower than in the baseline case. The total absorbed solar power is in both case the same since the exposed surfaces have the same optical property ("Single-layer") meaning that the general temperature reduction is due to the additional MLI shells.

In ARIEL 5.2, cold PLM temperatures are even lower of 1.3 K–1.4 K in respect of the 5.1 case. The silvered Teflon makes the external bottom MLI nodes to have a lower average temperature. The silver Teflon has both absorptivity and emissivity higher than the ones in the "Single-layer". Even if the solar absorbed power is higher (150 W instead of 129 W), the greater emissivity is able to lower significantly its average temperature. This has direct consequence in lowering also the SVM/PLM plate with general benefits for the PLM temperatures. Figure 6.7 shows the temperature distribution of the SVM top plate with MLI and PLM of ARIEL 5.2 for the "JT150mW-y25deg" case. The bottom nodes of the bipods feet and supporting struts are at around 230 K–260 K (coloured in dark red), higher temperatures than the upper surface MLI nodes (coloured in orange). Lower bipods' and struts' nodes are directly connected through contact zones to the upper surface of the top skin shell of the SVM/PLM plate. The

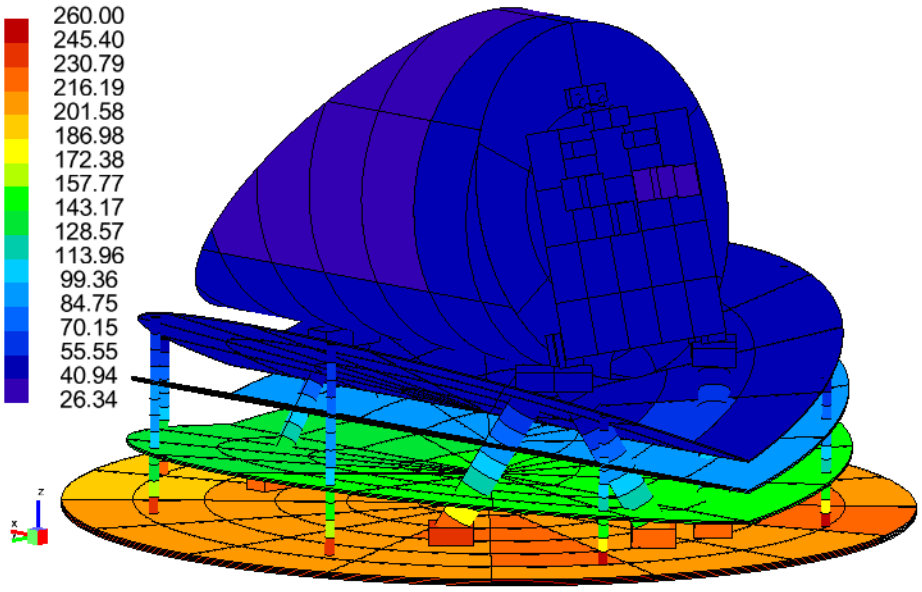

Figure 6.7: *ARIEL 5.2 SVM top plate with MLI shells and PLM temperatures for "JT150mW" BC and $\psi = 25°$ attitude rotation. The IB and the FGS/AIRS module boxes are hidden to show internal components.*

AIRS detector temperature is almost 10 K below its limit (5 K from the considered margin). This suggests that a BC with lower power absorbed by the JT cold end can be enough for the AIRS detector to satisfy the limit as well. Its temperature of the solved analysis case "JT100mW-y-25deg" is 36.1 K, which is just 1.1 K above the margined limit. In ARIEL 5.2 a JT cooling power of a little bit more than 100 mW is enough to respect the limit.

6.5 Outputs of the parametric analysis

This section summarizes the parametric analysis results and outputs the three models which fulfil the PLM temperature requirements with the assumed 5 K margin, highlighting advantages and drawbacks.

The first two sections of the parametric analysis have shown that the PLM ability to passively cool the scientific equipments is almost at the top of what is achievable with this configuration layout. The modification of the VG and baffle design parameters, like inclination, relative distance, and radius (remaining in shade of the SVM/PLM plate) has shown little temperature variations. The only significant case considered the VGs with incremental radii of 5 cm from the lowest ot the topmost (ARIEL 3.1). Anyway this case have shown a decrease around 0.2 K of PLM cold components at the cost of making each VG different, thus with higher cost. In the VG analysis, the geometrical shape has not been modified, maintaining always the original half-disc shells. Considering the general results of this analysis, little modifications in the VGs' shape should not bring sever consequence in the PLM passive cooling ability. One idea could be

Model name	Advantages	Drawbacks
ARIEL 4.6	Very stable temperatures of the SVM/PLM and consequently of the all PLM components	Large increase in dimensions, moderate in mass
ARIEL 4.8	Moderate dimension increment	Large increase in mass. VGs have different radii
ARIEL 5.2	No mass and dimension increment. SVM plates have the same radius. Requires less JT cooling power	Less robust since it relies on the hypothesis made on the MLI model in ESATAN-TMS Workbench

Table 6.10: *Advantages and drawbacks of the output models*

to cut the most external part of each VG geometry, obtaining a shape similar to a trapezoid. This would allow to consider a small SVM/PLM plate to shield the VGs from the Sun.

The sections on the SVM plates' dimension and MLI have shown that these parameters play a more decisive role in the PLM temperature influence on attitude variations. The solar power absorbed by the SVM/PLM plate for the considered environmental conditions, represents the bigger issue on the PLM temperatures and their stability. Solutions to counteract this problem is to enlarge the SVM bottom plate and/or enhance the insulating property of the MLI.

Three cases, ARIEL 4.6, 4.8 and 5.2, are presented as output of the parametric analysis since they fulfil the margined temperature requirements for the worst condition ($\psi = 25°$) with different design solutions. ARIEL 4.6 brings the SVM bottom plate at its extreme dimension, as much as to shield from the Sun to SVM top plate. ARIEL 5.2 considers a more refined method for simulating the thermal behavior of the MLI in ESATAN-TMS Workbench. ARIEL 4.8 is a compromise between S/C dimension and final PLM temperatures. Table 6.10 summarizes the advantages and drawbacks of these three models. Figure 6.8 shows an external view of the three output models. Figure 6.9 shows the temperature excursion between cold and hot conditions with respect to requirements and adopted margin. The dark grey bars describe intervals from the minimal node temperature in cold case to the maximal in hot case. Red bars represent, for each component, the temperature range over its requirement. The orange bars account for the assumed 5 K margin. ARIEL 4.6 is able to maintain FGS and AIRS temperature in a very close range (0.2 K), ARIEL 5.2 has the lowest absolute temperatures. The 5.2 case can be regarded as the best models since it achieves the lowest temperatures without mass and dimension increment. Anyway it relies on the assumptions made to model in ESATAN-TMS for the MLI thermal behaviour.

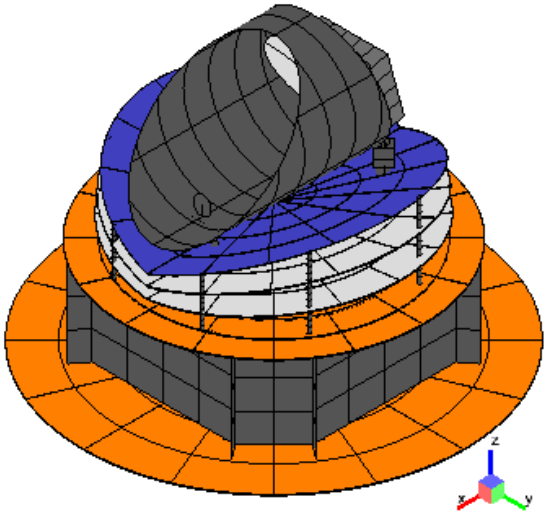

(a) ARIEL 4.6
SVM bottom plate radius:
1.72 m

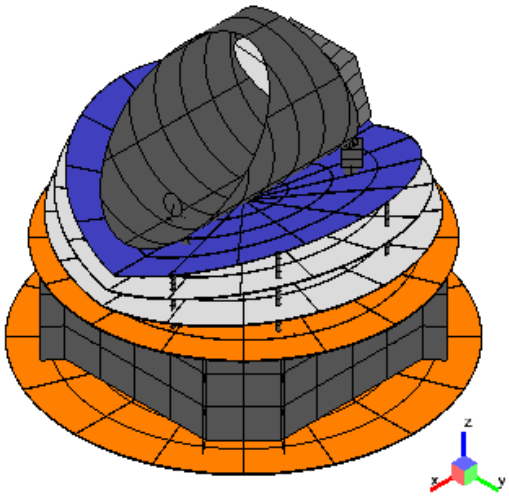

(b) ARIEL 4.8
SVM bottom plate radius:
1.55 m
SVM top plate radius:
1.40 m
VGs' radii: 1.30-1.25-1.20 m

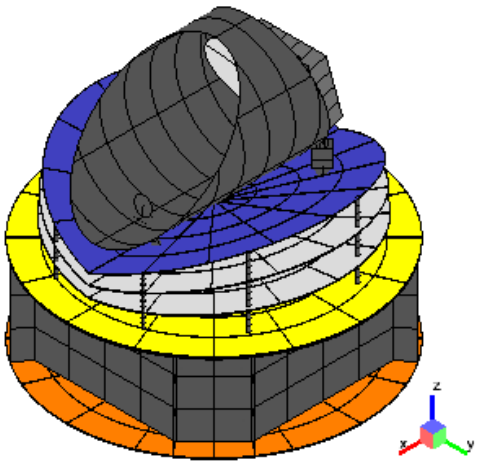

(c) ARIEL 5.2
Additional shells for MLI
with $\varepsilon^* = 0.03$

Figure 6.8: *ARIEL 4.6, 4.8, 5.2 external views*

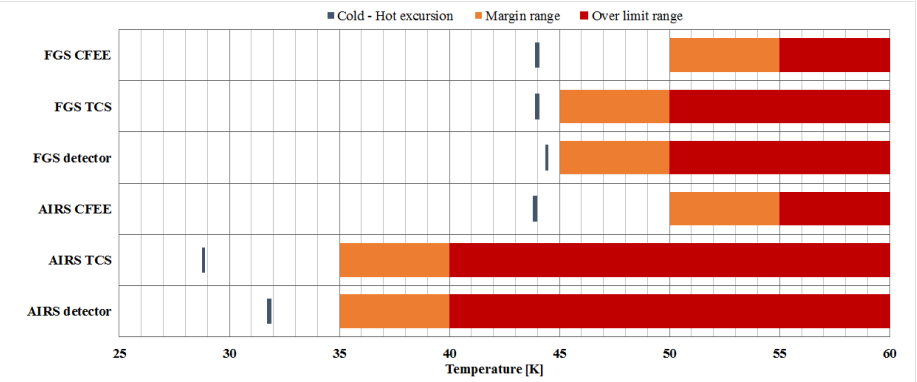

(a) ARIEL 4.6

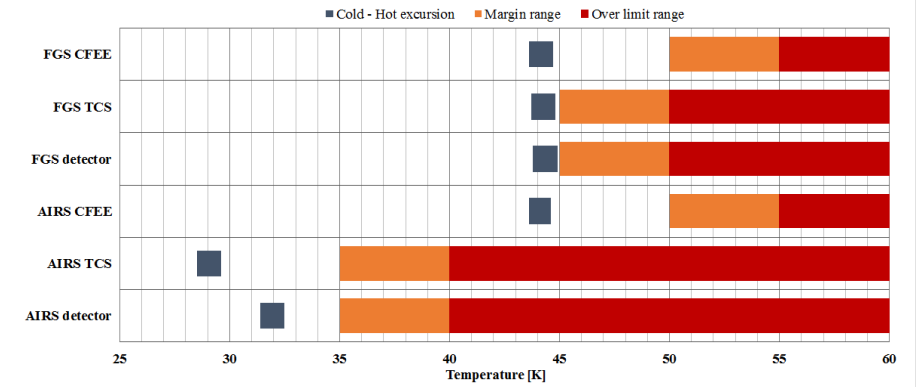

(b) ARIEL 4.8

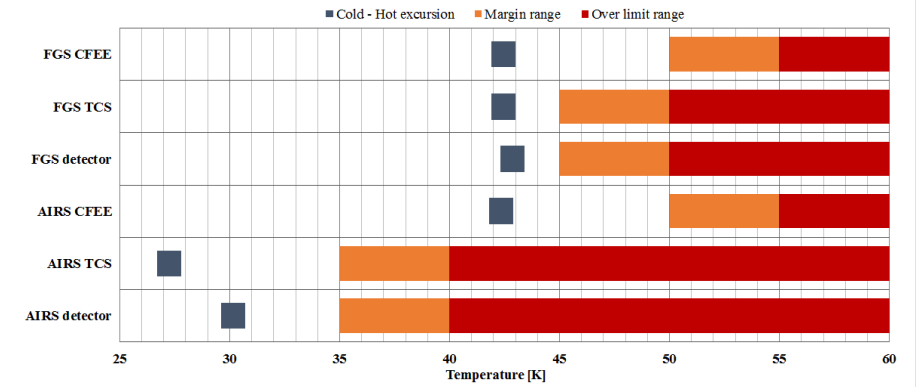

(c) ARIEL 5.2

Figure 6.9: *Temperature bar charts for FGS and AIRS units in ARIEL 4.6, 4.8 and 5.2*

Chapter 7

Conclusions

The analysis of the ARIEL S/C thermal architecture has shown that the adopted configuration is able to fulfil the PLM requirements on temperature including the margins used in the Phase A of a space project. The critical components are the detector units of the two main instruments, FGS/NIRP and AIRS, which are the closest to their respective temperature limits. At the L2 Earth-Sun system point the worst case thermal performances occur for the maximum rotation angle (25°) along the S/C Y, as the satellite is not symmetrical with respect to the Y-Z plane. In the ESATAN-TMS Workbench convention, this worst case corresponds to a positive rotation of the ψ Euler angle that causes the Sun to illuminate the X-negative satellite side. In this condition, the entering solar power is concentrated on the back side of the satellite, close to the optical bench where boxes containing the cryogenic scientific instrument are located.

The thesis has confirmed the need for an active cooling system dedicated to the AIRS instrument detector. The cryocooler option was first suggested by the ESA CDF study, as the mission proposal was based on a fully passive configuration. A simulation run on the thermal configuration with the best passive performances (model ARIEL 5.2) has demonstrated that, with no cooling power applied to the JT cooler cold end, the AIRS instrument is not meeting requirements. The AIRS detectors temperature is still more than 5K above its requirement (40 K) even in the most favourable attitude condition. In this model, a sort of best case in terms of passive performances, 100 mW of cooling power are needed at the JT cold end to lower the detectors temperature below the required temperature including a 5 K margin. In the thermal cases that show worse thermal passive performances, up to 150 mW might be required for the AIRS detectors to meet the margined requirement. Even in this worst case and including an extra 20% margin on the cooling power needed, the ARIEL JT cryocooler would anyway have the cooling capacity to support the mission, as the maximum heat lift of the cooler estimated by the RAL Space team in charge of the design is on the order of 200 mW.

The baseline ESATAN-TMS model (ARIEL 1.4, output of the chapter 5) has been developed from the information contained in the study documents. In order to avoid the solar rays hitting the VGs for the maximum considered attitude

rotation angle (25°), the VGs' dimension has been lowered while the SVM top and bottom plates' original dimensions have been left the same. This solution has been preferred to the opposite one, which considered enlarged SVM plates, since it would take advantage of an estimated mass save around of 30 kg without compromising the general PLM thermal performance. The baseline has both the SVM plates with a radius equal to 1.35 m and three VGs with the same radius equal to 1.15 m. With 150 mW of heat lift on the JT cold end and 500 mW heat load intercepted by the topmost VG (worst case assumption), the AIRS components are below the margined requirements but the FGS/NIRP ones are in the margined range for the hot case condition. An analysis on the most critical design parameters has been carried to try to improve efficiently the thermal architecture.

The parametric analysis, run on the configuration of the main components of the mission passive thermal design, has suggested three different solutions, each one with relative advantages and drawbacks. At the end of the analysis, the S/C parameters playing a key role in the thermal performance of the ARIEL PLM can be summarized in: (a) the insulating efficiency of the MLI on the SVM/PLM plate, (b) the dimension of the SVM bottom plate (the structure supporting the solar array), (c) the cooling power of the JT cryocooler, (d) the maximum attitude rotation angle at the operational orbit.

(a) *MLI insulating efficiency.* The outputs of the parametric analysis has shown that SVM/PLM plate MLI with different insulating efficiency affects particularly the thermal performance for rotated attitude cases. The MLI covering the bottom side of the plate has the function to protect it from the incoming solar radiation for rotated attitudes, while the upper side reduces the radiative coupling between the SVM and PLM. Two methods for modelling the MLI behavior have been considered in the ESATAN-TMS Workbench. The first one, adopted in the baseline, is more conservative, while the second is a more refined simulation (model ARIEL 5.2). Once a more detailed sketch of the SVM plate and its interfaces will be available, it will be possible to develop a more reliable model of the MLI. An efficient MLI shielding can help in increasing the design margins, allowing the relaxation on requirements on other parameters as the SVM bottom plate dimension, together with the allocated JT cooling power, or the maximum rotation angle for scientific observations.

(b) *SVM bottom plate dimension.* The dimension of the SVM bottom plate impacts the solar power absorbed by the external MLI layer covering the SVM top plate, which is mechanically connected by the bipods and the supporting struts to the PLM. Increasing the SVM bottom plate would lower the PLM sensitivity to attitude rotations. In the extreme case where the SVM bottom plate is so large to completely shield from the Sun the SVM top plate even for the maximum rotation angle (model ARIEL 4.6), the PLM units reach a high temperature stability. Simulations show a temperature excursion of circa 0.2 K in the FGS/NIRP and AIRS components between zero and maximum attitude rotation cases. The drawbacks of this configuration are the mass and the volume increment of the S/C.

(c) *JT cryocooler heat lift.* As previous said, the JT cryocooler has the function to cool down the AIRS detector below its temperature requirement.

Even if the estimated required power necessary to meet the margined requirement is below the maximum deliverable cooling capacity, it is preferable not to oversize the JT cooling power. Saving heat lift at the cold end has the benefit to require less power for the JT compressor and its driving electronics (located in the SVM, the warm part of the S/C) and less heat load interception by the VGs for pre-cooling of the high pressure Neon stream. The consequences are an improving of the VGs thermal performance and margins on the passively cooled stages, in particular the FGS/NIRP components and the telescope and instrument optics, as they rely on a passive cooling design.

(d) *Maximum attitude rotation angle.* This thesis has always considered the maximum angle equal to 25° for rotation along the S/C Y axis. This value comes from the observational requirements and is still TBC. If this maximum angle shall be incremented of few degrees in future developments, the margined design solutions adopted in this thesis should be sufficient to guarantee compliance with temperature limit requirements. On the other hand, if for particular reasons, there would be the need to reduce the key parameters governing the thermal performance, consequently the maximum allowed attitude angle should be adequately lowered.

Some of the characteristics of one model can be combined with the others resulting in new configurations able to meet requirements as well or even better. For example, one can consider a MLI with less insulating properties of the ARIEL 5.2 combined with a SVM bottom plate enlarged with respect to the baseline dimension. Thermal design solutions can be created recombining different values of these four parameters. In future studies, a more detailed analysis should trade-off a design among these parameters.

In the above parameters the VGs, the telescope baffle and the instrument box are not mentioned since the parametric analysis has shown very little influence on their design parameters on the PLM passive cooling performance. In order to achieve a substantial increment on the performance, the VGs' dimensions should be enlarged and therefore the general S/C dimension and mass increased to a level not compatible with the M4 mission constrains.

High thermal stability is another key issue of the ARIEL PLM design. ARIEL 4.6 and ARIEL 5.2 models show a PLM cold units temperature excursion of respectively circa 0.2 K and 1.1 K between cold and hot conditions, within the requirements stability of most of the PLM units. Once a more reliable opto-mechanical configuration of the telescope and instruments will be available, transient analyses should be performed with an updated model to characterise possible thermal stability issues and identify technical solutions to minimize them. As the requirements on temperature stability of the detectors are very challenging (50 mK peak-to-peak) it is likely that an active control system on each detector is necessary. Temperature variations are damped by dissipating a specific amount of heat calculated through a close loop control. In order to take this extra power dissipation into account, in all solved thermal analysis a heat load boundary condition of 5 mW has been applied in each Temperature Control Stage. This can be regarded as an additional margin to the overall robustness of the considered thermal model in this thesis.

Acronyms

AIRS	ARIEL IR Spectrometer
ARIEL	Atmospheric Remote-sensing Infrared Exoplanet Large Survey
AOCS	Attitude and Orbital Control System
BC	Boundary Conditions
CDF	Concurrent Design Facility
CDR	Critical Design Review
CFEE	Cold Front End Electronics
CFRP	Carbon Fiber Reinforced Polymer
CHEOPS	CHaracterising ExOPlanet Satellite
CNES	Centre National d'Études Spatiales
CO	Common Optics
COROT	COnvection ROtation and planetary Transits
EChO	Exoplanet Characterisation Observatory
E-ELT	European Extremely Large Telescope
EID-A	Experiment Interface Documents part A
EID-B	Experiment Interface Documents part B
ESA	European Space Agency
ESATAN-TMS	European Space Agency Thermal Analysis Network software Thermal Modelling Suite
ESO	European Southern Observatory
EU	Electronic Unit
FEE	Front End Electronic
FGS	Fine Guidance Sensor
FHTS	Fluid Heat Transport System
GFRP	Glass Fiber Reinforced Polymer
GUI	Graphical User Interface
HIRES	E-ELT High Resolution Spectrograph
IASF	Istituto di Astrofisica Spaziale e Fisica Cosmica
INAF	Istituto Nazionale di Astrofisica
IB	Instrument Box

ICS	Inertial Coordinate System
ICU	Instrument Warm Unit
I/O	Input/Output
IOB	Instrument Optical Bench
ITP	Industria de Turbo Propulsores
IR	Infrared
JT	Joule-Thomson
JWST	James Webb Space Telescope
L2	Second Lagrangian point
M1	Primary mirror
M2	Secondary mirror
M3	Third mirror
M3	Third M-class ESA mission
M4	Fourth M-class ESA mission
MCR	Mission Consolidation Review
MCRT	Monte Carlo Ray Tracing
MCS	Model Coordinate System
METIS	Mid-infrared E-ELT Imager and Spectrograph
MLI	Multi-Layer Insulation
MORTRAN	More Fortran
MPDB	Material Property Database
MRD	Mission Requirement Document
MSR	Mission Selection Review
NASA	National Aeronautics and Space Administration
NIR	Near Infrared
NIRP	Near Infrared Photometer
OB	Optical Bench
OBC	On Board Computer
OBDH	On Board Data Handling
PCDU	Power Conditioning and Distribution Unit
PDD	Payload Definition Document
PI	Principal Investigator
PID	Proportional Integral Derivative
PLATO	PLAnetary Transits and Oscillations of stars
PLM	PayLoad Module
RAL	Rutherford Appleton Laboratory
REF	Radiative Exchange Factor
R-OBS	Observational Requirement
R-THE	Thermal Requirement
RTU	Remote Terminal Unit

R-SCI	Scientific Requirement
RW	Reaction Wheel
SAF	Solar Absorbed Flux
S/C	Space/Craft
SciRD	Science Requirements Document
SDF	Solar Direct Flux
SI	International System of units
SPC	Science Programme Committee
STR	Star Tracker
SVM	SerVice Module
TBC	To Be Confirmed
TCS	Thermal Control Stage
TESS	Transiting Exoplanet Survey Satellite
TMM	Thermal Mathematical Model
TOB	Telescope Optical Bench
UD	Unidirectional
VDA	Vapour Deposited Aluminium
VG	V-Groove
VIS	Visible

Bibliography

[1] *ARIEL: The Atmospheric Remote-Sensing Infrared Exoplanet Large-survey*, Proposal submitted to ESA on January 15th 2015 in response to the call for the M4 mission.

[2] Concurrent Design Facility Team. *ARIEL Phase 0, Internal Final Presentation*, ESTEC, ESA, July 8th 2015.

[3] David Rodgers. *ARIEL Environment Specification*, ESA-ARIEL-EST-ENV-SP-001, August 28th 2015.

[4] The ARIEL study science team. *ARIEL Science Requirements Document (SciRD)*, ESA-ARIEL-EST-SCI-RS-001, October 5th 2015.

[5] The ARIEL study team. *ARIEL Mission Requirements Document (MRD)*, ESA-ARIEL-EST-MIS-RD-001, October 5th 2015.

[6] The ARIEL Payload Consortium & ESA ARIEL Team. *ARIEL Payload Definition Document (PDD)*, ESA-ARIEL-EST-PL-DD-001, September 10th 2015.

[7] NASA Ames/SETI/J Rowe. *Digital press kit - Kepler Planet Bonanza*, `http://www.nasa.gov/ames/kepler/digital-press-kit-kepler-planet-bonanza`, July 31st, 2015.

[8] Gilmore, D. G. *Spacecraft Thermal Control Handbook*, Vol. I: Fundamentals Technologies. El Segundo, California: The Aerospace Corporation Press, 2002.

[9] Baudouy, B. and Four, A. Low temperature thermal conductivity of Aluminum alloy 5056, *Cryogenics*, 60:1-4, 2014.

[10] Han, E. et al. Exoplanet Orbit Database. II. Updates to Exoplanets.org. *Publications of the Astronomical Society of the Pacific*, 126:827-837, October 2014.

[11] Hartwig, G. and Knaak, S. Fibre-epoxy composites at low temperatures. *Cryogenics*, 24(11):639-647, 1984.

[12] Morgante, G. et al. Thermal control system of the Exoplanet Characterisation Observatory Payload: design and predictions. *Experimental Astronomy*, 40(2):771-800, 2015.

[13] Tauber, J. A. et al. Planck pre-launch status: The Planck mission. *Astronomy and Astophysics*, 520:A1, 2010.

[14] Tinetti, G. et al. The EChO science case. *Experimental Astronomy*, 40(2):329-391, 2015.

[15] ITP Engines UK Ltd. *ESATAN-TMS Workbench User Manual*, Whetstone, Leicester, UK, December 2014.

[16] ITP Engines UK Ltd. *ESATAN-TMS Thermal Engineering Manual*, Whetstone, Leicester, UK, October 2014.

[17] SRE-FM and SRE-P and ESOC and D-TEC. *Margin philosophy for science assessment studies*, ESTEC, ESA, December 23rd 2014.

[18] Sheldahl®, a Multek brand. *Gold coated (one side) Polyimide*, Product Bulletin, `http://www.sheldahl.com/documents/Gold.pdf`, August 6th 2012.

[19] Hexcel Composites. *HewWeb^{TM}Honeycomb Attributes and Properties*, Hexcel Corporation, Pleasanton, California. `http://www.hexcel.com/Resources/DataSheets/Brochure-Data-Sheets/Honeycomb_Attributes_and_Properties.pdf`.